HEAT AND SMOKE TRANSPORT IN A RESIDENTIAL-SCALE LIVE FIRE TRAINING FACILITY: EXPERIMENTS AND MODELING

A Masters Thesis Submitted to the Faculty of the

WORCESTER POLYTECHNIC INSTITUTE

in partial fulfillment of the requirements for the

Degree of Master of Science in

Fire Protection Engineering

AUGUST 2010

Adam M. Barowy

Approved:

X

Kathy A. Notarianni
Advisor, Department Head

X

Daniel Madrzykowski
Co-Advisor, NIST

X

Nicholas A. Dembsey
Thesis Reader, WPI

For Engine Co. 3. Be Safe.

Abstract

Understanding fire behavior is critical to effective tactical decision making on the fireground, particularly since fireground operations significantly impact the growth and spread of the fire. Computer-based simulation is a flexible, low-cost training methodology with proven success in fields such as pilot training, space, and military applications. Computer-based simulation may enhance fire behavior training and promote effective fireground decision making. This study evaluates the potential of the NIST Fire Dynamics Simulator (FDS) and Smokeview to be utilized as a part of a computer-based fire fighter trainer.

Laboratory compartment fire experiments and full-scale fire experiments in a live-fire training facility were both conducted as part of the NIST Multiphase Study on Fire Fighter Safety and the Deployment of Resources. The laboratory experiments characterized the burning behavior of wood pallets to design a repeatable fire for use in the field experiments. The field experiments observed the effects of varying fire fighter deployment configurations on the performance times of fire fighter actions at a live fire training facility. These actions included opening the front door and fire suppression. Because the field experiments simulated numerous fire department responses to a repeatable fire, data were available to evaluate FDS simulation of heat and smoke spread, and changes in the thermal environment after the front door is opened and fire suppressed. In simulating the field experiments, the laboratory-measured heat release rate was used as an input. Given this assumption, this study has two objectives: 1) to determine if simulations accurately spread heat and smoke through a multi-level, multi-compartment live fire training facility 2) to determine if the simulations properly reproduce changes in the thermal environment that result from two typical fire fighter actions: opening the front door and fire suppression.

In simulation, heat and smoke spread to measurement locations throughout the test structure at times closely matching experimentally measured times. Predictions of peak temperatures near the ceiling were within approximately 20% for all measurement locations. Hot gas layer temperature and depth were both predicted within 10% of the floor to ceiling height. After the front door was opened, temperature changes near the door at the highest and lowest measurement locations matched with temperature changes in the experiments. After fire suppression, FDS simulated temperature decay at a rate within the range measured in the field experiments and approximated the total rise of the hot gas layer interface in the burn compartment 250 seconds after suppression.

Acknowledgments

The author would like to thank the United States Fire Administration for their support of the NIST computer-based fire fighter trainer project, especially Meredith Lawler. The author would also like to thank Daniel Madrzykowski and Jason Averill of the Building and Fire Research Laboratory (BFRL) at NIST, Dr. Lori Moore-Merrell of IAFF and Dr. Kathy Notarianni of WPI for their cooperation in conducting the residential fireground field experiments. The author would like to recognize Mr. Mike Selepak and Mr. Roy McLane of the for their technical support during field experimentation and Dr. Kevin McGrattan and Dr. Glenn Forney for their guidance and support during fire modeling. The author expresses gratitude to Professor Nicholas Dembsey of WPI for his review of this document and to Kelly Opert for technical writing support.

The author also wishes to express gratitude to the Montgomery County Fire and Rescue Service for providing their training academy facilities as a space in which to conduct the experiments, particularly Asst. Chief Michael Clemens, Capt. Doug Hinkle, Lt. Paul Neal, Master Fire Fighters Joey Fuller and Doug Dyer and Fire Fighter Chris Hinkle.

Thanks are also due to the dedicated staff of the Montgomery County and Fairfax County Fire and Rescue Services for tirelessly performing numerous simulated residential fire incident responses during the experiments on days often cold enough to freeze up charged hose lines.

Table of Contents

List of Figures

List of Tables

Nomenclature

A_v	area of compartment ventilation opening
A_T	total area of compartment enclosing surface excluding vent area
A_{fuel}	floor area of the fuel
c_p	specific heat at constant pressure
D_α	diffusion coefficient for species α
D^*	characteristic fire diameter
E	energy contained in fuel
f_b	external force vector (excluding gravity)
g	acceleration of gravity
g	gravity vector, normally (0,0,-g)
$\mathcal{H}$	total pressure divided by the density
H	compartment ceiling height
ΔH_c	effective heat of combustion
h_k	convective heat transfer coefficient
h_v	height of vent opening
k	thermal conductivity
$\dot{m}_\alpha'''$	mass production rate of species a per unit volume
$\dot{m}_f''$	burning rate
m_w''	local water mass delivered per unit area
m_c	moisture content by weight
m_{fuel}	fuel mass
Nu	Nusselt number
Pr	Prandtl number
$\overline{p_m}$	background pressure of m^{th} pressure zone
$\dot{q}_{rad}'''$	radiative heat flux
$\dot{q}_{conv}'''$	convective heat flux
$\dot{Q}''$	heat release rate per unit fuel area
$\dot{Q}$	total heat release rate
$\mathcal{R}$	universal gas constant
S	soot
T	temperature
T_g	true gas temperature
T_u	average upper (hot) gas layer temperature
T_l	average lower layer temperature
T_∞	ambient temperature
t	time, time after ignition
t_{solid}	burning duration of solid fuel
U	integrated radiant intensity
u = *(u, v, w)*	velocity vector
W_α	molecular weight of gas species α
x = *(x, y, z)*	position vector
Y_α	mass fraction of species α
Y_{O2}^∞	mass fraction of oxygen in the ambient
Y_F^I	mass fraction of fuel in the fuel stream

Z	mixture fraction
ΔH	heat of combustion
ε_{TC}	emissivity of thermocouple bead
υ_{α}	stoichiometric coefficient, species α
z_{int}	interface height above floor
ρ	density
ρ_o	ambient density
δx	nominal mesh cell size
τ_{ij}	viscous stress tensor
σ	Stefan-Boltzmann constant
$\omega = (\omega_x , \omega_y , \omega_z)$	vorticity vector

List of Acronyms

ASTM	American Society for Testing and Materials
BE	Benchmark Exercise
BFRL	Building and Fire Research Laboratory (at NIST)
BRE	Building Research Establishment
CFD	Computational Fluid Dynamics
CPSE	Center for Public Safety Excellence
DNS	Direct Numerical Simulation
DOE	United States Department of Energy
DVD	Digital Video Disc
FDS	Fire Dynamics Simulator
FM/SNL	Factory Mutual & Sandia National Laboratories
GLUT	Graphics Library Utility Toolkit
HGL	Hot Gas Layer
HRR	Heat Release Rate
HRRPUA	Heat Release Rate Per Unit Area
IAFC	International Association of Fire Chiefs
IAFF	International Association of Fire Fighters
IAFSS	International Association of Fire Safety Science
ICFMP	International Collaborative Fire Model Project
LES	Large Eddy Simulation
NBS	National Bureau of Standards (now NIST)
NFPA	National Fire Protection Association
NIST	National Institute of Standards and Technology
NRC	U.S. Nuclear Regulatory Commission
RANS	Reynolds-Averaged Navier-Stokes
SNL	Sandia National Laboratory
SOFIE	Simulation Of Fires In Enclosures
USFA	United States Fire Administration
VTT	Technical Research Centre of Finland (Valtion Teknillinen Tutkimuskeskus)
WPI	Worcester Polytechnic Institute

1 Introduction

Understanding fire behavior is critical to effective tactical decision making on the fireground, particularly since fireground operations significantly impact fire behavior. Incident commanders and company officers make tactical decisions based on their understanding of fire behavior. The outcomes of structure fires: deaths, injuries, and economic loss are strongly dependent on these tactical decisions. Therefore, it is crucial to maximize opportunities to advance and expand upon fire behavior training. The research reported in this thesis the first of multiple steps for validation of the NIST Fire Dynamics Simulator (v5), computational fluid dynamics (CFD) model, to simulate thermal conditions that result from fire in residential scale structures and to simulate changes in the thermal conditions due to fire fighter actions. With the support of NIST, this research will further efforts to develop a computer-based fire behavior training tool for the fire service using FDS and the companion visualization program Smokeview [1,2,3]

In 2005, the National Fallen Firefighters Foundation conducted the "National Fire Service Research Agenda Symposium" to identify and prioritize areas of research that will improve firefighter life safety [4]. The symposium identified two related needs: "Educational Methodologies to Effectively Reduce Fire Service Injuries and Fatalities" and "Effective Integration of Simulation into Training." Computer-based training software promises to meet these two needs. Computer-based training simulations have been successfully implemented in military applications as well as civilian applications such as driver education, flight training and countless other scenarios. Computer-based fire behavior training software could augment current fire behavior training methods. For example, a computer-based trainer could provide the opportunity to perform various different tactics at the same fire and allow the trainee to observe the results. This would ultimately equip the fire service to make improved tactical decisions that may reduce the amount of fire fighter and civilian deaths and injuries and economic loss.

The fire service responds to many different types of structures. This study considers only one type of structure, the single-family, detached two-story home. The single family two-story home is the most logical first step, because it is nationally recognized as the most commonly found structure in the United States [5]. It also recognized to have the most significant incidence of fire and subsequent losses. Section 2.1.1 discusses details about the incidence of fire in two-story homes in the U.S.

1.1 Current Fire Behavior Training

Currently, the fire service is educated about fire behavior through a combination of classroom instruction and live fire training exercises. Fire behavior training introduces the fundamentals of fire dynamics. Examples are: the "fire tetrahedron" (the four components necessary to maintain a fire: fuel, oxidizing agent, chemical chain reaction, thermal energy), the modes of heat transfer, conservation of mass and energy, buoyancy driven thermal layering, etc. [6,7,8]. The fundamentals of fire dynamics are used to educate the fire service about ignition, burn rate/rate of fire growth, the movement of heat and smoke, modes of fire spread, the stages of compartment fire growth and various other elements of fire dynamics. Fire dynamics is taught in the classroom to provide background for the traditional approaches to fire fighting tactics.

Live fire training demonstrates fire behavior and fire fighting tactics learned in the classroom. Fire fighters experience changes in fire behavior through the amount of thermal loading they perceive on their bodies as well as through visible changes in their environment. In particular, fire fighters observe how their actions affect fire behavior and their environment. For example, here is a potential observation that could be made by a fire fighter ventilating the window of a compartment fire:

- Opening the ventilation point above the thermal interface allows buoyant heated smoke and gasses to escape out the open window, causing the hot upper layer to diminish and elevating the thermal interface toward the ceiling.

Fire fighters must observe a live fire environment and obtain the physical experience necessary to be able to recognize fire conditions and how their actions immediately affect fire behavior. Trainees need to learn to communicate, navigate and cooperate on functions such as search and rescue or hose stream advancement in an environment that challenges their senses.

Live fire training acquaints fire fighters with the physiological demands of working in an elevated thermal and low-visibility environment representative of the structure fire environments they will encounter. Live fire training stresses the human body by a combination of factors including strenuous muscular work, intense heat, and heavy, restrictive, and highly insulative personal protective equipment. For fire fighters to function properly in real fire situations it is clearly essential that they gain an awareness and understanding of how elevated working temperatures can disorient the mind and make it difficult to think clearly and decisively. Fire fighters must be able to make judgments and decisions in conditions that directly affect their personal safety, as well as that of their fellow fire fighters and members of the public.

1.2 Enhancing Fire Behavior Training

Computer-based fire behavior training has the potential to expand upon current fire behavior training by:

- Increasing the availability/accessibility of fire behavior training materials
- Allowing trainees to study key phenomena and conditions that injure/kill many fire fighters
- Increasing the interactivity of fire behavior training
- Adding observational capabilities and perspectives to fire behavior training
- Offering fire incident scenarios that go beyond the capabilities of live fire training
- The ability to repeat training scenarios and change tactics/responses without limitation

The availability of classroom fire behavior instruction and live fire training is determined by the availability of resources. Qualified instructors are required in order to offer both forms of training and the training is offered only to groups, as opposed to the individual. In addition, live fire training requires training facilities, apparatus, equipment, planning and a budget all of which can limit the amount of live fire training a fire department is capable of conducting. This is particularly critical during demanding economic periods, such as during the writing of this work, when public service spending is under particular scrutiny.

Computer-based fire behavior training simulations developed through NIST using FDS would be beneficial to the fire service in light of the availability of fire behavior training resources (e.g. training budgets). FDS development and computer-based fire behavior simulation efforts are supported by NIST and the United States Fire Administration (USFA). FDS-produced structure fire simulations could be provided in cost-free and easily accessible formats (e.g. web-based or DVDs) that are appropriate for both classroom and individual use. Training with these simulations would be limited only by access to computers or televisions with DVD players, potentially placing a fire behavior training simulator in every firehouse in the country.

Computer-based fire behavior training simulations could provide a new, more interactive format of training material for the classroom as well as for the individual. The following is an example of how the classroom could benefit: during a fire simulation exercise, multiple tactical decisions are offered to classroom participants at particular points occurring along the fireground timeline starting with on-scene arrival. Instead of instructor-based determinations, changes in fire behavior resulting from tactical decisions are pre-calculated by FDS and based on real fire experiments. This reduces the burden on the instructors, allowing them to highlight their experience and expertise by discussing pre-decisional considerations, implementation of fireground tactics, changes in fire behavior, and critiquing tactical decisions and other logistical topics.

For the individual, the following is an example of how training could become more interactive: Between time spent on calls and ordinary work duties, an on-duty fire fighter works their way through fire simulations. The fire fighter observes fire behavior changes with respect to time and tactical decisions and has control over visual perspectives and the fireground timeline. In this format, fire behavior training would be available "on demand." Information delivery to fire fighters would be limited only by the development of the training simulations.

Computer-based fire behavior training simulations may also provide additional observational capabilities and perspectives over those available in live fire training. In live fire exercises individual fire fighters can only experience the changes in their local environment. A firefighter inside the room of fire origin will experience significantly different fire behavior than a fire fighter located in a remote location. Different fire fighter actions during an exercise will also result in significantly different fire behavior experiences. For example, a fire fighter performing window ventilation will not observe the same fire behavior that results from fire suppression. FDS and Smokeview possess the capabilities to provide multiple viewing angles and perspectives throughout a structure in a fire simulation. Section 1.3 discusses the details of how FDS and Smokeview may be able to provide these additional capabilities.

Computer-based fire behavior training has the potential to offer fire incident scenarios fire departments may not be capable of safely providing with live fire training. There are multiple factors that narrow the kinds of fire scenarios live fire training can be offered for. These factors are:

- Fire size
- Fuel type
- Impracticality of constructing training facilities representative of all types of building construction in a fire department's response area
- Construction differences between training facilities and structures in real fires

The primary concern in live fire training is trainee safety. The range of fire sizes and types of fuel that may be used are limited to the amount that can be trained with safely. Guidelines for fuel types in live fire training structures are provided by NFPA 1403: Standard on Live Fire Training Evolutions [9] in order to eliminate the hazards of flashover and backdraft for participants. However, the fuels for practically all real fire responses exceed the fuel loading and type recommended by NFPA 1403. For example, NFPA 1403 recommends that "pressure treated wood, rubber, plastics and straw or hay treated with pesticides" not be used in training fires. It is more than likely that these fuels will be present for any structure fire response. Subsequently, training fires in these facilities do not necessarily represent the type of fire growth and development that the fire service may encounter on an actual response. Computer-based simulations may be used to visualize fire behavior with fuels types and configurations that are outside the guidelines of NFPA 1403.

There are many different types of occupancies in the typical fire department's response area. For example, a single response area may include residences, office buildings, industrial facilities, educational facilities, etc. Within these categories there exist further classifications of building construction. As a matter of practicality, it is not possible to provide live fire training structures representative all of the types of building constructions that fire departments will respond to. Using data from NIST large-scale fire experiments, pre- and post-flashover fire scenarios could be simulated for multiple types of full-scale structures. As a minimum, it may be possible to produce training simulations that fire departments cannot provide fire behavior training for. Once FDS has been validated for fire simulation on a structural scale, computer-based fire behavior training simulations could be tailored to the specific needs of the fire service.

A final consideration is that training facilities differ in construction from structures that fire fighters may respond to during real fire incidents. Training facilities are designed to withstand the repeated abuse of extreme heat, moisture and general wear and tear. Construction is typically poured concrete, concrete block or all metal structures, which may be significantly different from the materials used in the construction for the buildings they are intended to represent.

The application of training software for incident command and fire fighting tactics has been recognized in the industry. Section 2.2.1 discusses current industry efforts to produce fire fighting tactics training software.

1.3 Computational Fluid Dynamics Models

Fluid dynamics is a field of science that studies the physics of fluids in motion. Computational fluid dynamics (CFD) is a branch of fluid dynamics that uses computers to apply numerical methods and algorithms to solve and analyze the physics of fluid flows. CFD models are computer programs which have been developed to solve the physics of fluid flow to generate simulations for specific applications. CFD models have been developed for research and commercial applications such as:

- Aerospace
- Automotive
- Marine
- Medical
- Weather
- Fire safety

CFD models work by applying equations that describe fluid flow to a volume known as the computational domain. The governing equations in almost all CFD models are the Navier–Stokes (N-S) equations, which define any single-phase fluid flow. In order to apply these equations, the volume of fluid being simulated is split into many smaller volumes or "cells", which together form a "computational mesh." The model then uses a numerical algorithm to apply the N-S equations to the computational mesh to solve the equations at consecutive discrete steps in time, or "time steps".

Most popular CFD models possess a graphical user interface (GUI) organizes and gathers user input data into all the physical information required to describe the condition they would like to simulate. The GUI also captures the user-defined resolution of the computational mesh (i.e., physical dimensions of the cells) and a simulation run time. For example, the user inputs information describing the shape of an aircraft wing and the speed of air flowing over the wing. The user also specifies the resolution of the computational mesh based on the level of detail desired, and a simulation run time. The CFD model would then use all of the inputs to march the N-S equations through the computational mesh at discrete time steps until the simulation is complete. The result is a set of numerical data that describes the physics of the fluid flow over the wing for length of the simulation. These numerical results can be viewed in a "post-processing" program designed to visualize output and they can analyzed with commercially available data analysis software. There are a number of variations in the details for how this process is carried out from model to model, but these are the general steps involved in CFD simulation.

CFD models, when applied to structure fire simulations, may be able to provide advances in current fire behavior training by using these physics-based calculations to present visualization and quantification of fire behavior in a meaningful manner to the fire service. Section 2.2.2 discusses FDS and two other specialized CFD fire models that have been developed to handle simulation of combustion as well as fluid dynamics.

The interactivity of classroom fire simulation exercises and individual fire behavior training could be enhanced by CFD simulations completed with FDS. As opposed to the local observations trainees make in live fire training, Smokeview provides different viewing locations and angles and the ability to move freely in 3-D space, so that trainees could observe how fire fighting tactics affect fire behavior and the environment inside an entire structure.

Currently, visualization options in Smokeview are accessible via pull down menus. Many of these visualizations available are not required to provide the information needed by the fire service, and the use of pull down menus would not be conducive to intuitive use in a training environment. Therefore work outside this study is underway at NIST to develop a fire-service specific version of Smokeview with intuitive controls for displaying fire behavior visualizations and information pertinent to fire service needs. Some example quantities of interest are: hot gas layer (HGL) temperature and depth, heat flux, heat release rate and gas concentrations. An example of how HGL temperature and depth could be used to demonstrate thermal layering was given in Section 1.1. Visualizations of these outputs reflect major concepts of fire behavior training currently offered to the fire service [6,7,8].

NIST has performed numerous fire reconstructions with FDS simulations, such as the Station Nightclub fire [10], a townhouse fire in Washington, DC [11], a two-story duplex fire in Iowa [12], and a one-story restaurant in Texas [13]. These simulations provide information and visualizations not available through standard fire fighting training and are examples of how FDS simulations can be used to augment fire fighting training. However, fire-behavior training simulations will require a pre-computational approach.

FDS inputs require a thorough understanding of heat and mass transfer and fluid dynamics as well as familiarity in computer programming, numerical methods and data reduction.

As a drawback to CFD, computers still perform computations much slower than in real-time. Even with the most advanced of technologies available, obtaining numerical predictions with practical accuracy is exceptionally computationally expensive. As a result, there are no CFD models with real-time user-interactivity. To produce a fire behavior training tool with FDS, simulations will require a decision tree that maps out possible fire fighting tactics during the course of a simulation. Changes in fire behavior resulting from tactical decisions will have to be pre-computed based on those tactical decisions and arranged in a database from which Smokeview loads visualization data.

1.4 CFD Fire Model Validation

Before a CFD model can be used in practice, it must be validated. The first step in performing a fire model validation is to understand the definition of validation. ASTM E1355 [14] defines model validation as:

"The process of determining the degree to which a calculation method is an accurate representation of the real world from the perspective of the intended uses of the calculation method."

In addition to the ASTM E1355 validation definition, the FDS developers provide the following definition of validation [2]:

"A process to determine the appropriateness of the governing equations as a mathematical model of the physical phenomena of interest. Typically, validation involves comparing model results with experimental measurement."

FDS requires further validation work to provide a better understanding of the accuracy of the model's HGL predictions, areas of the model that need development and acceptable uses of the model. Simulations must be compared with experimental data in order to evaluate the appropriateness of model inputs. The validation of FDS on the scale of compartment fires is dependent on the availability of reliable experimental data . Data can be found with relative ease for full scale compartment fire experiments; however the majority of those experiments were not conducted with the intent of FDS validation. As a result, much of the information required for performing a validation study is not available. Because of the complexity of FDS, a significant amount of information must be recorded before and during fire experiments. Ideally, this information should address all of the model inputs and be able to be compared directly to model simulations. Even having gathered this information, inputting it into the model using engineering judgment can be a difficult and convoluted process. In recognition of this difficulty and the lack of a standard approach, a guide similar to ASTM E 1591: Standard Guide for Obtaining Data for Deterministic Fire Models is currently being developed for field (CFD) models as well as more simple (zone, algebraic) models [15].

1.5 Scope of This Work

This thesis examines FDS simulations of the spread of heat and smoke throughout a two-story live fire burn facility designed to represent a single-family residential structure. Additionally, this thesis investigates changes in the simulated interior thermal environment resulting from two typical fire fighter actions on a fireground: front door ventilation and subsequent fire suppression. The analysis is conducted by comparing predictions of thermocouple temperatures, and hot gas layer temperature and depth, with full scale fire data from laboratory and field experiments. Input parameters that affect the FDS predictions and limitations imposed by the experimental data are discussed. The research reported here will further efforts to validate FDS on the residential scale and to develop a computer-based fire behavior training tool for the fire service.

2 Background

Section 2.1 provides an overview of fire incidents that the U.S. fire department responds to, concentrating on structure fires. Section 2.1.1 presents data that highlights the frequency and severity of residential structure fires. The data demonstrates why the one- and two-family residence represents an appropriate starting point for developing a fire behavior training simulation. Section 2.2.1 describes the current state of the art in computer-based fire behavior training simulations. The background of CFD fire models follows, which includes discussion of the applicability to structure fire simulations and the potential for advancing the state of the art in fire behavior training simulations.

2.1 The United States Fire Problem

Using NFPA data, Karter [16] shows that public fire departments in the United States responded to 1,451,500 fires in 2008. These fires resulted in:

- 3,320 civilian fire deaths
- 16,705 civilian fire injuries
- $15.5 Billion in property damage (including $1.4B from 2008 California wildfires)

What is most significant about the above loss totals is the disproportionate amount of all types of losses that are attributed to structure fires. Although structure fires accounted for only 34% (515,000) of the fire incidents in 2008, structure fires resulted in:

- 87% (2,900) of civilian fire deaths
- 90% (14,960) of civilian fire injuries, and
- 81% ($12.4B) of property damage

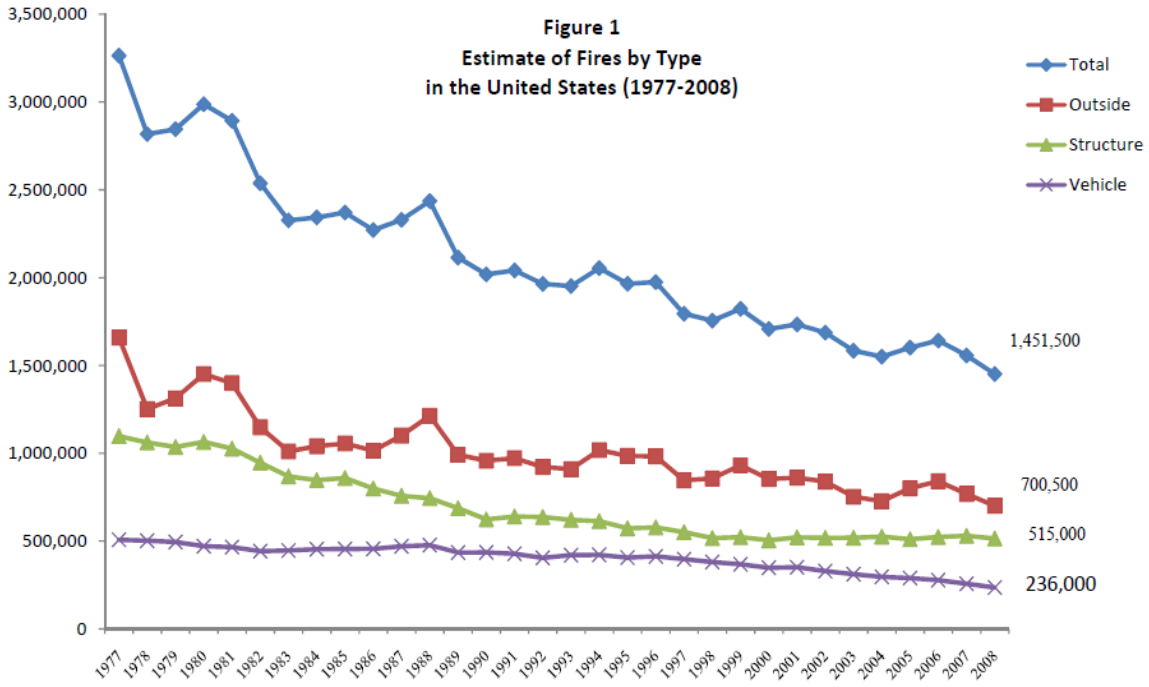

Figure 2-1: The incidence of fire from 1977-2008 [16]

Figure 2-1, taken from Karter's report, chronicles the incidence of fires from 1977-2008 and it provides comparison of the incidence of structure fires, outdoor/other fires, vehicle fires and the total incidence of fire. The data in this figure shows that although the incidence of fires has steadily trended downward since 1977, the proportion of fires occurring in structures has remained relatively constant. The proportion of losses resulting from structure fires has also remained relatively constant over the last three decades. Annual fire loss reports from prior years also reflect this observation. For example, 87%, 87% and 83% of civilian fire deaths occurred as a result of structure fires in 2008 , 2007 [17] and 2006 [18], respectively.

2.1.1 Fires in One- and Two-Family Residences

Residential fires dominate the incidence of structure fires in the United States. Karter's annual fire reports note that residential properties have experienced the largest number of fires in the three most recent years. The following is a list of the number of residential fires and the percentage they make up of the total number of structure fires for that year:

- 2006 - 412,500 fires or 79% [18]
- 2007 - 414,000 fires or 78% [17]
- 2008 - 403,000 fires or 78% [16]

Using Karter's 2008 fire loss report and NFPA data, Ahrens provides analysis of trends and patterns in 2008 fire losses. Residential properties are the most significantly affected by fires [19]. Ahrens provides Figure 2-2, which compares the incidence of fire by property class.

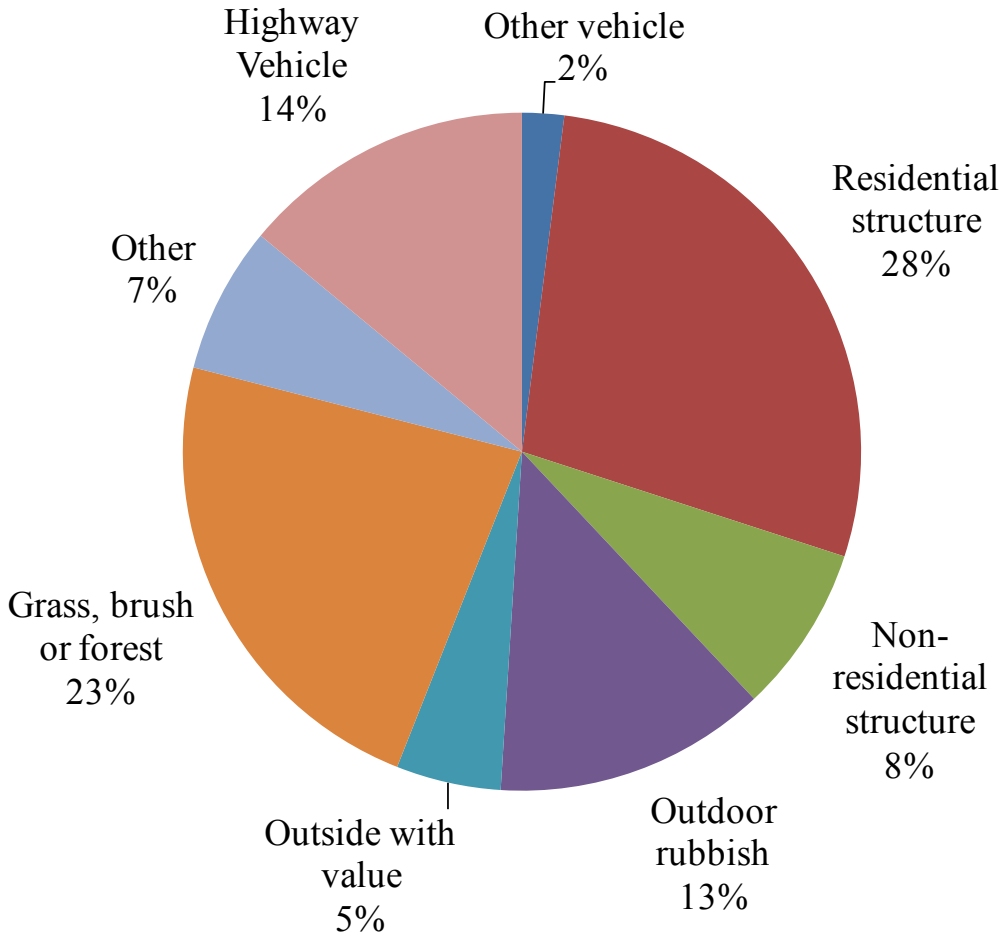

Figure 2-2: The incidence of fires in 2008 by major property class (recreated from [19])

Figure 2-2 shows that for the year 2008, residential fires dominated the incidence of fire even when including all non-structure fires (outside, vehicle, other). Ahrens's analysis extends further, organizing fire data into major types of residential properties and providing the quantity of civilian deaths, injuries and economic loss associated with each. All percentages shown in Table 1 are in relation to the total for each respective type of loss (deaths, injuries and property damage) that occurred in 2008.

Incident Type	**Fires in Structure Type**	**% of Total Fires in 2008**	**Civilian Deaths**		**Civilian Injuries**		**Direct Property Damage (In Millions)**	
Structure Fires	515,000	35%	2,900	87%	14,960	90%	$12,361	80%
Residential Structure Fires	403,000	28%	2,780	84%	13,560	81%	$8,550	55%
One- or two-family dwelling	291,000	20%	2,365	71%	9,185	55%	$6,892	45%
Apartment	95,500	7%	390	12%	3,975	24%	$1,351	9%
Other Residential	16,500	1%	25	1%	400	2%	$307	2%
Non-Residential Structure Fires	112,000	8%	120	4%	1400	8%	$3,811	25%
Vehicle Fires	236,000	16%	365	11%	1,065	6%	$1,494	10%
Outside and Other Fires	700,500	48%	55	2%	680	4%	$223	1%
California Wildfires 2008	-	-	-	-	-	-	$1,400	9%

Table 1: 2008 fires, civilian fire injuries and deaths and economic loss in 2008[1] [19]

The data in Table 1 clearly shows that the highest incidence of fires and the largest amount of resultant civilian fire deaths, injuries and property damage occurs in one- and two-family homes. For an additional perspective, Ahrens also provides graphical representations of the data in Table 1 that offer a proportional view of these losses compared across other property types including non-residential properties. Figure 2-3- Figure 2-5 are recreated from Ahrens' report.

[1] NFPA survey does not collect specific incident types for fire deaths and injuries caused by outside and other fires. Nor does it collect any dollar loss data for brush, grass, and wildland fires with no value or loss or for outside rubbish fires.

[2] In the analysis of the FDS source code it was found that the midpoint rule is actually used for the

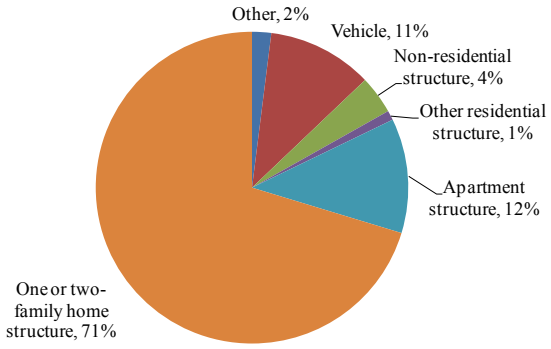

Figure 2-3: 2008 Civilian fire deaths by major property class (recreated from [19])

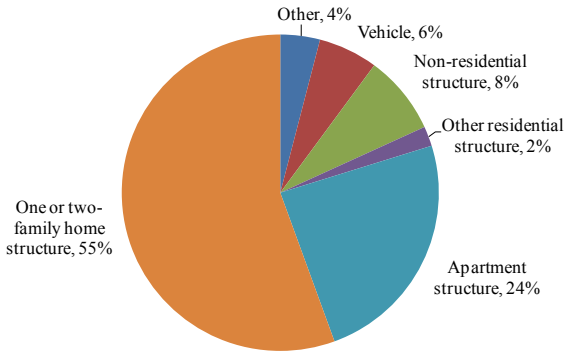

Figure 2-4: 2008 Reported civilian fire injuries by major property class (recreated from [19])

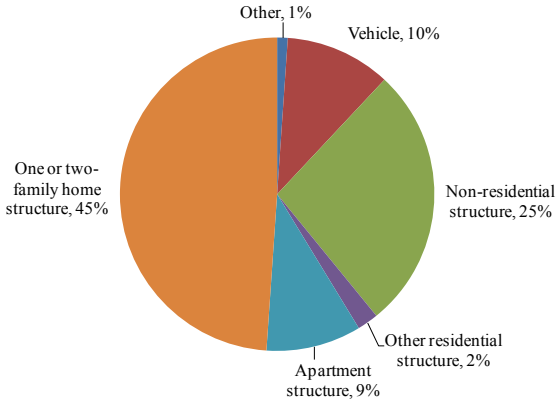

Figure 2-5: 2008 Direct property damage by major property class (recreated from [19])

The prevalence of residences is a factor in the relatively high incidence of residential fires. The one- and two-family residence is the most common structure in all regions in the United States. In 2005 the United States Department of Energy (DOE) conducted survey of residential properties known as the "Residential Energy Consumption Survey" [5]. This survey collected data from 4,831 households in housing units from the four regions (Northeast, Midwest, South, West) that make up the U.S. The DOE statistically selected housing units to represent the 111.1 million housing units in the nation. The survey shows that "detached single-family residences" (the closest match to one- and two-family dwellings) account for approximately 64.9 percent of the housing units in the United States.

The high incidence of fire for this type of structure is reflected in NFPA 1710: Standard for the Organization and Deployment of Fire Suppression Operations, Emergency Medical Operations, and Special Operations to the Public by Career Fire Departments. NFPA 1710 states that "all" communities respond to fire incidents at this type of structure, on a regular basis [20]. The most recent and detailed analysis of fire fighter injuries is given in a report by Karter and is based on fire fighter injuries occurring in various different occupancies, as opposed to property classes, during the years 2003-2006 [21]. Statistics reported in the analysis are based upon an average of the four years of data. The analysis shows that the trend in fire fighter injuries by occupancy agrees with the trends of losses presented by the analyses in the previously discussed reports; there is a high incidence of fires (57%) accompanied by a high incidence of fire fighter fireground injuries (61%) in one- and two-family dwellings. The table given in the report is recreated below as Table 2.

Occupancy	**Structure Fires**		**Fireground Injuries**	
Public assembly	13,500	3%	1,015	3%
Educational	6,600	1%	280	1%
Institutional	7,100	1%	135	0%
Residential	405,300	78%	27,600	80%
1 & 2 Family Dwellings	297,500	57%	20,930	61%
Apartments	92,800	18%	5,400	16%
Stores	22,900	4%	1,925	6%
Industrial, utility, manufacturing	11,600	2%	1,375	4%
Storage	30,800	6%	1,885	5%
Special	22,400	4%	225	1%
Total	520,200		34,450	

Table 2: Structure Fires, Fireground Injuries and Injury Rates By Occupancy, 2003-2006 Annual Average [21]

The USFA released the most detailed report analyzing firefighter fatalities in 2008 [22]. Fire fighter fatalities were classified by four types of fixed properties: residential, commercial, manufacturing and educational. Between the four types of fixed property identified, 15 (71.4%) of fire fighter fatalities occurred at the scene of a residential structure fire.

The literature makes it clear that between all of the types of fire incidents that the U.S. fire service responds to, structure fires account for the most injuries, deaths and economic loss for civilians and fire fighters. Specifically, the type of structure that results in the greatest amount of fire loss in the nation is the one and-two family residence. Therefore, performing a FDS validation for the one- and two-family residence is a logical step forward in fire behavior simulation development efforts. Fire simulations in one- and two-family residences could provide additional fire behavior training in the most common type of structure fire for the majority of U.S. fire departments.

2.2 Feasibility of Software for Fire Behavior Training

2.2.1 Current Fire Behavior Training Software

Presently, both the need for expanding the training resources of the fire service and the potential use of computer-based fire fighting trainers to fill this need have been recognized in the software development industry. Several commercial companies have developed or are currently developing fire behavior training software. The major focus of current training software is to provide representations of fire scenarios and fire behavior based on visual interpretations of fires, as opposed to visuals generated by physics-based calculations vetted by real fire data. Another significant focus is to provide incident command type training [23,24,25,26].

With current fire behavior training software, changes in fire behavior occur in one of two ways. Either the computer-based trainer has an interactive video game style and changes in fire behavior are pre-programmed into the software or changes in fire behavior are controlled by an instructor directing the simulation. In the former, fire behavior changes are controlled by algorithms designed to alter graphics based upon expected or likely changes in real fire behavior. In the latter, fire behavior changes are made based upon "expert" opinion and are dependent upon the personal experiences of the instructor. The following excerpt from a brochure for RescueSim is an example of how fire behavior is altered in an instructor-led simulation [25]:

"Not only in preparation, but also during the training, the instructor can influence the incident at all times. He can change elements such as fire, victims, explosions, smoke, gas cloud, wind direction, wind speed, weather conditions, availability of equipment, complexity of the incident, etc. This makes every scenario dynamic and realistic."

In either type of software, fire behavior visualizations are not generated using physics-based of fire phenomena using the current state of the art in fire research. Therefore current software fire behavior visualizations represent the current fire service interpretation and understanding of fire behavior.

It should be noted that although these types of fire ground simulations do not use physics based calculations to determine fire behavior, they are certainly useful for teaching incident command type issues such as apparatus positioning, scene size-up and fire department standard operating procedures.

Two previous studies demonstrate interest in, and the potential benefits of producing physics-based fire behavior training software. Tate, Sibert and King [27] developed a three dimensional model of the ex-USS Shadwell where users interact with shipboard spaces during a simulated fire. To simulate fire, previously recorded video of fires were overlaid into a 3-D model of the Shadwell. Fire growth was coupled to a smoke model that changed visual obscuration with time. The smoke model was developed based on previous fire experience inside the Shadwell. The extent of the value of this model is for familiarizing the trainee with a specific floor plan.

St. Julien and Shaw [28,29] used FDS (pre-version 4.0) in a research project at the Graphics, Visualization and Usability Center at the Georgia Institute of Technology. The Atlanta Fire Department offered fire service expertise during the development of the project. Instead of using Smokeview, the researchers chose to develop a separate visualization tool as part of their educational program. As of 2003 their research involved pre-computing multiple FDS simulations and compiling them into a single-scenario fire simulation. The simulation allows users to decide which actions to perform as the fireground timeline progresses. The goal of pre-computing many simulations was to provide the decision tree that would allow trainees to see the “realistic” change in fire behavior resulting from a selected action. This is a good process to approach, however the work was never validated with experimental data and no further efforts appear to have come out of the program since 2003.

Software fire behavior training simulators that generate visualizations of natural fire behavior from calculations of fire physics were not found in the literature. However, the fire fighting training simulators found in the literature identify the applicability of computer-based training software for fire fighting tactics training, especially when involving fire behavior. The development and commercial sales of these simulators identifies fire service interest in using computer-based simulations to expand upon fire behavior training; an interview with Shaw in [29] identifies the fire service interest in improving fire behavior simulations to be more representative of real-world fire behavior:

" The Atlanta Fire Department told us that accuracy is important. If the fire in our virtual environment doesn’t respond like a real fire would to a door opening, for example, then it’s not very useful as a training tool."

2.2.2 Current CFD Fire Models

A wide variety of CFD models have been developed for fire applications. The most significant difference between current fire models is their method for handling turbulence. Three major methods for handling turbulence in CFD have been applied to fire models: Direct Numerical Simulation (DNS), Reynolds-Averaged Navier Stokes (RANS), and Large Eddy Simulation (LES). The most well-known and supported current fire models, as well as their methods of handling turbulence are shown below in Table 3, along with the developer, country of origin and current license fee.

Name	Country of origin	Developer	Turbulence Model	Reference
Fire Dynamics Simulator	U.S.	NIST	LES/DNS	[1-2]
Smartfire	U.K.	Univ. of Greenwich	RANS	[30]
SOFIE	U.K./Sweden/ Finland	BRE/Lund Univ./VTT	RANS	[31]

Table 3: Current CFD fire models

The approach in DNS is to resolve all the relevant scales occurring in the flow in the simulation. DNS solves the Navier Stokes equations directly rather than using less-accurate, but time-saving turbulence models. This means that the whole range of spatial and temporal scales of turbulence must be resolved on a high resolution computational mesh. Direct Numerical Simulation is not yet of practical use in modeling compartment fires due to prohibitively expensive computational requirements; requirements exceed the capabilities of even the most powerful computing available today. Subsequently DNS modeling was not considered for this study.

The majority of the CFD fire models that have been developed to date use a RANS approach to simulating turbulence, but a more recent approach is LES. FDS is currently the only CFD model that uses the Smagorinsky form of LES with a mixture-fraction combustion model to simulate fire-driven fluid flow [1-2]. The most important differences between the RANS and LES approaches are in how each handles the effects of turbulence during simulation. The advantage of the RANS approach is that it requires less computational resources than LES. RANS models have been developed as a time-averaged approach to solving the conservations equations of fluid dynamics. The smallest resolvable length scales are dependent on the averaging time and local velocity. However, results of RANS simulations have been shown to be less accurate than LES and to have a "smoothed" appearance [2,32].

As opposed to RANS, the smallest resolvable length scales in LES are determined by the user-specified computational grid. The effects of turbulent eddies smaller than the spatial dimensions of the computational mesh are approximated. Eddies on a scale larger than the computational mesh are solved for directly. It is assumed that large-scale turbulence carries the majority of the energy in the system. This is particularly important for modeling structure fires. Fluid flow in structure fires is driven by the fire plume which is dominated by large eddies. By approximating small eddies, as opposed to solving for them by direct numerical simulation, computational demands are reduced but results are still improved over the RANS approach. Additionally, the scale of the computational domain for structure fire simulations can be quite large. This makes it possible to perform simulations on a structural scale in a reasonable amount of time with a relatively "coarse" computational grid. As opposed to the limitations of RANS, the fidelity of LES solutions is controlled by the size of the underlying spatial mesh. As computer processors improve in computational speed, it becomes possible to further reduce the spatial size of the computational mesh. However, even though the assumptions in LES and in RANS significantly simplify the calculations involved in fire modeling, simulations are still highly computationally expensive and run slower than real-time. Even with the most powerful computing resources currently available it is still not possible to perform CFD simulation in real-time. FDS was chosen for this study for four reasons:

- FDS takes advantage of LES, an improved method for handling turbulence that is relatively new to fire modeling
- FDS is a free and open source fire model with ongoing support and development from NIST.
- A highly interactive post-processing scientific visualization tool, Smokeview, has been developed in parallel with FDS.
- Work outside this study is underway at NIST to develop a fire-service specific version of Smokeview

2.2.3 FDS Validations

A search of the literature identified a wide range of FDS validation studies. Some of the major validation topics identified are: pool fires [33], tunnel fires [34], flame spread [35] and compartment fires. This section focuses on compartment fire validation studies germane to the simulation of thermal conditions due to fire in a residential-scale structure.

Two major FDS validation studies have been completed for recent versions of FDS. Both studies include validation of HGL temperature and depth in compartment fires. Both studies used the rigorous verification and validation guidelines recommended in ASTM E 1355 [14]. NIST completed the first study as a review of the capabilities of FDS [2]. In their validation, NIST compared FDS outputs to measurement data from 15 different experiments as well as two different correlations. One of these 15 experiments (NBS Multi-Room) were compartment fire experiments. The majority of the predictions of

HGL temperature and depth for the NBS experiments fall within the reported 13% combined uncertainty.

The U.S. Nuclear Regulatory Commission (NRC) completed the second significant verification and validation study [36]. This study was completed in order to document the accuracy of FDS v4.0 in predicting the results of six different compartment fire experiments relevant to the nuclear power plant industry. Two of the experimental series included in the NRC validation study are the same series used in the validation completed by NIST, the remainder are single compartment fire studies. Figure 2-6, given below, shows the that the relative difference between the predicted and measured HGL for the majority of the experiments falls within a ±13% range. Figure 2-6 provides a visual of the results of from the NRC validation study.

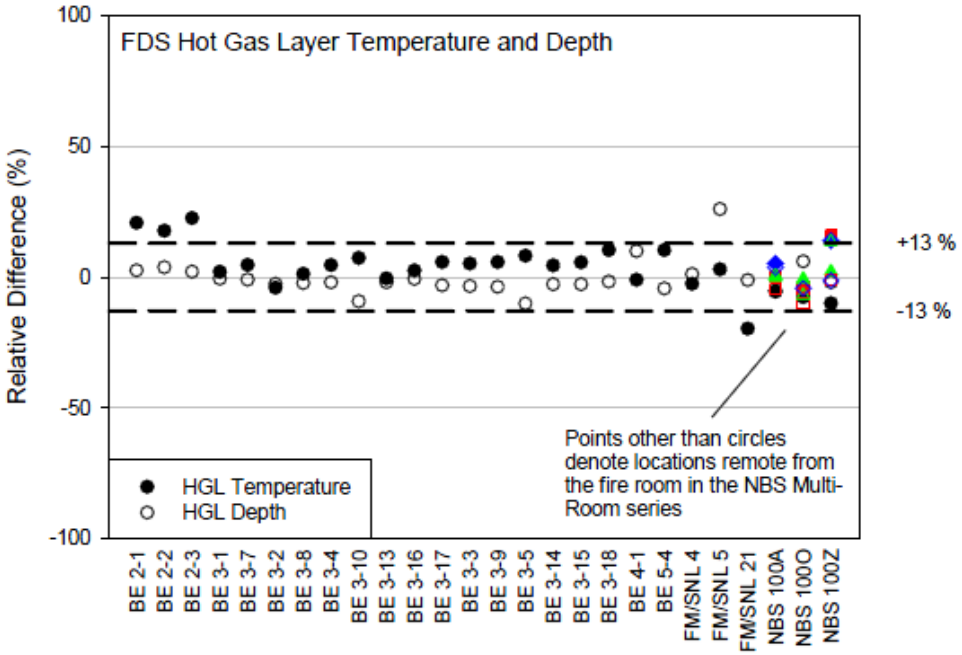

Figure 2-6: Summary of HGL calculation results from U.S. NRC validation study

A pair of multi-level, multi-compartment fire experiments were used by Floyd [37] in a validation study of FDS v2.0 in 2002. These experiments were conducted in a decommissioned nuclear power plant located in Germany [38]. However, the construction and compartment geometry of a nuclear power plant does not well-represent a residential structure. In addition, the validation study should not be considered a suitable evaluation of FDS v.5 because a pre-release version of FDS 2.0 was used. Significant changes have been implemented since FDS 2.0 that have altered the predictions calculated by the program. In addition, the arrangement and size of compartments in the nuclear plant are significantly different from that of a residential structure.

Numerous FDS validation studies have been carried out, but no studies evaluate the ability of the model to predict hot gas layer temperature and depth on the scale of a multi-level and multi-compartment residential structure. This study improves on the empirical

basis to determine how FDS can be used to simulate multi-level and multi-compartment residential structure fires for the future development of fire behavior training software.

3 Brief Description of FDS & Smokeview

The first version of the FDS was released in February of 2000 and written in Fortran 90. Prior to 2000, NIST was engaged in researching large outdoor oil fire plumes, which contributed significantly to the development of large eddy simulation for fire modeling and ultimately formed the foundation for FDS. More recently, FDS development has been more focused on solving practical problems in fire protection engineering, but is also used as a tool for researching fire dynamics and combustion. Currently, the major uses of the model are in performance based fire protection system design [39,40] and also in fire forensic scene reconstructions [10,11,12,13]. Since 2000, numerous improvements have been made and new features added, such as the multiple mixture fraction combustion model, and multiple mesh and parallel computation capabilities. This study was carried out using FDS version 5.4.2 (Subversion #4957) released Oct 19th, 2009.

Smokeview is a post-processing program developed using Fortran 90 and C and is used to visualize the time-varying fire phenomena as numerically output by FDS. Smokeview uses the 3D graphics library OpenGL to render graphics and the Graphics Library Utility Toolkit (GLUT) to provide a user interface. Smokeview visualizes smoke and other attributes of fire using traditional scientific methods such as displaying tracer (massless) particle flow, 2D or 3D animated color contours of gas flow data such as temperature and flow vectors showing flow direction and magnitude. Aside from visualizing fire phenomena, Smokeview is immensely valuable for visual inspection of physical obstructions (compartment/content geometry) when writing an FDS input file. Smokeview version 5.4.6 (svn # 4991) was used in this study.

FDS and Smokeview may be obtained from (http://fire.nist.gov/fds). Unless otherwise referenced, the majority of the information in Section 3.0 describing how FDS works is extracted from the user's manual and technical reference guide [1-2].

3.1 Hydrodynamic Model

In FDS, simulations can be completed using LES or DNS. This study was completed with LES. This section describes the hydrodynamic model used to compute fluid flow with LES.

The core algorithm of FDS is an explicit predictor-corrector scheme, second-order accurate in space and time. This means that discretization error is proportional to the square of the time step or cell size. The basic set of conservation equations solved by the hydrodynamic model in FDS as given in the FDS Technical Reference Guide [2] are presented below. The conservation of energy is incorporated into the conservation of mass:

Conservation of Mass:

$$\frac{\partial \rho}{\partial t} + \mathbf{u} \cdot \nabla \rho = -\rho \nabla \cdot \mathbf{u}$$

Conservation of Momentum:

$$\frac{\partial \mathbf{u}}{\partial t} + \mathbf{u} \times \omega + \nabla \mathcal{H} = \frac{1}{\rho}\left((\rho - \rho_0)\mathbf{g} + \mathbf{f}_b + \nabla \cdot \tau_{ij}\right)$$

Pressure Equation:

$$\nabla^2 \mathcal{H} = -\frac{\partial(\nabla \cdot \mathbf{u})}{\partial t} - \nabla \cdot \mathbf{F} \quad ; \quad \mathbf{F} = \mathbf{u} \times \omega - \frac{1}{\rho}\left((\rho - \rho_m)\mathbf{g} - \mathbf{f}_b - \nabla \cdot \tau_{ij}\right)$$

Conservation of Species:

$$\frac{\partial \rho Y_\alpha}{\partial t} + \mathbf{u} \cdot \nabla \rho Y_\alpha = -\rho Y_\alpha \nabla \cdot \mathbf{u} + \nabla \cdot \rho D_\alpha \nabla Y_\alpha + \dot{m}_\alpha'''$$

Equation of State:

$$\overline{p}_m(z,t) = \rho T \mathcal{R} \sum_\alpha Y_\alpha / W_\alpha$$

3.2 Combustion Model

In order to resolve combustion FDS uses a mixture fraction combustion model. The mixture fraction is a conserved scalar quantity defined as the ratio of the mass fraction of fuel and the mass fraction of undepleted oxygen in ambient air, as follows:

$$Z = \frac{sY_F - (Y_{O_2} - Y_{O_2}^{\infty})}{sY_F^I + Y_{O_2}^{\infty}} \quad ; \quad s = \frac{\nu_{O_2} W_{O_2}}{\nu_F W_F} \quad ; \quad \nu_F = 1$$

Practically speaking, the mixture fraction describes the amount of gaseous fuel within a grid cell with respect to the total gaseous mass contained in that cell. The mixture fraction inside a fuel-rich region is equal to one and equal to zero in a volume containing only ambient air. This model assumes that combustion is controlled by the rate of mixing and that the reaction occurs instantaneously, giving rise to the phrase "mixed is burned." As a result, once combustion has occurred within a grid cell, that cell will contain only combustion products and any remaining unburned fuel.

The default option in FDS assumes that combustion occurs in a single step reaction:

$$C_x H_y O_z N_a M_b + \nu_{O_2} O_2 \rightarrow \nu_{CO_2} CO_2 + \nu_{H_2O} H_2O + \nu_{CO} CO + \nu_S S + \nu_{N_2} N_2 + \nu_M M$$

It should be noted that in the above equation the S on the right hand side represents the soot formed during the reaction of the fuel and oxygen. This single step reaction becomes less accurate in the prediction of combustion products if the compartment fire becomes under ventilated. The single step reaction assumes that for each fuel molecule a fixed amount of CO_2, H_2O, and CO, are produced and persist in the plume with no further reaction. To address under-ventilation with greater accuracy, a two step-reaction is available in FDS. If sufficient oxygen is available, CO2 is produced in the second step. This two-step reaction calculation is more computationally expensive, causing a longer simulation run time when invoked. As the prediction of combustion products and species transport is not a focus of this study, the single step reaction is a more appropriate assumption for this study. An assessment of the change in simulation results of the two-step reaction compared with the single-step reaction is not within the scope of this study. However, the two-step reaction would be a good feature to explore in future work as the transport of toxic species through residential scale structures is of significant interest.

3.3 Rectilinear Calculation Mesh

3.3.1 Obstruction Geometry

FDS performs calculations of the governing equations on a rectilinear grid. Therefore the dimensions of physical obstructions (walls, wood pallets, etc.) in the fire model must conform to the size of the underlying grid. Obstructions smaller than the spatial resolution of the mesh are either stretched to fit the mesh, or rejected and displayed as a surface with zero thickness. In practice this is not always possible, as some rooms can be non-rectangular, have sloped ceilings, etc. Objects not conforming to the rectilinear grid can be represented by breaking the surfaces into numerous smaller rectangular obstructions. The result is a "sawtooth" surface. An optional feature in FDS that lessens the effect of "sawtooth" surfaces by preventing vorticity from being generated at the sharp corners. This smoothes out the flow field in the region of the surface by preventing additional drag due to the multiple sharp corners. This feature should not be used where the boundary layer is important. It was not necessary to use this feature in the simulations in this study, because all surfaces could be confidently assumed to conform to the specified rectilinear mesh.

3.3.2 Mesh Sizing

The FDS User's guide recommends that optimal grid size be chosen using a ratio of the characteristic fire diameter and cell size $D^*/\delta x$, where

$$D^* = \left(\frac{\dot{Q}}{\rho_\infty c_p T_\infty \sqrt{g}}\right)^{\frac{2}{5}}$$

A mesh sensitivity study conducted by the U.S.NRC [36] found that $D^*/\delta x$ values from 4 (coarse mesh) to 16 (fine mesh) adequately resolved plume dynamics as well as other geometric characteristics of the model. The model developers recommend performing an analysis of grid size to determine the resolution necessary for a given simulation.

3.3.3 Multiple Meshes

"Multiple meshes" implies that instead of a singular rectilinear mesh of a constant spatial resolution, the computational domain in a simulation can be split into multiple separate computational meshes of different (or uniform) spatial resolution. The benefits of using multiple meshes to define the computational domain are two-fold. First, meshes with a fine spatial resolution can be prescribed to regions of increased resolution requirements (e.g., in a volume containing a flame sheet or when more precise ventilation adjustment is required). Second, and of greater significance to this study, is to take advantage of the relatively recent development of parallel processing of FDS simulations. Computation time increases exponentially as the total number of cells in a computational mesh increases linearly. In order to determine cell size and how many meshes were necessary to simulate fire behavior in the full-scale structure without significant detriment to the fidelity or accuracy of FDS predictions, a grid cell sensitivity analysis was performed. This analysis is discussed in Section 5.1.

3.4 Model Inputs and Outputs

The input parameters required to run an FDS simulation as well as desired output quantities are contained in a single text input file (*.fds format). The type of information contained in FDS input files describes the computational mesh(es), initial and boundary conditions (temperature, wind), thermo-physical material properties (thermal conductivity, density), obstruction (walls, furniture) geometry, chemical reaction parameters, control logic (e.g., a set time or temperature that causes a window to open) and an abundance of numerical and visual output quantities.

Determining appropriate material input parameters is still a significant challenge to the user. Current research efforts are being focused into developing a standard guide that provides the user with methods for determining appropriate material input parameters [15]. Regarding the chemical reaction (combustion of fuel), it is necessary to specify the stoichiometric coefficient of the ideal reaction, soot yield, heat of combustion and the radiative fraction of energy release. Chemical reaction parameters and thermo-physical properties such as density, specific heat, thermal conductivity, and emissivity can be found in a number of handbook references, material submittal sheets from the manufacturer, or by conducting bench-scale experiments.

Numerical results for user specified outputs are written to comma-separated-value files. These outputs can be in Smokeview or analyzed with commercial or open-source data analysis software. Regarding output quantities, the FDS user's guide phrases it best [1]:

"Much like in an actual experiment, the user must decide before the calculation begins what information to save. There is no way to recover information after the calculation is over if it was not requested at the start."

3.5 Suppression Model

Currently, FDS simulates fire suppression with water by the use of an empirically derived algorithm based on sprinkler suppression research by Yu, et al. [41]. The research was conducted for two different commodities in various different rack storage configurations, with suppressing water applied at the top of the storage array. From this research, FDS developers have implemented the following algorithm to simulate sprinkler suppression:

$$\dot{m}''_f(t) = \dot{m}''_{f,0}(t)e^{-\int k(t)dt}$$

Where $\dot{m}''_f(t)$ represents the burning rate of the fuel as a function of time, $\dot{m}''_{f,0}(t)$ is the burning rate of fuel immediately prior to sprinkler activation and $k(t)$ is the function:

$$k(t) = \text{E\_COEFFICIENT}\ m''_w(t)$$

Above, m''_w represents the local water mass per unit area, and E_COEFFICIENT. This algorithm applies for cases in FDS where a HRR is prescribed to a surface, i.e. the surface is assigned a fuel flux that corresponds to this HRR. The algorithm works by exponentially reducing the burning rate as a function of time, water mass per unit area m''_w, and the E_COEFFICIENT. The parameter E_COEFFICIENT must be obtained experimentally, and it is expressed in units of $m^2/kg/s$ [1].

This built-in suppression algorithm is not appropriate for use in suppressing the simulated fire in this study. The scenario of fire suppression in this study (hose stream suppression) is significantly different than the intended use of the algorithm. A separate approach was taken to simulate suppression in that manually manipulated the HRR based on analyses of previous suppression research for a highly similar fuel configuration and video analysis. More details of the approach to simulating suppression are discussed in Section 5.2.4. Currently, work is ongoing at NIST to develop a model of hose stream water spray impact on fire generated conditions, and to implement the hose stream model in FDS [42]

3.6 Hot Gas Layer Reduction Method

Interest in the average hot gas layer temperature and depth originated with the development of zone models. Zone models are fire models that divide a compartment into two-spatially homogenous control volumes, a hot upper layer and a cool lower layer, and calculate a mass and energy balance between the control volumes. Therefore, zone models must calculate HGL temperature and depth by their very nature. Because FDS is a field model, and not a zone model, FDS does not calculate HGL temperature and depth by default. Nevertheless, due to the popularity of the HGL calculations in practice, FDS provides the option to calculate and output HGL temperature and depth. In order to determine HGL temperature and depth, FDS must perform an additional calculation using values obtained from numerical temperature predictions made for each "cell." To do this FDS utilizes the “hot gas layer reduction method." This method was originally developed to provide estimates of average layer temperature and depth from experimental data describing vertical temperature profiles. The following is an excerpt from the FDS User’s Guide [1] describing the hot gas layer reduction method:

"Consider a continuous function T(z) defining temperature T as a function of height above the floor z, where z = 0 is the floor and z = H is the ceiling. Define T_u as the upper layer temperature, T_l as the lower layer temperature, and z_{int} as the interface height. Compute the quantities:

$$(H - z_{int})\, T_u + z_{int}\, T_l = \int_0^H T(z)\, dz \;=\; I_1$$

$$(H - z_{int})\, \frac{1}{T_u} + z_{int}\, \frac{1}{T_l} = \int_0^H \frac{1}{T(z)}\, dz \;=\; I_2$$

Solve for z_{int}:

$$z_{int} = \frac{T_l(I_1 I_2 - H^2)}{I_1 + I_2 T_l^2 - 2 T_l H}$$

Let T_l be the temperature in the lowest mesh cell and, using Simpson's Rule[2], perform the numerical integration of I_1 and I_2. T_u is defined as the average upper layer temperature via:

$$(H - z_{int})\, T_u = \int_{z_{int}}^H T(z)\, dz$$

Unlike the "N% rule" [43], the method pre-dating the hot gas layer reduction method, predictions of interface height are not confined to thermocouple locations. The integral form of the hot gas layer reduction method calculates the interface height by locating the inflection point in the vertical temperature profile of the compartment. Therefore, the prediction is non-discrete and continuous.

A propagation of error analysis of the hot gas layer temperature and depth, calculated from experimental values, was carried out in [44]. The algebra in the uncertainty analysis is complicated, as error is propagated through the many terms that involve I_1 and I_2 and that present themselves in the determination of T_u and z_{int}. The report includes uncertainties in experimental hot gas layer temperature and depth for six test series. It was found that the "largest uncertainties were associated with experiments that had relatively coarse instrument density", where thermocouple instrument density is: $\left(\frac{\#\ thermocouples\ in\ an\ array}{floor-to-ceiling\ height}\right)$.

[2] In the analysis of the FDS source code it was found that the midpoint rule is actually used for the integration, however the result is the same for HGL calculations

One of the six test series includes a single-floor, multi-compartment experimental structure with the same thermocouple density used for the laboratory and field experiments in this study. The uncertainties reported for hot gas layer temperature and depth are 10% and 13%, respectively. The remaining five series had significantly more coarse thermocouple densities. It is therefore assumed that the experimental uncertainties for hot gas layer temperature and depth are the same for the laboratory and field experiments

4 Description of Experiments

Two sets of experiments are described in this section. Section 4.1 prefaces the descriptions of the experiments by providing measurement uncertainties common to both experimental series. Section 4.2 describes a series of full-scale compartment fire experiments conducted in the Large Fire Laboratory at NIST. Section 4.3 describes a series of residential-scale field experiments conducted by five partner organizations (NIST, IAFF, WPI, IAFC, CPSE) called the "Multiphase Study on Fire Fighter Safety and the Deployment of Resources" [45]. Section 4.2 serves to preface Section 4.3 by providing background for the design of the fuel package used in the field experiments. Section 4.4 presents experimental results from the field experiments series that describe the thermal environment inside the residential-scale structure and the effects that fire fighter actions have on the thermal environment. Additional detail regarding the selection of two fire fighter actions (front door ventilation and suppression) for analysis is provided in Section 4.4.5. In Section 4.5, previous research of numerous environmental variables that affect fire growth is discussed. This discussion provides insight into the variation of the burning behavior of the fuel in the field experiments.

4.1 Measurement Uncertainty

The measurements taken in the two series of experiments that follow Section 4.1 have unique components of uncertainty that must be evaluated in order to determine the fidelity of the data. These components of uncertainty can be grouped into two categories: Type A uncertainty and Type B uncertainty [46]. Type A uncertainties are those that are evaluated by statistical methods, such as calculating the standard deviation of the mean of a set of measurements. Type B uncertainties are based on scientific judgment using all available and relevant information. Using relevant information, the upper and lower limits of the expected value are estimated so that the probability that the measurand falls within these limits is "for all practical purposes, 100%" [46]. After all the component uncertainties of a measurement have been identified and evaluated it is necessary to use them to compute the combined standard uncertainty. The combined standard uncertainty is computed using the law of propagation of uncertainty (A.K.A. the “root sum of squares”). Although this expresses the uncertainty of a given measurement, it is more useful in fire model validation to define an interval for which the measurand will fall within a certain level of statistical confidence. This is known as the expanded uncertainty. The current international practice is to multiply the combined standard uncertainty by a factor of two (k=2), giving a confidence of 95%.

The total expanded uncertainty of the NIST oxygen-consumption calorimeter HRR measurements was estimated at ± 11 %, based on a propagation of uncertainty analysis by Bryant [47]. This estimation is based on the calorimetry system alone. It does not account for the uncertainty that exists due to the experimental configuration. There is a delay time for the combustion gases to reach the hood and calorimetry instrumentation.

Components of length measurement error were estimated as Type B uncertainties. Length measurements were taken using a steel measuring tape with a resolution of 0.5mm (0.02in). On the compartment scale, poured concrete construction resulted in uneven surfaces and unlevel walls and floors which made it difficult to lay the tape measure flat and straight. This yields an estimated uncertainty of ± 0.6%. Exterior building measurements were additionally affected by the uneven surface and grade of the paved surface around the structure, yielding an uncertainty estimate of approximately ± 0.8%. Total expanded length measurement uncertainties are therefore ± 1.2% and ± 1.6%, respectively.

Previous work done at NIST has shown that the uncertainty of the environment surrounding thermocouples in a full scale fire experiment has a significantly greater uncertainty than the uncertainty inherent with thermocouple design [48,49]. Furthermore, while a vertical thermocouple array gives a good approximation of the temperature gradient with respect to height, temperatures cannot be expected to be uniform across a plane at any height because of the dynamic environment in a compartment fire. Inaccuracies of thermocouple measurements in a fire environment can be caused by:

- Radiative heating or cooling of the thermocouple bead
- Soot deposition on the thermocouple bead that changes its mass, emissivity and thermal conductivity
- Heat conduction along thermocouple wires
- Flow velocity over the thermocouple bead

To reduce the effects of radiative heat transfer, thermocouples with smaller diameter beads were chosen. This is particularly important for thermocouples below the interface because the radiative transfer between the surrounding compartment surfaces will be significantly less uniform than if the thermocouple were in the hot gas layer. It is suggested in [49] that it may be possible to correct for radiative transfer given enough sufficient knowledge about thermocouple properties and the environment, however measurements of local velocity and the radiative environment were not taken. A report by NIST quantifies the components of uncertainty for compartment fire thermocouple measurements and suggests a total expanded uncertainty of -20% to +6% [50], where the lower bound represents the uncertainty of thermocouples in the lower layer. It is assumed that the uncertainty in the layer depth calculation is not significantly impacted by erroneously high lower layer TC readings, since the layer calculation seeks locations of significant temperature change, rather than, for example, the absolute value of that difference. Neglecting uncertainty in the lower layer temperature measurement reduces the total uncertainty [44] in the calculation.

Moisture content was measured using an electrical resistance-type moisture meter with a moisture measurement range of 5% to 40% [51] and an accuracy of <0.5% of the measured value between 5% and 12% moisture content. Mass measurements were made prior to each test with an industrial bench scale having a range of 0-100kg, a resolution of 0.1kg and an uncertainty of ± 0.1 kg.

All timing staff were equipped with the same model of digital stopwatch with a resolution of 0.01 seconds and an uncertainty of ± 3 seconds per 24 hours; the uncertainty of the timing mechanism in the stopwatches is small enough over the duration of an experiment that it can be neglected. A test series described in the NIST Recommended Practice Guide for Stopwatch and Timer Calibrations [52] assessed the reaction times of test participants for traceable audio and visuals time signals. Because of the lack of knowledge regarding the mean bias of the timers, a rectangular distribution was assumed and the worst case reaction time bias of 120 ms was used, giving a standard deviation of ±69 ms. The standard deviation of the reaction time was assumed to be the worst case of ±230 ms. The magnitude of the delay in the refreshing of the stopwatch display was estimated to be 5ms. Using k=2, the estimated total expanded uncertainty of task times measured in these experiments is ±0.5s.

4.2 Laboratory Experiments

The National Institute of Standards and Technology conducted several large-scale fire tests to quantify the heat release rate (HRR) of burning wooden pallets in a free-burning condition and in a multi-room enclosure (two rooms plus a corridor) . The purpose of these experiments was to characterize the burning behavior of wooden pallets as a function of:

- The number of pallets in a stacked configuration
- Compartmentalization
- Changes in ventilation
- Effect of excelsior loading on fire growth rate

In addition to the heat release rate, additional measurements were taken within the enclosure to determine the thermal conditions during the fires. Experimental data from this test series was used to design a repeatable, NFPA 1403 [9] compliant fuel package to be used in the field experiments described in Section 4.3[3]. A single set of test data from the multi-room enclosure experiments corresponding to the final fuel configuration used in the field experiments is considered in this study. This single set of data is used for the grid cell sensitivity analysis discussed in Section 5.1 and for the simulation of the field experiments discussed in Sections 5.2 and 6.

[3] NFPA 1403 is the Standard on Live Fire Training Evolutions and requires that fuel materials shall have known burning characteristics and that the fuel load shall be limited to avoid conditions that could cause an uncontrolled flashover or backdraft.

4.2.1 Burn Compartment

Two identical compartments measuring 3.66 m (12ft) x 4.88 m (16ft) were connected by a hallway measuring 3.83 m (12.6 ft) x 1.22 m (4 ft). At one end of the hallway, an open doorway measuring 0.91 m (3ft) x 1.92 m (6.3ft) connected the hallway to the burn compartment. The ceiling height throughout the structure was 2.44 m (8ft). The other end of the hall opened directly into the second compartment. In the burn compartment the single window measuring 1.52 m (5ft) x 1.52 m was sealed with non-combustible board and opened only to extinguish the remaining burning material at the end of each test. In the second compartment an open doorway connected the compartment to the rest of the test laboratory. This doorway allowed combustion products to flow into the main collection hood for measurement of heat release rate. The structure was constructed of two layers of gypsum wallboard over 20-gauge steel studs. The floor of the structure was lined with two layers of gypsum wallboard directly over the concrete floor of the test facility. In the burn compartment, an additional lining of cement board was placed over the gypsum walls and ceiling surfaces in the corner of the fire source to minimize fire damage to the structure after multiple fire experiments. Figure 4-1 shows a schematic view of the multi-room enclosure and the location of the thermocouple array described in Section 4.2.3.

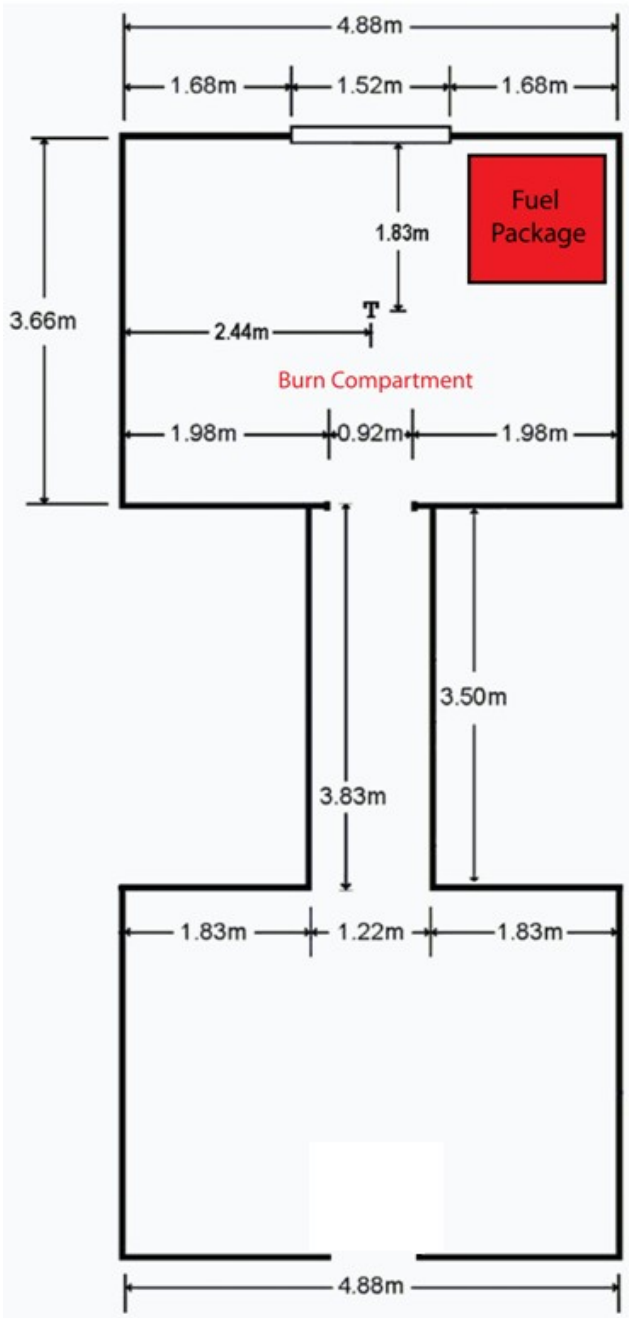

Figure 4-1: Multi-room enclosure[4] used in laboratory experiments. The "T" designates the location of the vertical thermocouple array.

[4] Multi-room enclosure schematic view modified from [76].

4.2.2 Fuel Package

The fuel source for the tests was used hardwood pallets constructed from several lengths of hardwood boards nominally 83 mm (3.3in) wide by 12.7 mm (0.5in) thick. Lengths of the individual boards ranged from nominally 1 m (3.3ft) to 1.3 m (4.3ft). The finished size of a single pallet was approximately 1 m (3.3ft) by 1.3 m (4.3ft) by 0.11 m (0.4ft). Figure 4-2 shows the fuel source used in this study, including four stacked pallets (total weight of 71.1kg (156.7lb)) and an ignition source. The ignition source consisted of wood excelsior (total weight of 0.8kg (1.8lb)) placed within the pallets and two cardboard matchbooks with 20 matches. The matchbooks were wrapped with Ni-Chrome resistance heating wire and remotely energized to cause ignition. This device will be referred to as an electric match in this report.

Figure 4-2: Fuel source used in laboratory experiments

4.2.3 Experimental Measurements and Results

Heat release rate (HRR) measurements were recorded using the 3 m x 3 m oxygen depletion calorimeter at the NIST Large Fire Research Laboratory. It is capable of measuring HRRs in the range of 0.03MW to 3.0MW with brief peaks of up to 5MW [47]. The HRR measurement was based on the oxygen consumption calorimetry principle first proposed by Thornton [53] who showed that for a large number of organic liquids and gasses, a relatively constant net amount of heat energy is released per atom of oxygen reacted in complete combustion. Huggett [54] rediscovered Thornton's study and further developed the concept to show that the same relationship was obeyed for materials used in buildings. The measurement of exhaust flow velocity and gas volume fractions (O2, CO2 and CO) were used to determine the HRR based on the formulation given by Parker [55] and Janssens [56].

Prior to experimentation, ten of the wooden pallets used in the fuel packages were randomly selected for measurement. The average pallet moisture content was 10.2% ± 2.2%. Statistical analysis of the pallet data resulted in an average fuel package mass of 72.5kg ± 13.9kg.

Gas temperature measurements were made in the burn compartment using 24-gauge bare-bead chromel-alumel (type K) thermocouples positioned in a vertical array. Eight thermocouples were located at the center of the compartment, vertically spaced 0.3 m (1ft) apart, measured from the ceiling. Moisture content was measured for each pallet using an electrical resistance-type moisture meter. All measurements registered below the operational range of the meter (<5% by wt.).

Other measurements in the experiments were: additional gas temperature locations, heat flux and gas concentration (CO, CO_2, O_2). Descriptions of these measurements can be found in [45]. Figure 4-3 shows the time-history of the HRR that corresponds to the burning of the fuel loading shown in Figure 4-2. The peak heat release rate of 1960 ± 215kW occurs at approximately 238 seconds. Figure 4-4 shows that a resultant peak temperature of 820 ± 123 °C was recorded at 0.03m below the ceiling approximately 313 seconds after ignition.

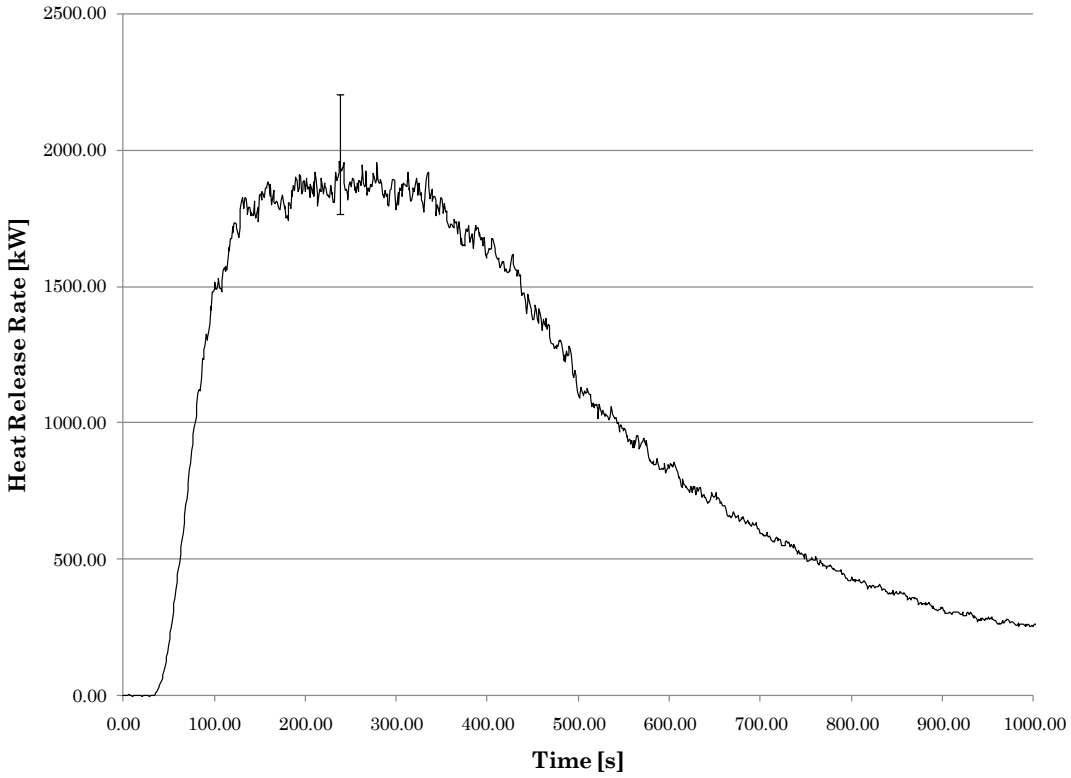

Figure 4-3: Heat release rate versus time for a 4-pallet fire in the multi-room enclosure

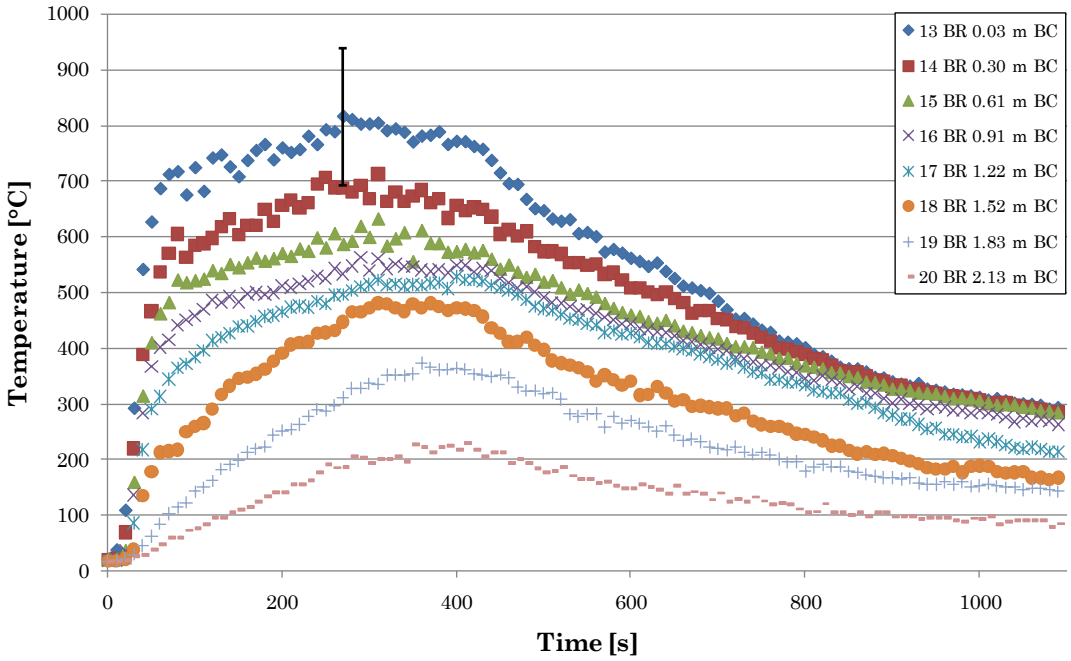

Figure 4-4: Temperature versus time for the vertical thermocouple array located in the center of the burn compartment

4.3 Field Experiments

This section describes a series of residential-scale fire experiments conducted in the field for the Multi-Phase Study on Firefighter Safety and the Deployment of Resources [45]. A two-story burn facility representing a low hazard[5] residential structure was designed and built at the Montgomery County Public Safety Training Academy in Rockville, MD. This study was involved in the design and construction of the burn facility as well as the design and implementation of the instrumentation plan.

The field experiments were split into two phases. In the first phase, fire fighters from Montgomery County, MD and Fairfax County, VA fire departments performed a simulated first alarm response to a "confirmed fire in a bedroom in the first floor rear of the structure." The "confirmed fire" consisted of pallets and excelsior designed as part the laboratory experiments explained in Section 4.2.2. Arrival times of the first and subsequent fire apparatus were systematically varied and crew size was incrementally varied from two- to five-person staffing. Each deployment configuration performed a series of twenty-two timed fire fighter actions, while the thermal and toxic environment inside the structure was measured. In total, 24 tests were conducted. The various deployments configuration resulted in a distribution of fire fighter action start and completion times. The results for all fire fighter action times and discussion of the causes of the distribution of action times are included in [45]. Two of these 22 actions, front door opening and bedroom window ventilation, are chosen for inputs for ventilation times in the FDS simulations. Thermocouple data from the matching phase one tests are used for comparison with the thermal conditions predicted by FDS.

The second phase of the experiments used a different fuel package. Simulation of the thermal conditions inside the burn facility using the second fuel package is not included in this study.

[5] A low hazard occupancy is defined in the NFPA Fire Protection Handbook as one, two, or three family dwellings and some small businesses 69].

4.3.1 Design of Structure

The burn facility was comprised of two 186 m^2 (2,000 ft^2) floors totaling 372 m^2 (4,000 ft^2). An exterior view of the A-B corner of the burn facility is shown in Figure 4-5. The structure was constructed as a duplex with a common stairwell and sliding partition walls that divided the structure into halves. Dividing the facility permitted one half of the building to cool down and dry-out after fire suppression, while the other side was set-up and used for testing. This enabled multiple tests daily.

Figure 4-5: View of A-B corner of the burn facility

The placement of the sliding partition walls created a floor plan representative of a two-story, 186 m^2 (2,000 ft^2) single family residence on each side of the burn facility. Note that the structure does not have a basement and includes no exposures (e.g., nearby buildings or hazards). The overall dimensions are consistent with the general specifications of a typical residential structure that many fire departments respond to on a regular basis, as described in NFPA Standard 1710 . Further details about typical single family home designs are not provided in the standard. Therefore, a floor plan representative of a typical single family home was created by the project team and used in the experiments. Details and floor plan dimensions are shown in Figure 4-6. Note that the burn compartment is identical in size to the laboratory experiments.

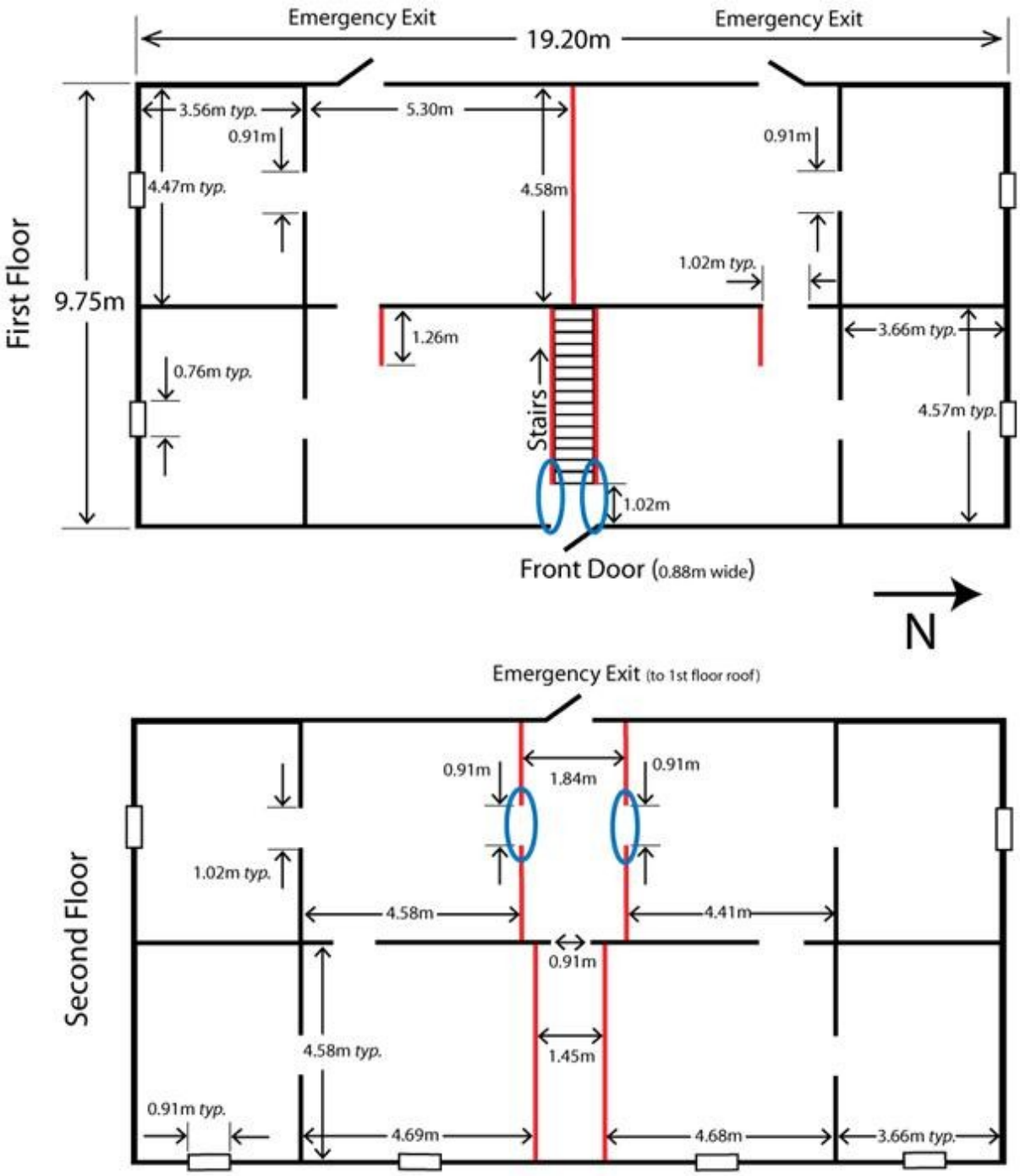

Figure 4-6: Schematic view of the burn facility with dimensions. Locations of sliding walls circled in blue

The black lines in Figure 4-6 indicate load-bearing reinforced concrete walls and red lines indicate the gypsum over steel stud partition walls. The areas circled in blue are the locations of the sliding partition walls. The ceiling height was 2.4 m (94 in) throughout the entire structure. Figure 4-7 shows an example test configuration, the live fire test location corresponding to the right side of the structure. The shaded area on the left is designed to represent the area sealed off and not involved in the test. Figure 4-7 also shows the location of the fire source and the naming convention for the windows on the first and second floors.

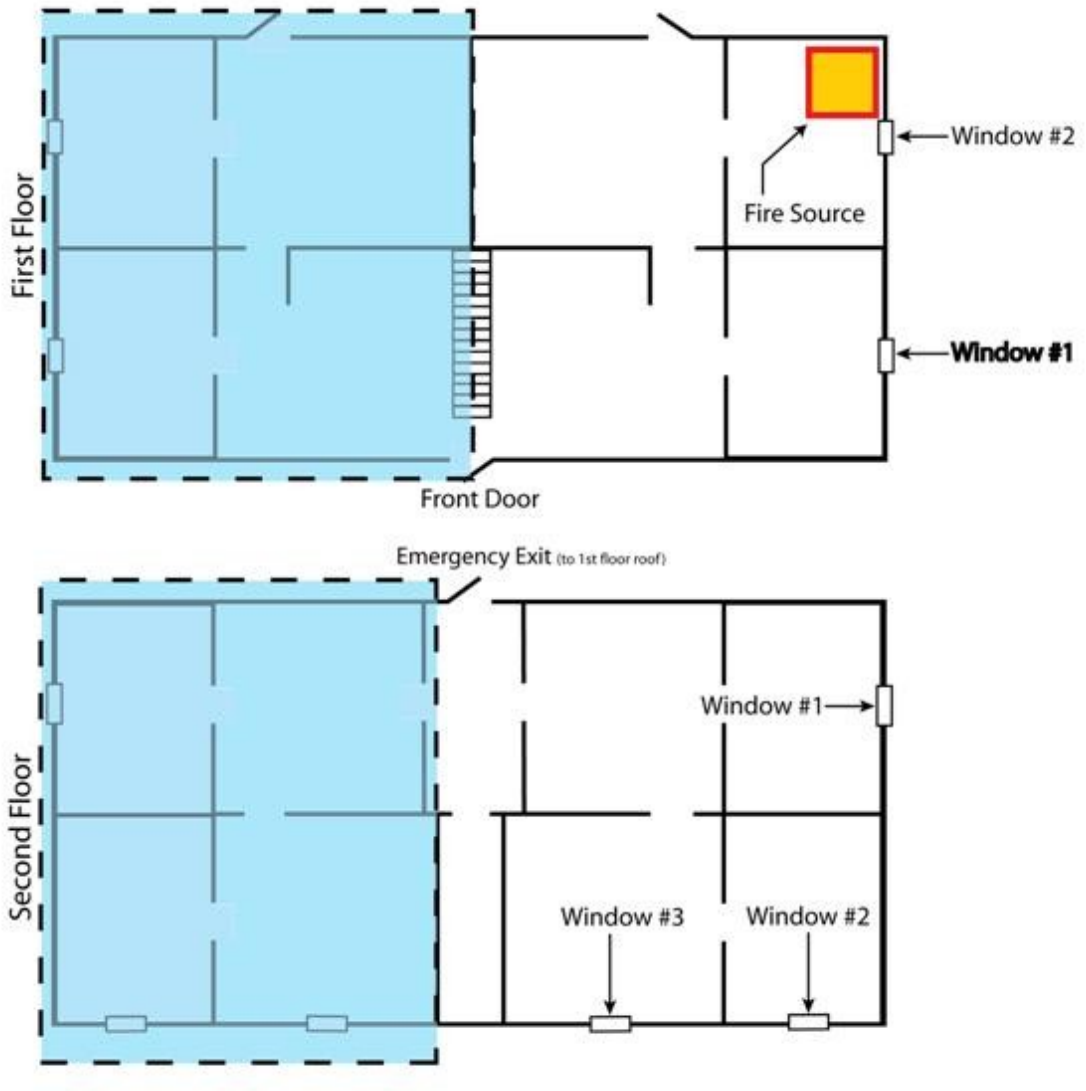

Figure 4-7: Schematic view of floor plan with naming scheme for windows and location of fire source. Area shaded in blue is "sealed."

The concrete walls original to the burn facility were 8 in (204 mm) thick steel reinforced poured concrete and the floors on the first level and second levels were 4 in (102 mm) thick poured concrete. The support structure for the second floor and the roof consisted of corrugated metal pan welded to open web steel joists. The dimensions of the joists are shown in Figure 4-8. The ceiling was constructed from ½ in. (13 mm) thick cement board fastened to the bottom chord of the steel joists. Partition walls were constructed from 5/8 in. (17 mm) thick gypsum panels attached to 20 gauge steel studs fastened to steel track, spaced 16 in. (407 mm) on center.

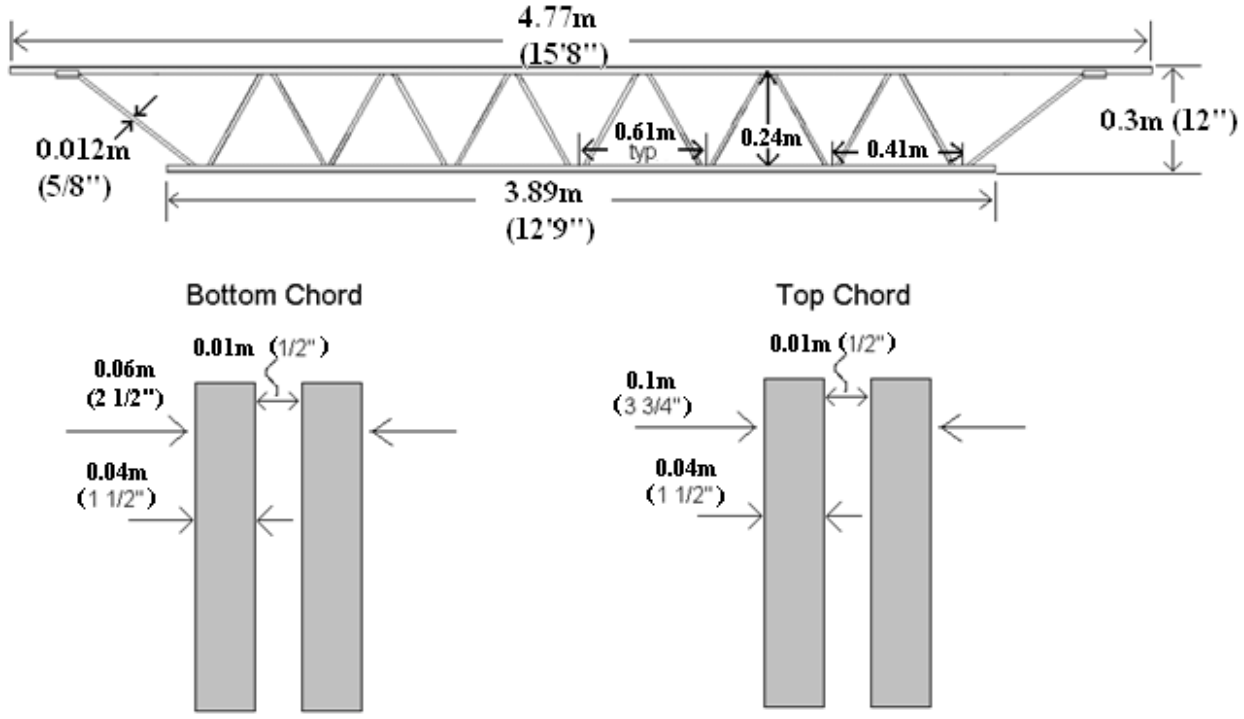

Figure 4-8: Structural steel dimensions

Additional construction was implemented in the burn compartments to address thermal loading and hose stream impingement concerns. Spray-on fireproofing was applied to the steel joists prior to fastening the ceiling, as shown in Figure 4-9. The ceilings were constructed with three layers of ½ in. (13 mm) cement board, as opposed to one layer construction in the rest of the building. Each layer was fastened in a different direction so that seams of adjacent layers ran orthogonally, to minimize leakage. The burn compartment walls were constructed from a single layer of ½ in. (13 mm) cement board over a single layer of 5/8 in. (16 mm) gypsum board, attached to 7/8 in. (22 mm) offset metal furring strips. After construction of the ceiling was complete, a dry-standpipe deluge system was installed with one head in each burn compartment to provide emergency suppression. During an experiment, a 2.5 in (104 mm) ball valve fitting was attached and charged from a nearby hydrant. Figure 4-10 shows the additional construction implemented in the burn compartment as well as the deluge sprinkler head.

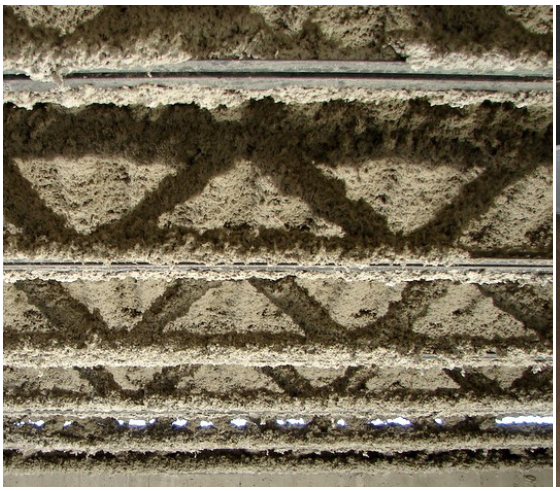

Figure 4-9: Fireproofing added to structural steel

Figure 4-10: Additional construction of burn compartment walls and ceiling and deluge sprinkler head.

Exterior doors, and shutters designed to represent windows, were of non-combustible construction. "Windows" were fabricated from 0.25 in. (6 mm) thick steel plate and the exterior doors were of prefabricated hollow-core steel design. The "windows" on the first floor were 30 in. (0.76 m) width x 36 in. (0.91 m) height and 36 in. (0.91 m) width x 40 in. (1.02 m) height on the second floor. Exterior doors were 35.8 in. (0.88 m) width x 80.5 in. (2.03 m) height. There were no doors attached to the doorways inside the structure. Figure 4-11 shows the construction of the "windows." Figure 4-12 is a picture of the interior of the burn facility taken just outside the burn compartment, showing the construction of the ceiling, interior doorway construction, gypsum wing wall and the joint compound used to seal seams in the ceiling and walls.

Figure 4-11: Window & Latch Construction

Figure 4-12: Interior view of Burn Facility

4.3.2 Fuel Package

The fuel source for the field experiments was recreated from the laboratory experiments described in Section 4.2. Figure 4-13 shows the fuel source, including four stacked pallets with excelsior. The fuel source consisted of used hardwood pallets constructed from several lengths of hardwood boards nominally 83 mm wide by 12.7 mm thick. Lengths of the individual boards ranged from nominally 1 m to 1.3 m. The finished size of a single pallet was approximately 1 m by 1.3 m by 0.11 m. The average mass of the stacked pallets was 72.5kg ± 13.9kg. Moisture content readings were taken in three different locations on each pallet for eight pallets. The average pallet moisture content was 7.8% ± 1%. As in the laboratory experiments, the fuel source was ignited remotely by electric match.

Figure 4-13: Fuel package researched in laboratory experiments

4.3.3 Time to Task Scenario

This section contains a synopsis of the "time to task" scenario conducted in phase one of the Multiphase Study on Fire Fighter Safety and the Deployment of Resources. Fire crews from Montgomery County, MD and Fairfax County, VA were deployed to the burn facility simulating a "first alarm" response. Specifically, the scenario was dispatched as a "confirmed fire in a bedroom in the first floor rear of the structure." The response included three engines, one ladder truck and one battalion chief. The elapsed time between the first due and subsequent fire apparatus were systematically varied between "close" and "far" scene arrival staggers. Crew size was incrementally varied from two- to five-person staffing between tests. Each first alarm deployment configuration was repeated three times. This resulted in 24 total tests. Table 4 shows the experimental matrix.

Apparatus Staffing Level	Scene Arrival Stagger	
2 Persons	Close	X3
2 Persons	Far	
3 Persons	Close	
3 Persons	Far	
4 Persons	Close	
4 Persons	Far	
5 Persons	Close	Total = 24 experiments
5 Persons	Far	

Table 4: Matrix for phase one experiments of the Mutliphase Study on Fire Fighter Safety and the Deployment of Resources

The following list describes the response time assumptions used in each test:

- Fire ignition = time zero
- 60 seconds for recognition (detection of fire) and call to 9-1-1
- 60 seconds for call processing/dispatch
- 60 seconds for turnout[6]
- **Close Stagger** = 240 second travel time FIRST engine with 60 second ladder-truck lag and 90 second lag for each subsequent engine
    - Ladder truck arrives at 300 seconds from notification
    - Second engine at 330 seconds from notification
    - Third engine at 420 seconds from notification
- **Far Stagger** = 240 second travel time FIRST engine with 120 second ladder-truck lag and 150 second lag for each subsequent engine
    - Truck arrives at 360 seconds from notification
    - Second engine arrives at 390 seconds minutes from notification
    - Third engine arrives at 540 seconds minutes from notification.

[6] . After the experiments were complete, the NFPA 1710® technical committee released a new edition of the standard that prescribes 80 seconds for turnout time.

Fire fighters performed a series of 22 fire fighter actions[7] after arriving on the fireground. These actions ranged from tagging the water supply hydrant (first action) to implementing positive pressure ventilation (final action). Ten observers/timers were used to record the start and the end time for each fire fighter action as they were performed. Timers were provided clipboards, stop watches, and data recording sheets. Career fire fighters were used as timers to ensure an understanding of tasks to be observed. Figure 4-14 shows a member of the timing staff shadowing a fire fighter participant and recording action start/ stop times.

Figure 4-14: Trained timing staff recording fire fighter action times

Significantly more detail describing the 22 fire fighter actions performed on the fireground, the timing criteria for these actions, data control measures and the logistical coordination of the experiments is provided in [45].

[7] The technical experts involved in the Multiphase Study on Fire Fighter Safety and the Deployment of Resources determined that there are 22 critical actions that must be performed at the typical two-floor, single family residential structure fire in order to fully mitigate all hazards.

4.3.4 Measurement Equipment

After construction, instrumentation was installed throughout the facility to measure the thermal environment. The instrumentation plan was designed to measure gas temperature, video, and time during the experiments. It should be noted that heat release rate was not recorded in the field experiments. It is not possible to implement structural scale calorimetry in the field. Data were recorded at 1-second intervals on a computer-based data acquisition system. Non-combustible furniture props made of steel and gypsum panels were included to simulate contents that exist in a typical residence. In two locations, the furniture was utilized to provide measurement equipment protection from physical contact with fire fighters. A schematic plan view of the instrumentation and furniture prop arrangement is shown in Figure 4-15. Measurements corresponding to dimensions in Figure 4-15 are provided in Table 5.

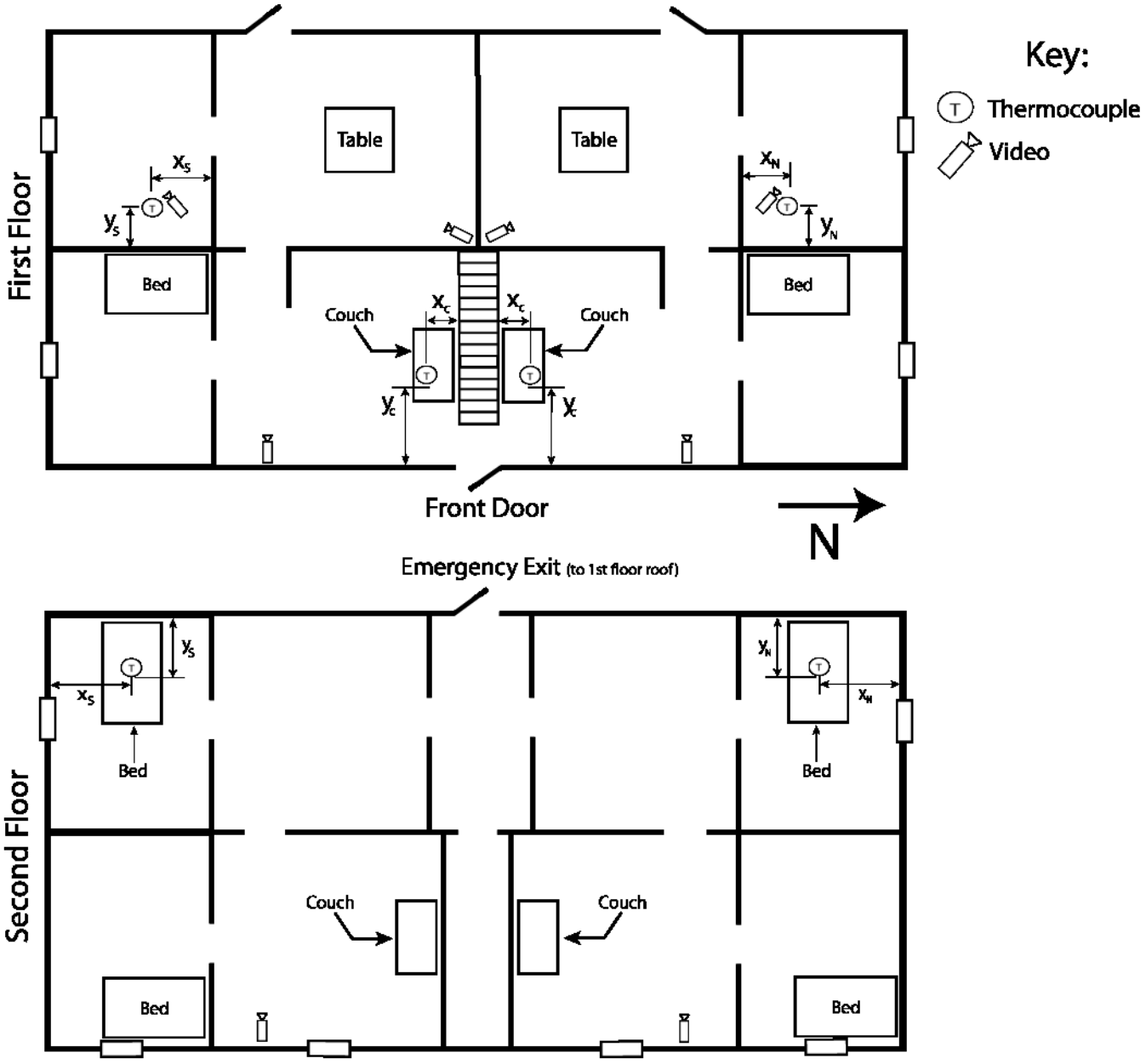

Figure 4-15: Instrumentation & furniture prop location layout

Floor	X_S [m]	Y_S [m]	Z_S [m]	X_N [m]	Y_N [m]	Z_N [m]	X_C [m]	Y_C [m]	Z_C [m]
1	0.76	0.51	0.3, 0.61, 0.91, 1.22, 1.52, 1.83, 2.13	0.76	0.51	0.3, 0.61, 0.91, 1.22, 1.52, 1.83, 2.13	0.8	2.0	0.91, 1.52, 2.41
2	1.83	0.91	0.3, 0.61, 0.91, 1.22, 1.52, 1.83, 2.13, 2.41	1.83	0.91	0.3, 0.61, 0.91, 1.22, 1.52, 1.83, 2.13, 2.41			

Table 5: Detailed thermocouple locations by floor

Measurements taken prior to the compartment fire experiments were length, wood moisture content, individual pallet mass and excelsior mass. Gas temperatures were measured with two different constructs of type K (Chromel-Alumel) thermocouples. All thermocouples outside the burn compartments were fabricated from 30 gauge glass wrapped thermocouple wire. Vertical arrays of three thermocouples were placed near the front door on the north side and south sides of the stairwell on the first floor. On the second floor, vertical arrays of eight thermocouples were placed near the center of each bedroom. Figure 4-16 is a photograph of the West wall of the North bedroom, showing the thermocouple array, the smoke obscuration meter, and a gas sampling probe used during the phase two experiments.

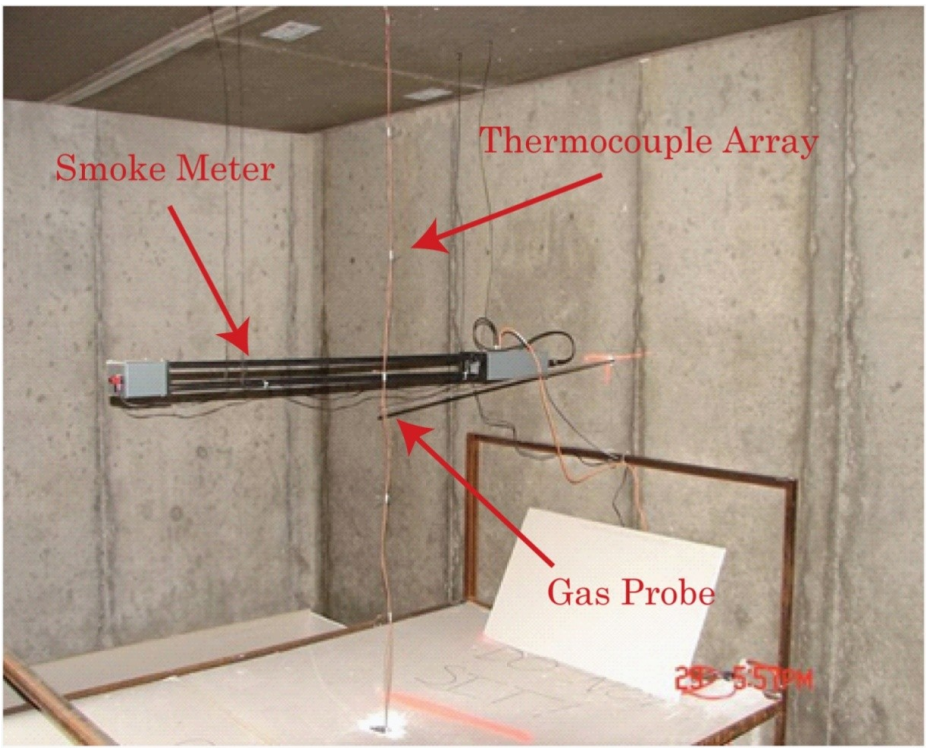

Figure 4-16: Bedroom instrument cluster

Inside the burn compartments, seven 3.2 mm (0.125 in.) exposed junction thermocouples and 0.76 m (30 in.) SUPER OMEGACLAD XL® sheathed thermocouple probes were arranged in a floor-to-ceiling array. Figure 4-17 shows the vertical array in the burn compartment. Type K thermocouple probes were chosen for their ability to withstand high temperature, moisture and physical abuse resulting from physical contact with hose streams and fire fighters. To protect the extension wire and connectors from the effects of heat and water, through-holes were drilled in the burn compartment walls and the sheaths were passed through from the adjacent compartment. To prevent leakage through the holes, all void spaces were tightly packed with mineral wool. Inside the burn compartment the end of each probe was passed through an angle iron stand and fastened to the floor and ceiling to provide additional protection from physical contact with firefighters. The stand also ensured that the measurement location did not change if probes were to come in contact with fire fighters. In consideration of the risk associated with heating the open web steel joists, additional thermocouples were placed above each burn compartment to monitor the temperature of the interstitial space.

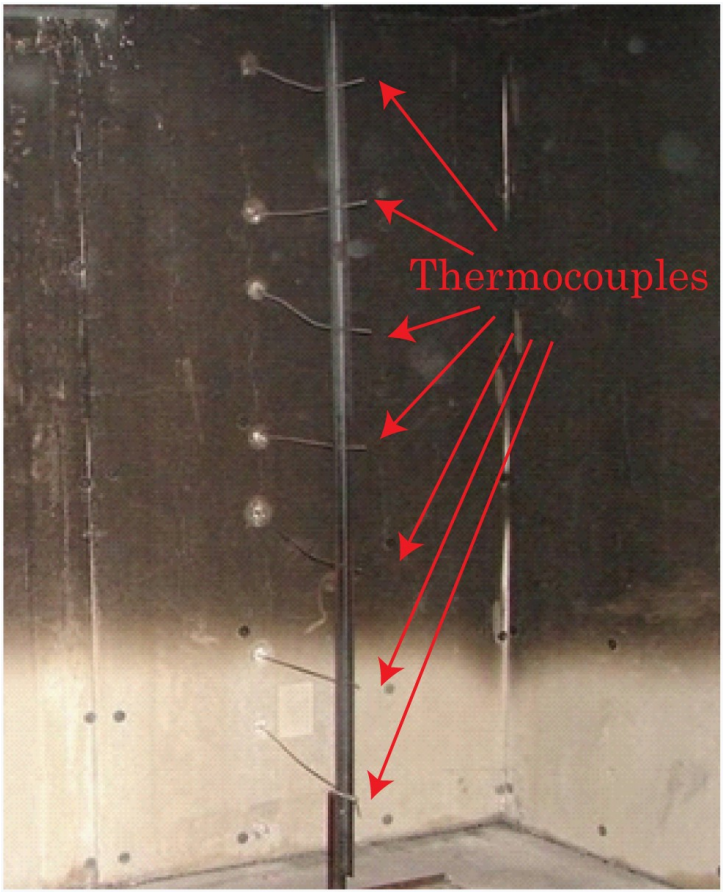

Figure 4-17: Burn compartment T.C. array

All length measurements were made using a steel measuring tape. Wood moisture content measurements were taken using an electrical resistance-type moisture meter [51]. Fuel mass was measured prior to each experiment using a platform-style heavy duty industrial scale. Mass was not measured after each experiment due to the absorption of fire suppression water.

Non-combustible "prop" furniture was fabricated from angle iron stock and gypsum wallboard. The purpose of the furniture was twofold. The furniture was placed inside to represent interior furnishings that fire fighters would encounter during interior operations. The second use was to locate equipment within the frames of the furniture to provide protection for measurement equipment from physical damage caused by contact with firefighter and their tools. Figure 4-18 shows an example of a table placed outside the burn compartment.

Figure 4-18: Non-combustible "prop" table

4.4 Results of Field Experiments

Section 4.3.3 described the testing matrix for the field experiments. Twenty-four tests were conducted with eight different deployment configurations, resulting in a range of fire fighter action completions times. There were three thermocouple (TC) arrays in the experimental setup: a 7-TC array in the burn compartment, a 3-TC array near the front door and an 8-TC array in the bedroom. Sections 4.4.1-4.4.3 present temperature results in each of these measurements locations. In each section temperatures recorded for each test by the highest thermocouple in one measurement location are displayed on a single plot. The purpose of the plot is to qualitatively demonstrate the repeatability of each measurement[8]. Having established the repeatability with this plot, a second plot is provided that presents the measurements of the entire vertical thermocouple array on one plot for a single test[9]. The purpose of the second plot is to demonstrate the typical temperature behavior measured in the experiments (i.e., the same plot using a different set of test data would appear nearly the same). This prevents an unwieldy analysis of the large amount of test data, however additional examples of this second plot can be found in the report of the fireground experiments [45]. Section 4.4.4 presents the hot gas layer temperature and depth results in the burn compartment calculated using the hot gas layer reduction method and the data presented in Section 4.4.1. HGL calculations are available only in the burn compartment. Near the front door more TCs are needed to provide the resolution of the vertical temperature profile necessary for HGL calculations. In the bedroom a two-zone approximation is not appropriate; the relatively long transport from the burn compartment along cold concrete surfaces cooled the hot gasses such that the temperature profile more closely resembles a single zone, where no clear thermal interface is present. In Section 4.4.5 justification is provided for selecting two fire fighter actions, the front door opening and fire suppression, for further analysis and simulation with FDS.

[8] Quantification of repeatability relevant to the comparison of simulated and experimental measurements is provided in Section 6.

[9] It should be noted that for consistency, the test chosen for display is the same test analyzed in Section 6.1

4.4.1 Temperatures in Burn Compartment

The temperature rise recorded by the highest TC in the vertical array in the burn compartment is presented for all 24 tests in Figure 4-19. The data in each test was adjusted in time such that time zero in the plot corresponds to the time of ignition. The temperature rise is adjusted by subtracting the ambient temperature for each TC measurement. Seventeen sets of temperature rise data are shown with solid lines in a multitude of colors. Seven sets of test data are shown in dotted black lines. These seven sets of data represents tests in which poor ignition resulted in partial burning of the pallets and excelsior. Consequently these tests are excluded from the rest of this study; the seventeen tests with successful ignition remain the focus.

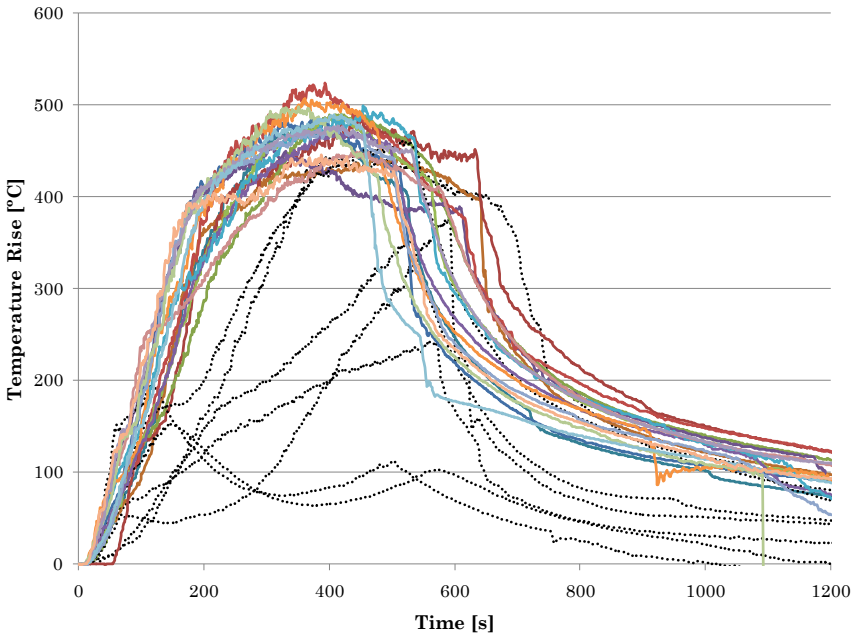

Figure 4-19: Temperature rise measured by the 2.1 m (7ft) TC in the burn compartment for all 24 tests

Figure 4-19 shows that the seventeen tests with successful ignitions grew to peak temperatures in the range of approximately 420 to 520° C in 350 to 400 seconds. After peak burning and during the decay phase of the fire, a rapid drop in temperature is evident in each set of test data. This rapid drop, resembling a single-phase exponential decay, corresponds to the application of suppression water to the burning pallets by the fire fighters. Suppression occurred at different times for each set of test data due to the variation of deployment configurations used, as discussed in Section 4.3.3. Although suppression occurred at different times, the rate and magnitude of temperature decay appears similar from test to test. Quantification of this temperature decay is provided in detail in Section 6.3, as part of the comparison with simulated temperature decay.

The repeatability of the rate of temperature rise for the 17 fires was ascertained by analyzing temperatures measured by a TC located 2.1m above the floor in the burn compartment. Figure 4-20 shows the remaining 17 fires used in the analysis. Among the seventeen field experiments shown, there was an approximate ±21% relative difference in the rate of temperature rise.

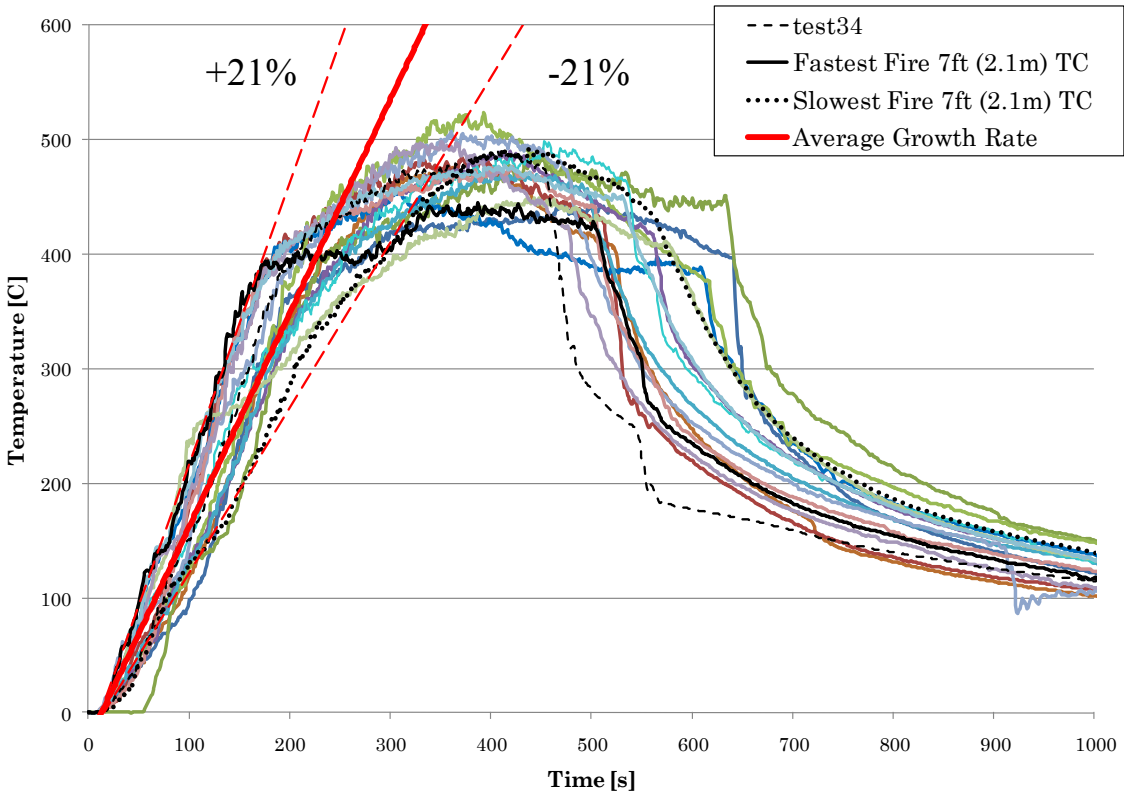

Figure 4-20: Repeatability of experimentally measured temperature growth rate

Figure 4-21 shows the temperature rise measured by the 7-TC array in the burn compartment for one test representative of the 17 successfully ignited tests. The temperature rise behavior is representative of the other 16 tests conducted. Additional plots that display this behavior are available in the full report of the residential fireground experiments [45]. After approximately 100 seconds, temperatures at and above 1.2 m (4ft) rose at virtually the same rate, and peaked between approximately 470 and 490 °C at approximately 410 seconds. At 0.9 m (3ft) similar behavior occurred but the temperature rose more slowly, and the peak temperature was slightly lower. Below 0.9m, temperatures rose at effectively the same rate and peaked at temperatures well below the temperatures recorded above 0.9 m. This data indicates that the hot gas layer formed during the first 100 seconds and descended to a level near to, but below 0.9 m.

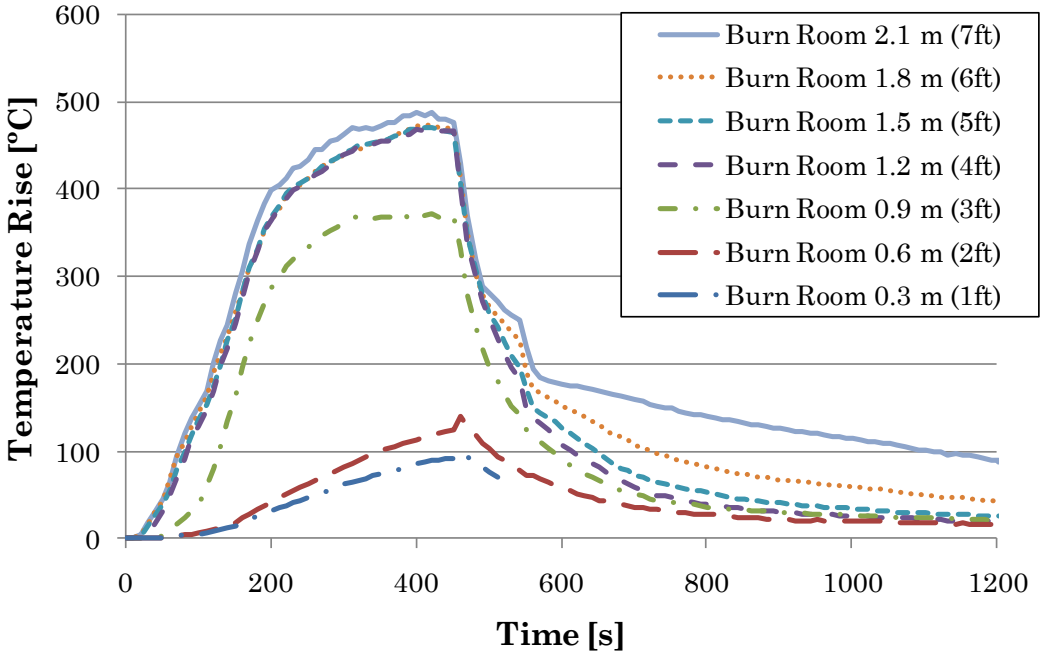

Figure 4-21: Temperature rise measured by 7 TC array in the burn compartment for one test

4.4.2 Temperatures Near Front Door

The temperature rise recorded by the highest TC in the vertical array near the front door for the 17 tests chosen is presented in Figure 4-22.

The data in each test was adjusted in time such that time zero in the plot corresponds to the time of ignition.

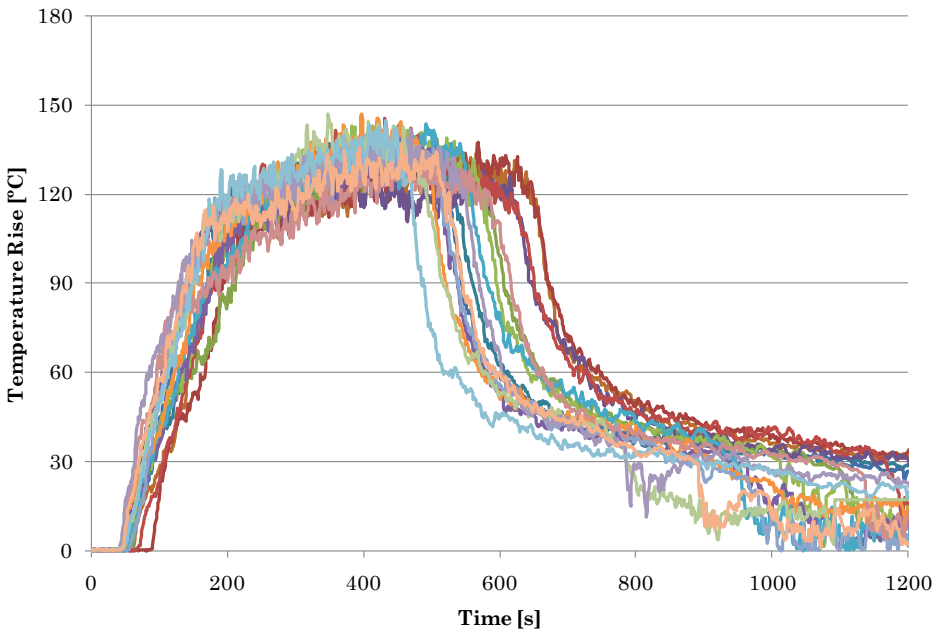

Figure 4-22: Temperature rise measured by the 2.4 m (8ft) TC near the front door for 17 tests

Figure 4-22 shows the temperature near the front door began to rise approximately 45-70 seconds after ignition, indicating the arrival of hot gasses. Temperatures at this location peaked in the range of approximately 110-145 °C between 350 and 450 seconds. After peaking, temperatures remained relatively constant until fire suppression. As in Figure 4-19, post-suppression temperatures decayed in a manner resembling a single-phase exponential decay. In Figure 4-23 the distribution of suppression times is more clear than in Figure 4-19; prior to suppression, temperatures are grouped more closely from test to test (i.e., the temperatures have nearly the same starting point on the plot, before beginning to decay).

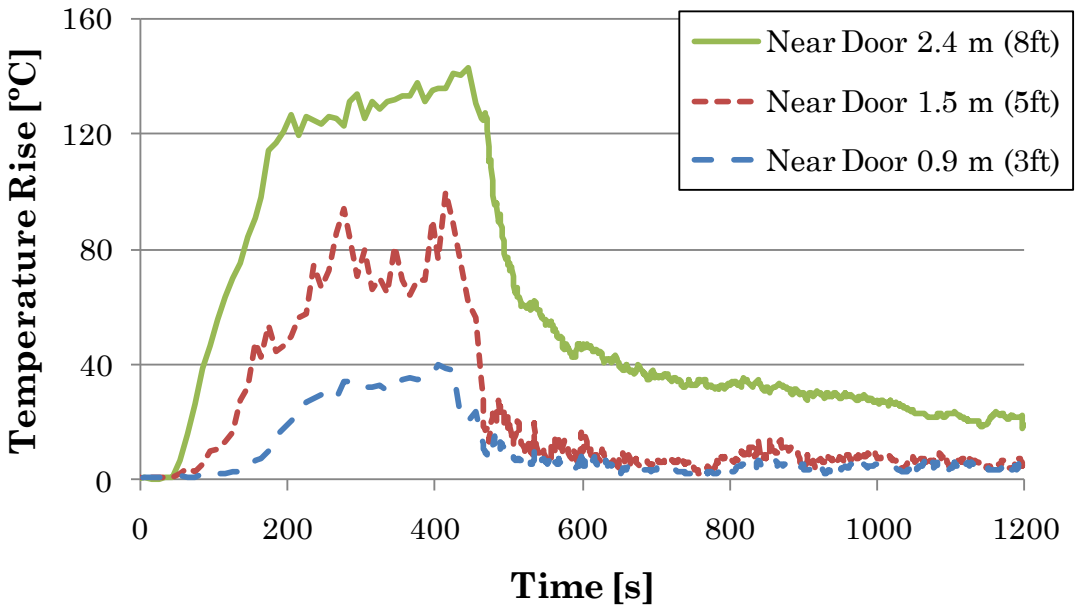

Figure 4-23: Temperature rise measured by 3 TC array near the front door for one test

Figure 4-23 shows the temperature rise measured by the 3-TC array located near the front door, for the same test displayed in Figure 4-21. Additional plots that display this behavior are available in the full report of the residential fireground experiments [45]. In Figure 4-23, temperatures began to rise first at the 2.4 m (8ft) TC location after approximately 40 seconds. As hot gasses continued to flow into and accumulate in the room adjacent to the front door, at lower TC locations; the temperature began to rise at the 1.5 m (5ft) location after approximately 100 seconds and after approximately 180 seconds the temperature rose above ambient at the 0.9 m (3ft) TC location.

Given the relatively coarse instrument density in this location, it is not possible to identify the location of the hot gas layer interface with certainty. However, a simple observation can be made that qualifies the location of the hot gas layer post-suppression: After suppression (at approximately 450 seconds), the temperature quickly decayed to ambient at locations at 1.5 m and below. The temperature at 2.4 m also decayed rapidly, but after 50 seconds the rate of temperature decay became approximately linear and remained well above ambient. This indicates that the 2.4 m TC was in the diminishing but still existent hot gas layer, whereas the two TCs below are in a ambient temperature environment.

4.4.3 Temperatures in Bedroom

The temperature rise recorded by the highest TC in the vertical array in the bedroom for 17 tests is presented in Figure 4-24. The data in each test was adjusted in time such that time zero in the plot corresponds to the time of ignition.

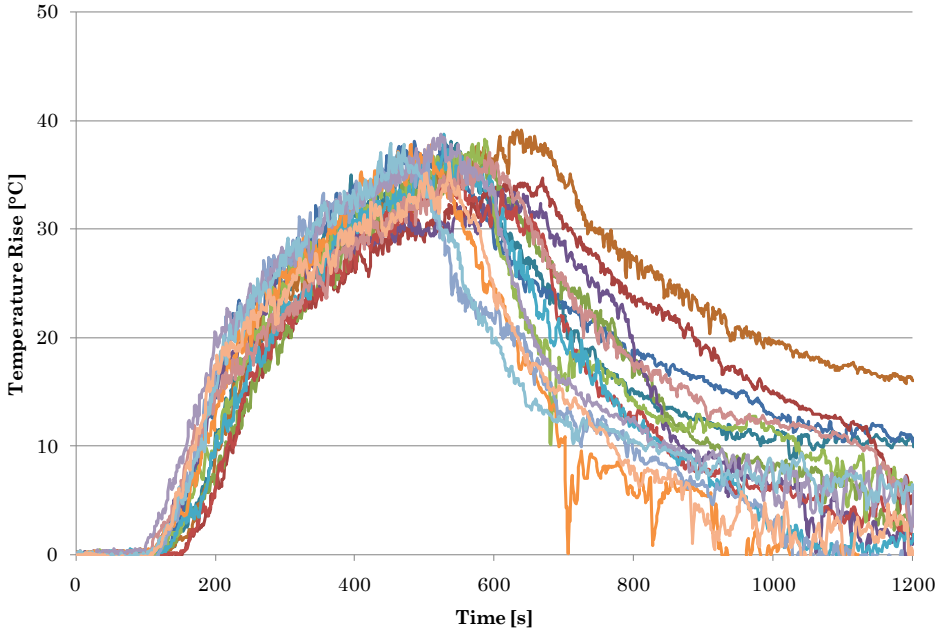

Figure 4-24: Temperature rise measured by the 2.4 m (8ft) TC in the bedroom for 17 tests

Figure 4-24 shows that temperatures in the bedroom began to rise approximately 100-160 seconds after ignition, indicating the arrival of hot gasses. Temperatures in the bedroom peaked in the range of approximately 33-39 °C between 460 and 650 seconds. Temperatures in the bedroom are much lower than near the front door, indicating a significant amount of energy loss to the cold concrete surfaces of the structure and dilution of the hot gasses with ambient air. The time at which temperatures remained at or near peak temperatures was relatively short. Due to the long transport time of the hot gasses from the burn compartment to the bedroom, the fires in each test were suppressed very near the time that temperatures were near their peak.

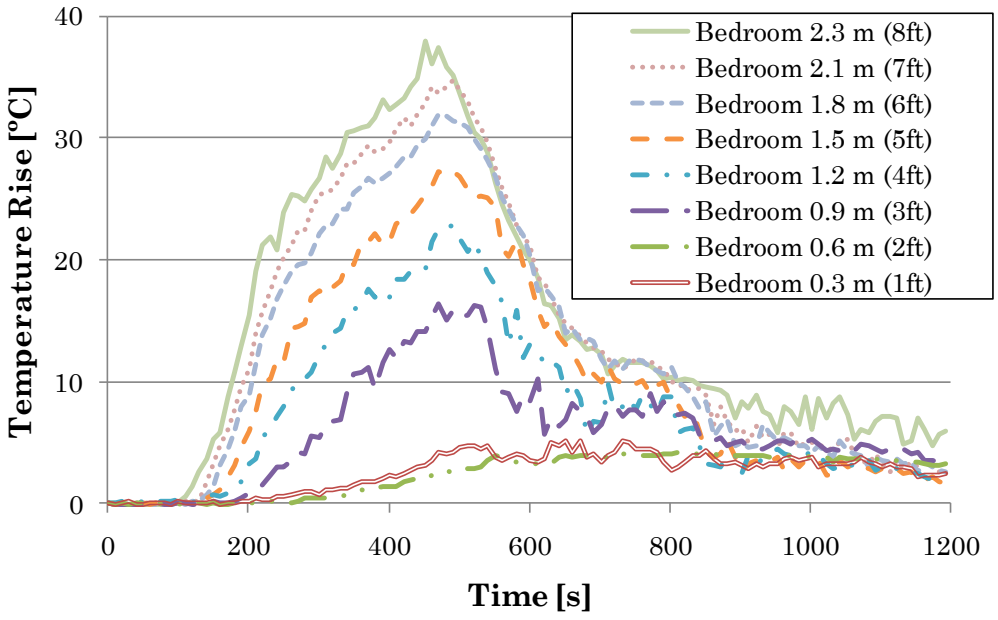

Figure 4-25: Temperature rise measured by 8 TC array in the bedroom for a single test

Figure 4-25 shows the temperature rise measured by the 8-TC array located in the bedroom for the same test displayed in Figure 4-21 and Figure 4-23. Additional plots that display this behavior are available in the full report of the residential fireground experiments [45]. In the burn compartment, it was seen that temperatures above 0.9 m rose at similar rates and peaked near the same temperatures. In the bedroom, the rates of temperature rise above 0.9 m are instead widely separated. Temperatures above 0.9 m also peaked in a wider range, relative to the maximum temperature. It is still seen that the temperatures below 0.9 m appear closely grouped at temperatures much lower than the temperatures above 0.9 m, but the temperature gradient in the room is very small (i.e., between 0.6 m and 0.9 m the maximum temperature difference is approximately 10 °C). Although this separation in temperatures weakly indicates a hot gas layer interface between 0.9 m and 0.6 m, the separation was too small to produce reliable hot gas layer calculations in the bedroom for any test.

4.4.4 Hot Gas Layer in Burn Compartment

The HGL temperature rise calculated using the HGL reduction method and temperature measurements from the vertical array of TCs in the in the burn compartment for 17 tests is presented in Figure 4-26.The data in each test was adjusted in time such that time zero in the plot corresponds to the time of ignition.

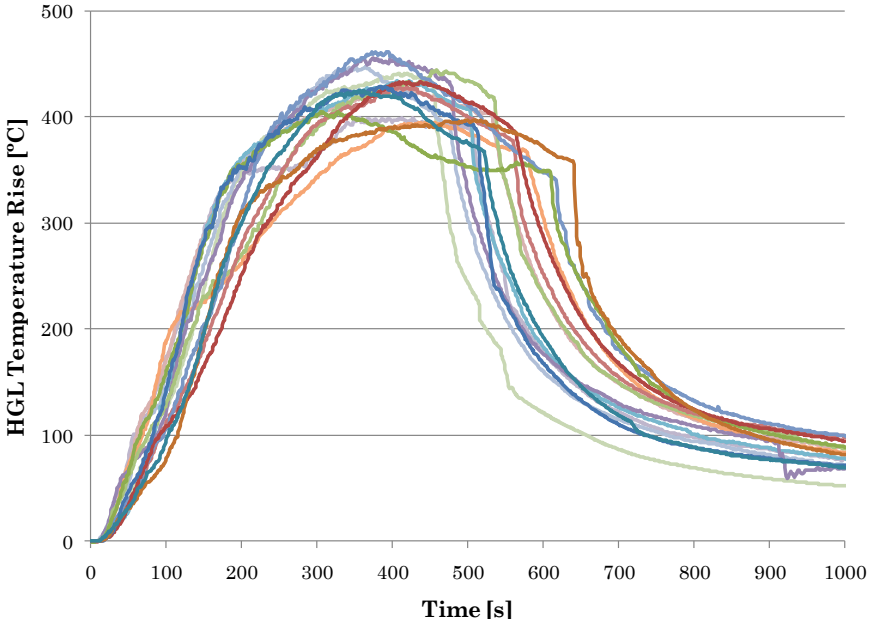

Figure 4-26: HGL temperature for 17 tests

The behavior HGL temperatures curves shown in Figure 4-26 closely resembles the behavior of temperatures curves in Figure 4-19. The HGL temperature is essentially a weighted average of temperatures measured above 0.9 m, which Figure 4-21 shows are closely grouped. The majority of HGL temperatures peaked from approximately 390-460 °C from 350-450 seconds. In comparison with measurements from the 2.1 m TC, the range of peak temperatures is lower and occurs at a slightly larger range of times. This is expected as TCs measuring hotter temperatures near the ceiling are averaged with TCs that are slightly cooler, but still in the hot gas layer. The distribution of suppression times is again shown well; the magnitude and rate of HGL temperature change is shown to be repeatable.

The HGL temperature is an effective means of showing the effects of fire suppression in the burn compartment. Because the HGL reduction method averages temperatures above the thermal interface, it is insensitive to the transience of single thermocouple measurements. Because the thermal changes in the burn compartment due to fire suppression are large at all measurement locations in the HGL prior to suppression, the HGL temperature is superb for capturing the effects of fire suppression on the thermal environment in the burn compartment.

The HGL depth calculated using the HGL reduction method and temperature measurements from the vertical array of TCs in the in the burn compartment for 17 tests is presented in Figure 4-27. The data in each test was adjusted in time such that time zero in the plot corresponds to the time of ignition.

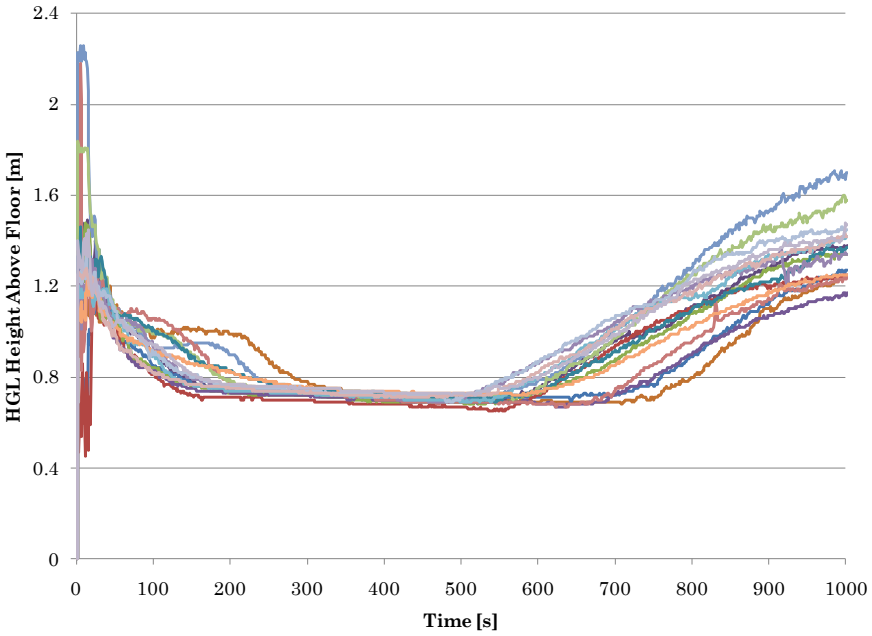

Figure 4-27: HGL depth for 17 tests

After ignition, the HGL reduction method outputs spurious results for approximately 50 seconds. To produce a reliable HGL depth calculation is it first necessary to accumulate enough hot gasses near the ceiling to form a thermal interface that descends below sufficient measurement locations in the vertical array. This process took approximately 50 seconds for these particular tests. After 50 seconds, the HGL interface descends from 1.1 to 1.2 m until approximately 180 seconds. After 180 seconds the HGL interface remained steady in the region of 0.7-0.75 m, until suppression occurred in each test. The effects of suppression on the HGL depth were the same for all tests, the HGL interface steadily rose, although the rate showed some variance. In the tests, suppression was initiated as early as 450 seconds and as late as 700 seconds. It is seen that the reaction of the HGL interface height to suppression is not as immediate as the reaction in HGL temperature. Additional analysis of the effects of suppression on the HGL temperature and depth are provided in Section 6.3.

4.4.5 Selection of Fire Fighter Actions for Simulation

Seven fire fighter actions from the 22 total fire fighter actions conducted on the fireground during the field experiments can be identified as interactions that may change the interior thermal environment and fire development [45]. These fire fighter actions, listed chronologically in order of completion, are :

1. Front door is breached for fire company to make entry (i.e., door is opened)
2. Fire suppression
3. Second floor window #1 (bedroom) ventilated
4. Second floor window #2 ventilated
5. Second floor window #3 ventilated
6. First floor window #1 ventilated
7. First floor window #2 ventilated

Two of these seven fire fighter actions are chosen for simulation with FDS, forced entry of the front door and fire suppression. The reason for choosing these two actions is simple. These are the first two actions that occur in the chronological sequence of fire fighter actions in the experiments, and as stated in [45], the typical order of events on the fireground for a residential structure. It is important to look at the first actions that typically occur on the fireground because this evaluation is a first step in determining if FDS appropriately simulates changes in the thermal environment resulting from these actions. The effects of later actions, and how the thermal environment is affected by the time at which these actions are performed, may be studied with future validation work.

Figure 4-28 through Figure 4-30 are photos that show the front door being opened and suppression during the fireground of the experiments. Figure 4-28 also shows one of the trained timing staff and the fireground safety officer recommended by NFPA 1403.

Figure 4-28: Fire fighter crews preparing to make entry through the front door. Timing staff standing in left of photo.

Figure 4-29: Fire Fighters entering structure

Figure 4-30: Fire Fighters just before suppressing fire in burn compartment

4.5 Influence of Environmental Variables

In the laboratory, a significant amount of control could be employed to reduce the effects of environment variables. Although the best efforts were carried out to control the testing environment in the field as much as possible, the testing environment was less controllable than in the laboratory. This section addresses common environmental variables that affect fire behavior and have been identified with previous research. Based on this information, it is expected that the HRR and fire growth rate were somewhat reduced in the field experiments as compared to the laboratory experiments. This section is intended to provide insight into the differences between the field experiments and the laboratory experiments and how that affects the outcome of the simulations.

4.5.1 Ambient Temperature

Ambient temperature has an effect on fire growth rate. According to Tamanini [57], an approximate 15% increase in fire growth rate can be expected as ambient temperature is changed from 4 to 32 °C, assuming all other parameters are constant. Therefore, it is suspected that colder ambient temperatures contributed to slower fire growth rates in the field, as compared to the laboratory experiments.

4.5.2 Relative Humidity

Relative humidity can significantly affect the oxygen concentration of ambient air. In environments with higher temperatures and relative humidity, water vapor acts as a diluent. An analysis by Tamanini [57] shows that a "hot and steamy environment" of 32.2 °C and 100% RH results in a 1% drop in oxygen concentration from the dry value of 20.95%. In the same article, Tamanini furnishes an example of a pool fire experiment where oxygen concentration was decreased from 21 to 20% by volume. Tamanini estimated an approximate 10-15% change in fire growth rate. With the equipment available, it was not possible to take measurements of the moisture content of the air inside the structure. It is expected that the total moisture content of the air inside the burn compartments was significantly higher than the moisture content of the outdoor ambient air due to evaporation from moist compartment surfaces.

4.5.3 Fuel Mass

The pallets used in the field experiments consistently measured the same exterior physical dimensions (1 m by 1.3 m by 0.11 m). Variance in pallet mass was primarily due to stringer thickness and deck spacing. A theoretical analysis by Buchanan [58] can be used to quantify the burning duration:

$$\dot{Q} = \frac{E}{t_{solid}}$$

where $\dot{Q} = \dot{Q''} A_{\ fuel}$ and $E = m_{fuel} \Delta H_C$

$$t_{solid} = \frac{m_{fuel} \Delta H_C}{\dot{Q''} A_{fuel}}$$

Heat release per unit area, the area of the fuel (floor space occupied) and the heat of combustion of wood can be held constant given that the pallets were set up the same for each test. The variance in burning duration is then affected only affected by mass. Pallet mass varied by ±19.2% therefore burning duration, had the pallets been ignited and allowed to burn until fuel depletion, would have varied by approximately ±19.2%. It is important to consider burning duration, because it seen in the field experiments that the some of the fires began to decay prior to any fire fighter action. Although Buchanan's analysis shows that fuel mass will affect burning duration it does not address fire growth rate. Varying stringer thickness and deck spacing will affect the ignition propensity of the pallets by increasing the thermal capacitance with increasing dimensions. For example, a thin wood board will ignite more readily than a very thick wood board.

4.5.4 Fuel Moisture Content

The burning rate was affected by the moisture content of the wood used in pallet construction. In the laboratory, moisture content measurements registered below the operational range of the wood moisture meter. During the field experiments, pallets were

stored in a closed steel shipping container located outdoors. The moisture content of the wood pallets used in the fuel package was recorded in three different locations on ten randomly sampled pallets immediately prior to the test series. Moisture measurements averaged 10.2% ± 2.2%. Buchanan [58] provides a means for estimating the effect of moisture on the calorific value of wood:

$$\Delta H_C = H_C(1 - 0.01m_C) - 0.025m_C$$

With a ±2.2% variance in moisture content, the effective calorific value of the wood pallets varies by approximately 21.3%. Given that heat release rate is the product of fuel flow rate and heat of combustion, heat release rate may have varied by approximately 21.3% had the pallets burned individually. It is likely that the moisture content of the wood pallets increased after placement in the burn compartment because of the relatively high amount of moisture in the compartments and the significant hygroscopicity of wood. There are numerous phenomena that decrease the burning rate of wood with increase in moisture content. Some examples of how moisture content affects the burning rate of wood are:

- Increase in thermal inertia
- Thermal energy required for phase change of water into water vapor
- Convective cooling as water vapor escapes through the face of the burning wood

4.5.5 Moisture of Wall Linings

Moisture content affected the interaction of the porous cement board compartment surfaces with the thermal environment. Surfaces were exposed to suppression water spray and the high temperature/humidity environment that resulted from suppression. Three measures were taken to reduce moisture as much as possible. Suppression water was immediately drained, surfaces were heated with high output kerosene torpedo heaters and no two consecutive tests were run in the same burn compartment. However, visual inspection revealed that the porous cement-board and the concrete floor absorbed a significant amount of moisture.

The thermo-physical properties of moist porous materials, particularly thermal conductivity, are strongly dependent on moisture content. Generally, the thermal conductivity linearly increases with moisture content [59]. Density and specific heat also increase. Voids in the porous material are filled with water which has a higher density and specific heat than air. Further complicating the thermal behavior of moist porous materials, is the phase change of water to water vapor. As the thermal gradient moves through the material, the temperature "plateaus" at approximately 100°C, until water transitions to water vapor and escapes the material. With the equipment available, it was not possible to take measurements of the moisture content of the compartment surfaces.

4.5.6 Thermo-physical Properties of Construction Materials

Thermo-physical properties for the construction materials used in the burn facility were gathered from manufacturer's data sheets where possible. The accuracy of these values is subject to the manufacturer's testing and material production. Properties for materials without data sheets are referenced to the most appropriate values from commonly used fire protection engineering literature. Determining appropriate values for fire model inputs remains a significant challenge. For that reason, efforts are underway to produce guidelines for the determination of fire model thermophysical inputs [15].

4.5.7 Wind Direction/Magnitude

Wind direction, velocity and gust data was not recorded during the field experiments. It is clear that this will affect the thermal environment inside the structure, particularly after fire fighter actions have been performed. For example, the rate that buoyant smoke and gasses exit the bedroom window after ventilation may be affected by a positive pressure created by an opposing wind velocity. Without wind data, the existence or magnitude of this effect cannot be quantified. Additionally, wind may have changed ventilation conditions during the initial stages of fire growth.

4.5.8 Building Envelope Leakage

Leakage from the building envelope was documented by measuring the physical dimensions of leak paths (scuppers, seams around window frames, gaps under exterior doors). It is assumed that the paths measured represent the majority of leakage from the building, however there were numerous unsealed seams in wall and ceiling panels that likely added to a greater total building leakage. Therefore the true total leakage of the structure is not known.

4.5.9 Total Effect of Different Testing Environments

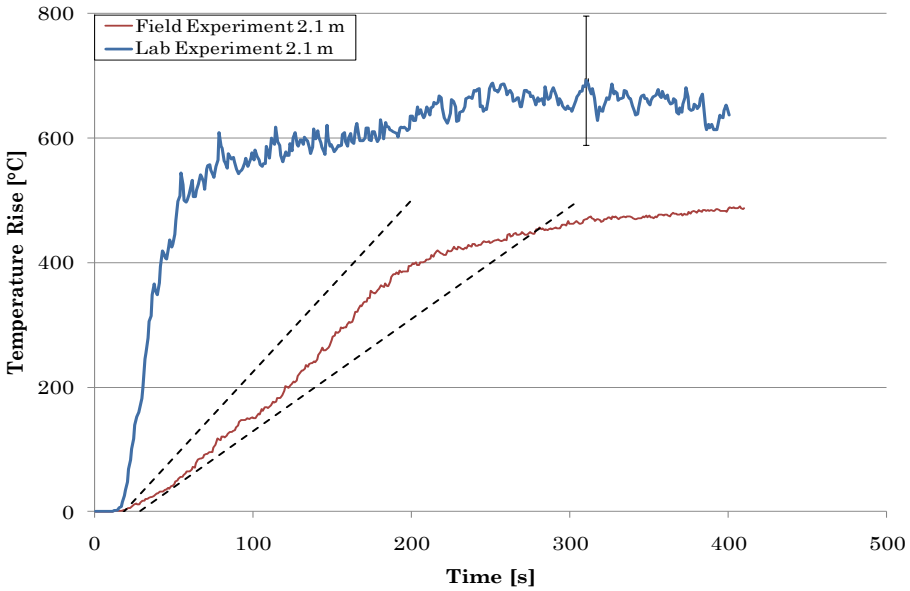

Figure 4-31: Comparison of the temperature at 7ft in the lab burn compartment and the field burn compartment

The total effect of the difference between the testing environments of the laboratory and the field experiments on the temperature at 7ft inside the burn compartment is shown in Figure 4-31. The data shown from the field experiment was selected from the test which most closely matched the average rate of temperatures rise. The ±21% variation in the rate of temperature rise is shown by the dotted black lines. Some variation in the rate of temperature rise and peak temperature is expected due to the natural variability in the burning behavior of wood. However, the separation between the +21% bound and the laboratory temperature plot qualitatively shows the conditions of testing in the field experiments significantly reduce the rate at which the fire grew and the intensity with which it burned. This change in the burning behavior is especially important to consider, because of the use of the laboratory measured HRR as an input parameter for the field experiments. The differences shown between these two environments will also be reflected in the simulation of the field experiments.

5 Description of FDS Simulations

Two stages of simulations were conducted ; a grid cell sensitivity study simulating the laboratory experiment, followed by simulation of the live-fire training facility. All simulations were run using a Linux cluster with multiple-core 3.16Ghz processors. Parallel processing was used in the second stage of simulation. The sensitivity study simulated the fire growth and thermal conditions measured in the laboratory experiments. The sensitivity study had multiple purposes:

- To investigate the mesh resolution requirements for resolving combustion and plume dynamics in the residential-scale burn facility.
- To benchmark the computational demands imposed by varying grid cell resolutions in a single-mesh arrangement.
- To serve as a less computationally-expensive domain for testing model assumptions before performing simulations in the larger domain containing -the burn facility.
- To provide a base of comparison for temperature and HGL predictions with the burn facility simulations and with experimental data.

5.1 Grid Cell Sensitivity Simulations

The grid cell sensitivity was performed in order to determine a favorable mesh resolution for the full scale burn facility simulations. This process was carried out by starting with a resolution known to be "coarse" and decreasing cell size until differences between the numerical predictions of thermocouple temperatures for consecutive simulations were effectively collinear. A favorable cell size lays in a range of possible sizes. Cells that are too large prevent accurate specification of dimension-critical parameters that affect calculations. For example, the mesh resolution is too coarse to represent compartment geometry and it is not possible to sufficiently characterize ventilation and fuel configuration. On the other hand, reducing cell size increases simulation run times exponentially and numerical predictions eventually converge towards a final value that no longer depends on mesh resolution.

The discretization error of FDS is proportional to the square of the time step or cell size. By default, FDS adjusts each time step as the model performs sequential steps, so that the CFL (Courant, Friedrichs, Lewy) condition is satisfied [2]. The CFL condition states that the solution of the equations (i.e., the governing equations) cannot be updated with a time step larger than that allowing a parcel of fluid to cross a grid cell, otherwise the simulation will produce wildly incorrect results. The CFL condition is shown below:

$$\delta t \ \max\left(\frac{|u_{ijk}|}{\delta x}, \frac{|v_{ijk}|}{\delta y}, \frac{|w_{ijk}|}{\delta z}\right) < 1$$

x, y, and z are the spatial dimensions of the smallest grid cell in the mesh and u, v, and w are the components of the velocity of fluid flow in that cell. For this scale of simulation convective heat transfer is the driving force of fluid velocity and the CFL condition restricts the time step. Therefore, reducing cell size forces a reduction for every time step in the simulation. In theory, reducing the grid cell size by a factor of 2 reduces the discretization error by a factor of 4. However, it also increases the computing time by a factor of 16. This implies that there are diminishing returns for reducing mesh size.

The grid cell sensitivity simulations were designed after the laboratory experiments described in Section 4.2. Simulations were run using three mesh cell sizes. The process of choosing these sizes was iterative and was based on the results of each simulation. This provided valuable insight into choosing a final mesh size for the full-scale simulations.

5.1.1 Domain & Mesh Resolution

The size of the computational domain for the three simulations was determined using the dimensions of the burn compartment from the laboratory experiments. The domain measured 5m (16.4ft) x 5.1m (16.7ft) x 2.5 m (8.2ft). The domain was extended 1 m (3.3ft) in the direction of the hallway to resolve flow in and out of the compartment door. The edges of the domain lay at the exterior surfaces of the compartment walls, excluding the hallway side of the compartment. Figure 5-1 shows the domain used in the simulations.

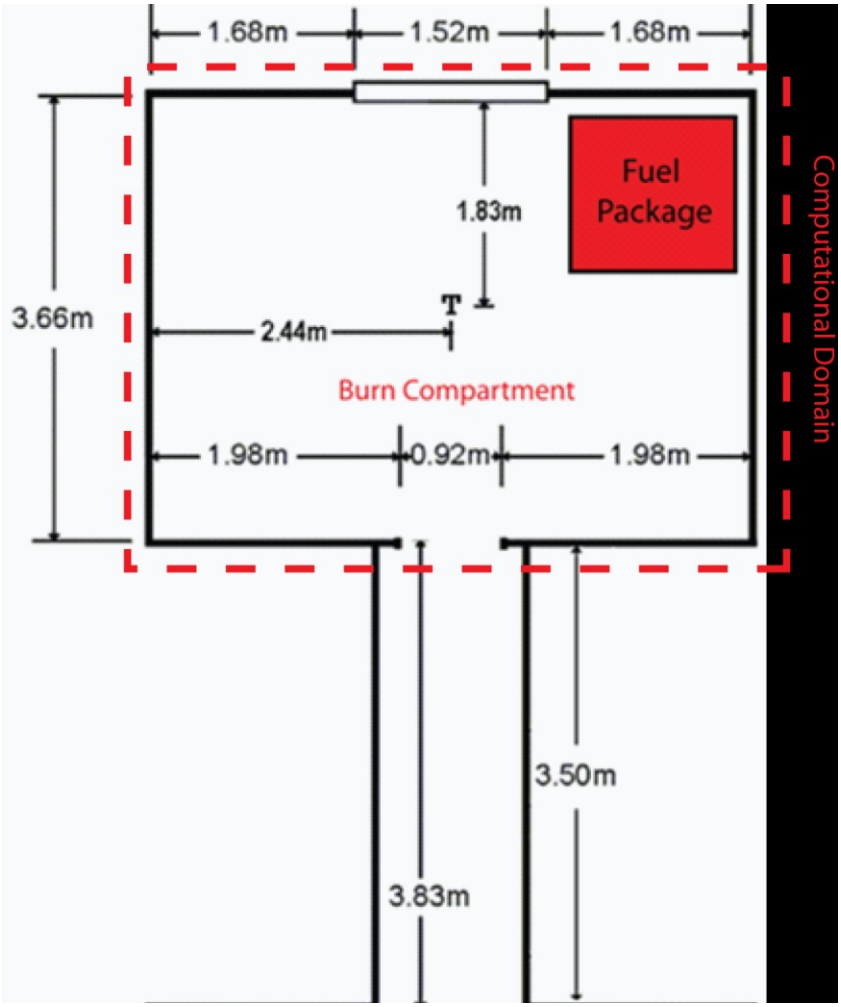

Figure 5-1: Floor plan of laboratory experiments showing domain

In the experiments the stack of pallets burned out after 1100. Therefore the simulations were run for 1100 seconds. A cell size of 0.2m x 0.2m x 0.2m was chosen as a starting point for the simulations. This size was chosen because it has been used in previous residential-scale fire reconstructions simulated with FDS [10,11,12,13]. The ratio of $\frac{D^*}{\delta x}$ (calculation given in Section 3.3.2) falls within the range of 4-16 reported successful in simulating plume dynamics and geometries by the U.S. NRC [36], using the laboratory

measured HRR of 2MW. The elapsed time was relatively short for this simulation, so a second simulation was run with a 0.1m cell size. Again, 0.1m resulted in a relatively short run-time, so the simulation was run a third and final time with a 0.05m mesh. The specifics of these mesh cell sizes for each simulation and their run times are provided in Table 6. Visuals of the different mesh resolutions are shown in Figure 5-4-through Figure 5-6

Grid Cell Size	# of cells in domain	$D^*/\delta x$	Wall Clock Simulation Time [s]
20cm3	8125	6	1482
10cm^3	63750	13	11990
5cm3	510,000	25	114688

Table 6: Details of three resolutions used to simulate laboratory experiments

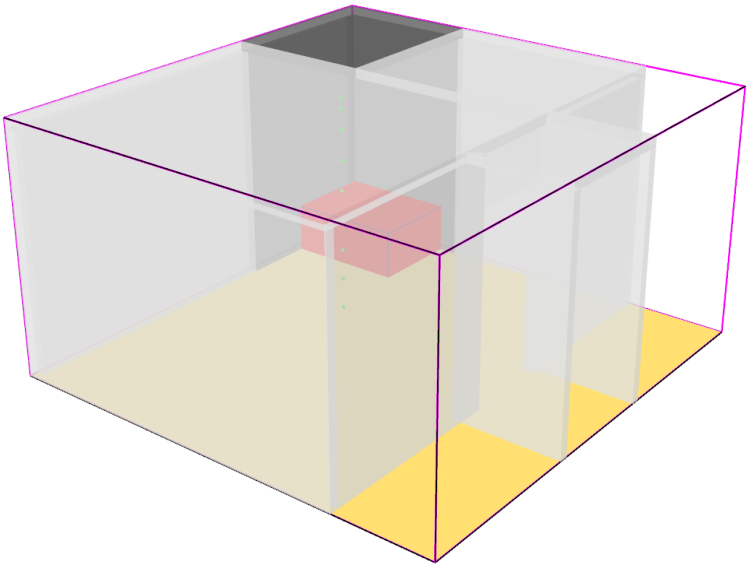

Figure 5-2: Laboratory experiment domain

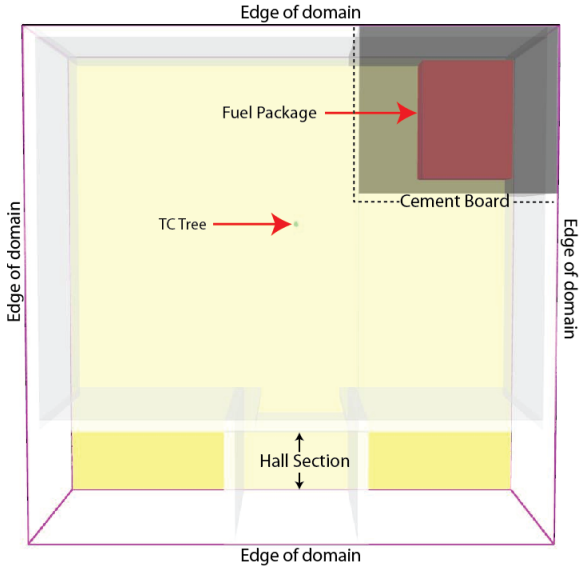

Figure 5-3: Overhead view of compartment and domain

5.1.2 Geometry

The compartment and fuel geometry were input into the model using the dimensions from Figure 5-1 and a ceiling height of 2.4 m. Figure 5-2 shows an isometric view of the laboratory test compartment, with the outer wire frame indicating the boundaries of the computational domain. Figure 5-3 provides an overhead view of the compartment which shows the locations of the thermocouples in relation to the fuel package and the door to the hallway. All of the geometry was prescribed using rectangular obstructions that were forced to conform to the rectilinear grids described in the previous domain description. This only became a minor issue for the 0.2m grid size. The width and height of the compartment door and the pallet stack were automatically adjusted to meet the

underlying mesh. This is evident when comparing Figure 5-4 and Figure 5-5. The pallet stack was constructed by creating a solid obstruction with the same dimensions and applying vents at the surface to represent the fire. The size of this obstruction was 1m x 1.3m x 0.5m. The compartment walls were 1 cell thick, but specified with the appropriate thickness in the SURF parameter line in FDS. This was 0.032m for the walls, floor and ceiling and an additional 0.013 m the corner with the fuel package.

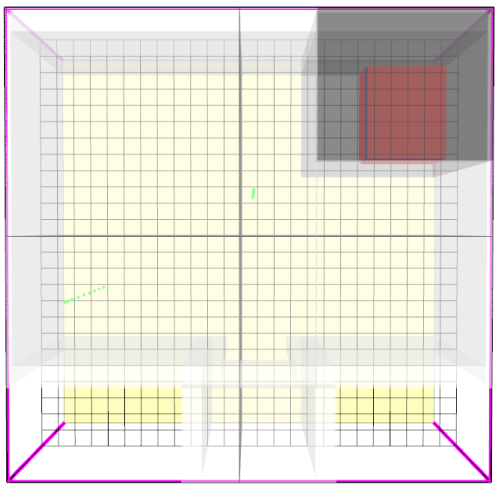

Figure 5-4: Burn Compartment with 0.2cm mesh

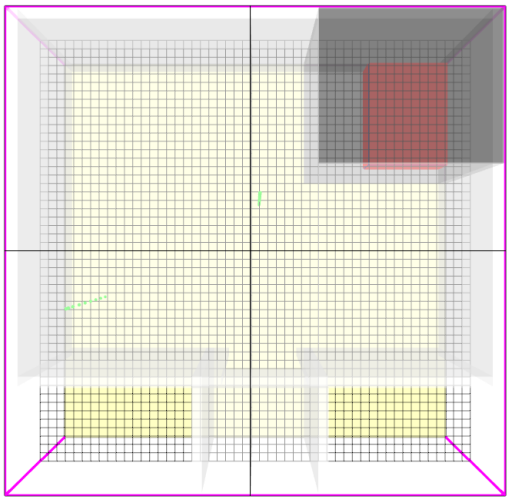

Figure 5-5: Burn compartment with 0.1m mesh

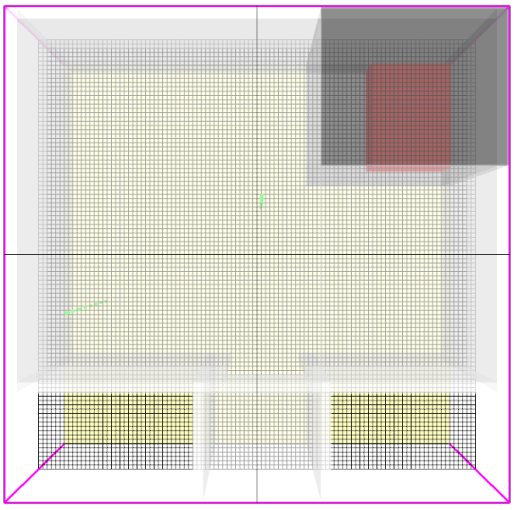

Figure 5-6: Burn compartment with 0.05m mesh

5.1.3 Materials

The gypsum and cement board were assigned thermo-physical properties for the simulation. Where the cement board overlapped the gypsum in the corner of the fuel package, the multiple layer material feature of FDS was implemented to account for heat transfer through the solids. Material properties were obtained from manufacturer's specifications. Table 7 lists these properties.

Material	Specific heat [kJ/kg·K]	Conductivity [W/m·K]	Density [kg/m3]	Thickness [m]	Location
Cement Board [60]	0.84	0.12	1153.0	0.013	Corner w/ fuel package
Gypsum [61]	1.09	0.18	677.6	0.032	Entire compartment (including behind cement board)

Table 7: Thermo-physical properties used in simulation

The pallets were approximated as Douglas Fir, with a chemical formula of $CH_{1.7}O_{0.74}N_{0.002}$, a heat of combustion of 16400 J/kg·K, a CO yield of 0.01 kg/kg and a soot yield of 0.015 kg/kg [62]

5.1.4 Vents & Initial/Boundary Conditions

The hallway door, measuring 0.9m x 1.9m, was the only vent in the burn compartment. All domain boundaries were set to an open condition. Boundary conditions for construction materials were set to "void", to simulate heat transfer through the solid to an ambient environment. The fire was simulated by an obstruction representing the pallet stack, shown in red, in Figure 5-2. The vents covering the surface area of the pallet stack were prescribed a heat release rate per unit area (HRRPUA) that varied based upon a time dependent function. The function was created by discretizing the heat release rate (HRR) measured in the laboratory. The laboratory HRR and the discretized HRR used in the FDS simulations are shown in Figure 5-7.

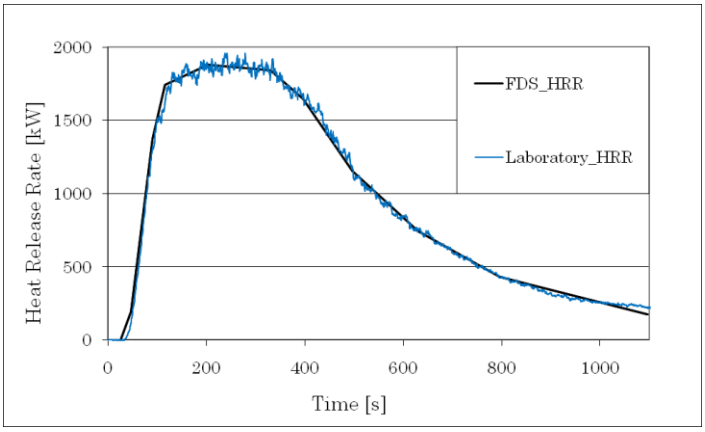

Figure 5-7: Laboratory & Discretized FDS HRR

An approximate relationship is known in regards to how HRR will affect HGL temperature and depth. A sensitivity analysis in [44] shows that when the HRR is varied by 15%, the HGL temperature varies by approximately 10% and the HGL depth varies by 1%. Using the same analysis, 11% variation of the HRR due to the measurement uncertainty of the NIST calorimeter would result in approximately 7% in the predicted HGL temperature and less than 1% variation in HGL depth.

5.1.5 Methodology for Comparing Simulated and Calculated HGL Temperature and Depth

This section describes the method used to compare the HGL temperature and depth calculated from experimental values with the HGL temperature and depth from FDS simulations. The method used here, a relative difference range, is suggested in ASTM E 1355 (11.3.8.2 (a)). This method is developed further in [44]. The formula used for comparing experimental and simulated values is defined as follows:

$$\varepsilon = \frac{\Delta M - \Delta E}{\Delta E} = \frac{(M_t - M_0) - (E_t - E_0)}{(E_t - E_0)}$$

where ΔM is the difference between the model prediction (M_t) at time t and its baseline value (M_0), and ΔE is the difference between the HGL value calculated from experimental measurements (E_t) at time t and the baseline experimentally measured value (E_0). The parameter ε is a ratio that represents the relative difference between the model HGL predictions and HGL calculations. Therefore the zero axis in a plot of ε represents exact agreement between the two values.

The error bounds used in the relative difference plots are based on a weighted expanded combined uncertainty also included in the report [44]. This uncertainty is the result of combining estimated measurement uncertainty and model input uncertainty in quadrature. For the HGL temperature and depth, these uncertainties are 14% and 13%, respectively.

If the relative difference curves fall within the error bounds, FDS and the experimental measurement are considered to be in agreement.

5.1.6 Results

Temperature measurement devices were prescribed to the same locations as in the experimental layout using FDS's thermocouple input. Heat release rate was continually recorded in the domain. Hot gas layer temperature and depth were specified as devices co-located with the thermocouple array. For heat release rate and temperature, error bars are applied to peak experimental values. For the relative difference curves, error bounds are placed corresponding to the error for each quantity of interest.

Heat Release Rate

Figure 5-8 shows a comparison of the experimental HRR and the FDS HRR for each grid cell size.

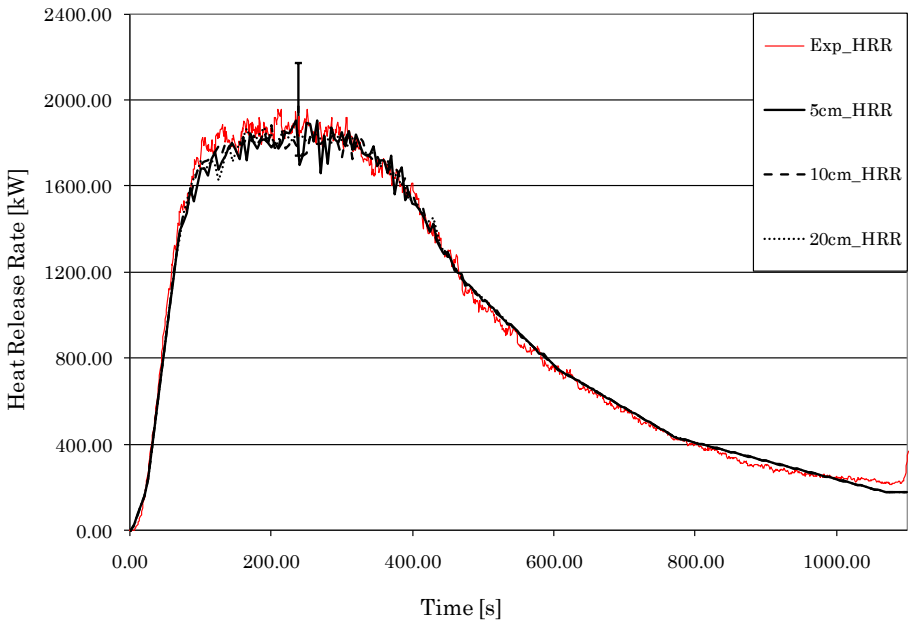

Figure 5-8: Laboratory-measured and FDS-simulated HRRs for each grid cell size

Temperature comparisons between experimental and simulated temperature measurements are made in Figure 5-9 through-Figure 5-12. Comparisons of data from all the remaining thermocouple locations can be found in Appendix A. Error bars for measured temperatures are provided based on measurement uncertainty. Error bars for FDS temperature predictions are not provided. The error of FDS temperature predictions is complicated and beyond the scope of this thesis. The total error of FDS temperature predictions is dependent on a propagation of all input uncertainties through the model combined with the errors caused by the assumptions made in the governing equations of the model and the errors introduced by the numerical solver. As shown in Figure 5-11, temperatures for locations within 1.2m of the ceiling were under-predicted for approximately 100 seconds after ignition. This is in large part because of the experimental design. FDS matched the measured HRR because the HRR in FDS is a user-defined input. The element that is difficult to account for in the experimental design is the filling of the upper region of the compartment structure required before smoke exits and registers in the calorimeter. Thus, it should be expected that temperatures will register first in the FDS simulation and appear to rise "faster." After 100 seconds, FDS over-predicted temperatures to values outside measurement error at thermocouple locations further than 1.2m from the ceiling for 0.2m and 0.1m cell sizes. Temperature predictions at all heights with a 0.05m cell size lay within measurement error. Reducing

the grid cell size reduced the magnitude of over-predictions, particularly at lower thermocouple locations.

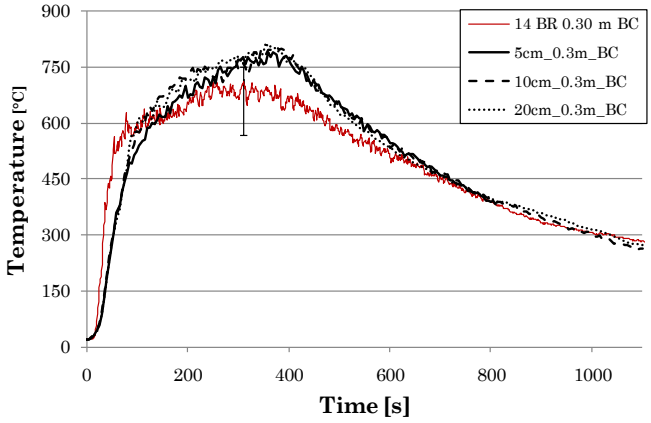

Figure 5-9: Predicted vs. measured temperatures 0.3m below the ceiling

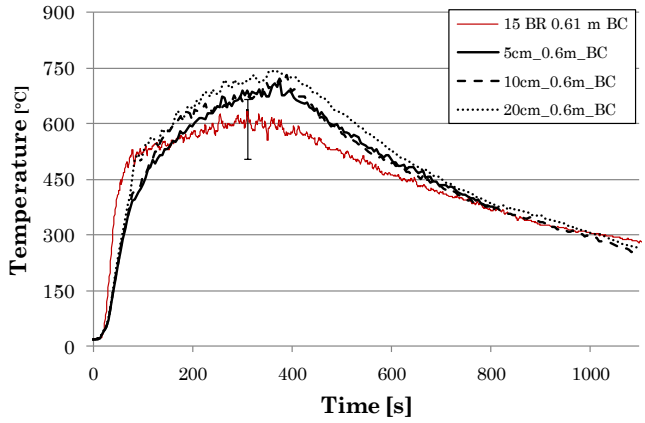

Figure 5-10: Predicted vs. measured temperatures 0.6m below the ceiling

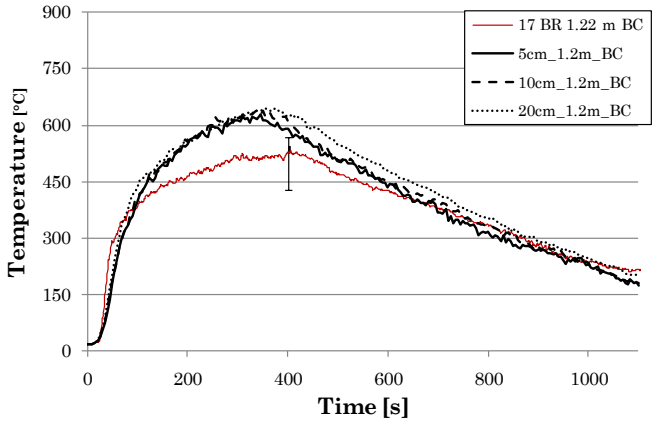

Figure 5-11: Predicted vs. measured temperatures 1.2m below the ceiling

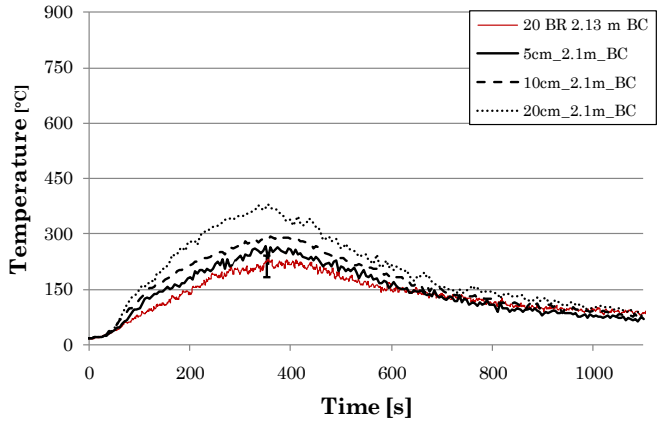

Figure 5-12: Predicted vs. measured temperatures 2.1m below the ceiling

HGL Temperature

HGL temperatures are under-predicted, like the temperature predictions near the ceiling, for the first 100 seconds of simulation. After this period, HGL temperature matches within previously cited uncertainty for all grid cell sizes. Though still within uncertainty, reducing the grid cell size from 0.2m causes predictions to converge towards the experimental HGL temperature. Figure 5-14 shows that for all grid cell sizes, HGL temperature predictions agree to within the 14% weighted expanded combined uncertainty presented in [44], after the approximate 100 second period of under-prediction.

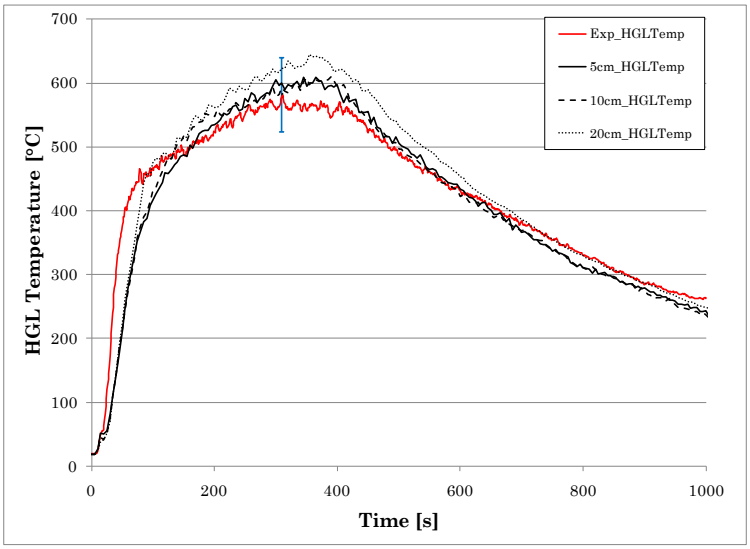

Figure 5-13: Calculated Experimental HGL Temperature and simulated HGL temperature with respect to grid cell size

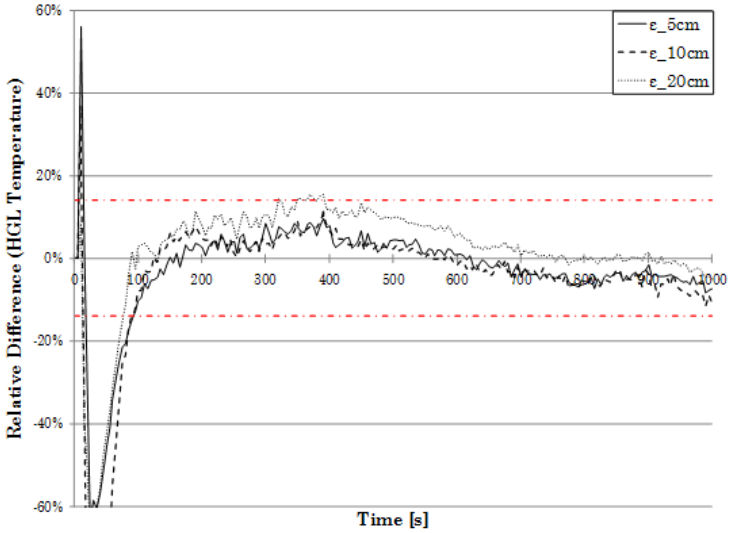

Figure 5-14: Relative difference, ε, versus time for HGL temperature

HGL Depth

Calculation of the hot gas layer depth is spurious for a brief period before generating a stable numerical output. The HGL calculation is designed to find the inflection point in the vertical temperature profile of the room. Until a thermal interface (inflection point) is clearly defined, the calculation produces spurious results.

Figure 5-15 highlights behavior present in the temperature versus time curves. HGL depth is over-predicted for the majority of the simulation. The underlying cause of this over-prediction is evident in the temperature versus time curves. Temperatures at lower thermocouple locations are shown to be over predicted for the duration of the simulation. As a result, the calculated location of the thermal interface depth moves toward the floor. As the size of the grid is reduced the amount that the HGL depth is over-predicted decreases; a smaller grid cell size reduces the amount that temperatures at lower thermocouple heights are over-predicted. Figure 5-16 shows that although the HGL depth is over-predicted, values for 0.05m and 0.1m cell sizes fall within uncertainty after approximately 110 seconds. It should be noted that for the first 35 seconds, the value of ε was set to zero to account for the time needed for a hot gas layer to form. The spurious values of the HGL calculation that occurred before a thermal interface was formed produced erroneous relative difference values.

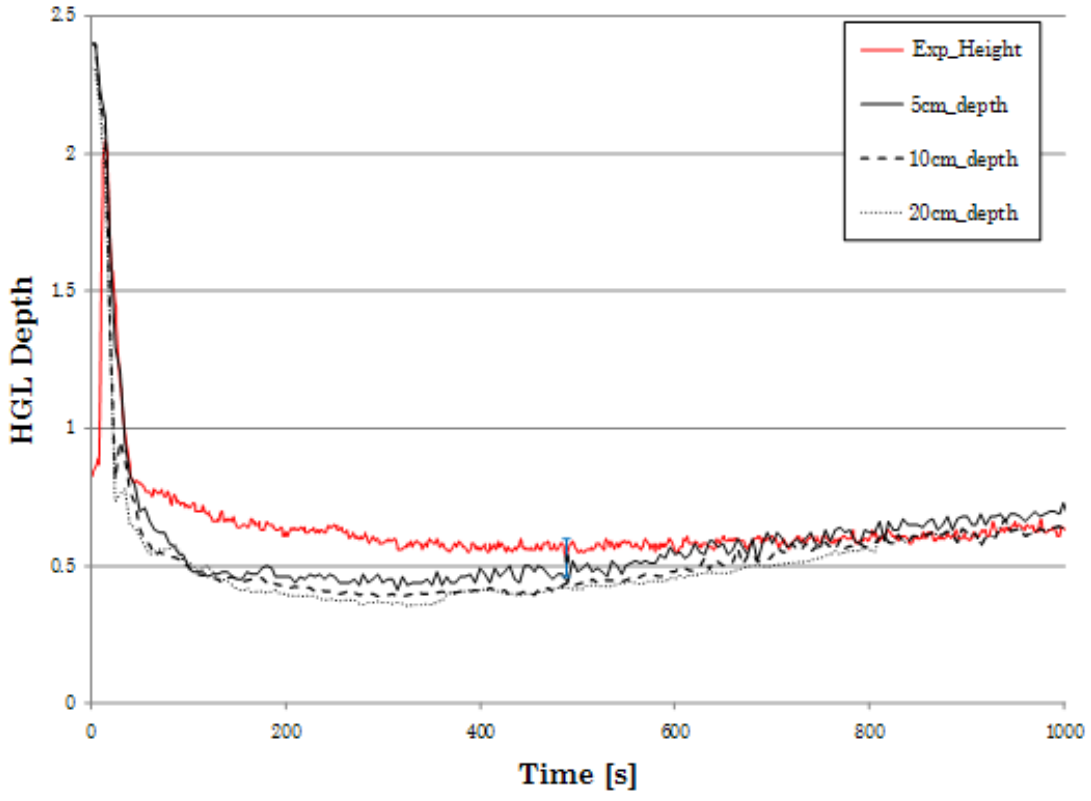

Figure 5-15: Calculated Experimental HGL depth and FDS HGL depth with respect to grid cell size

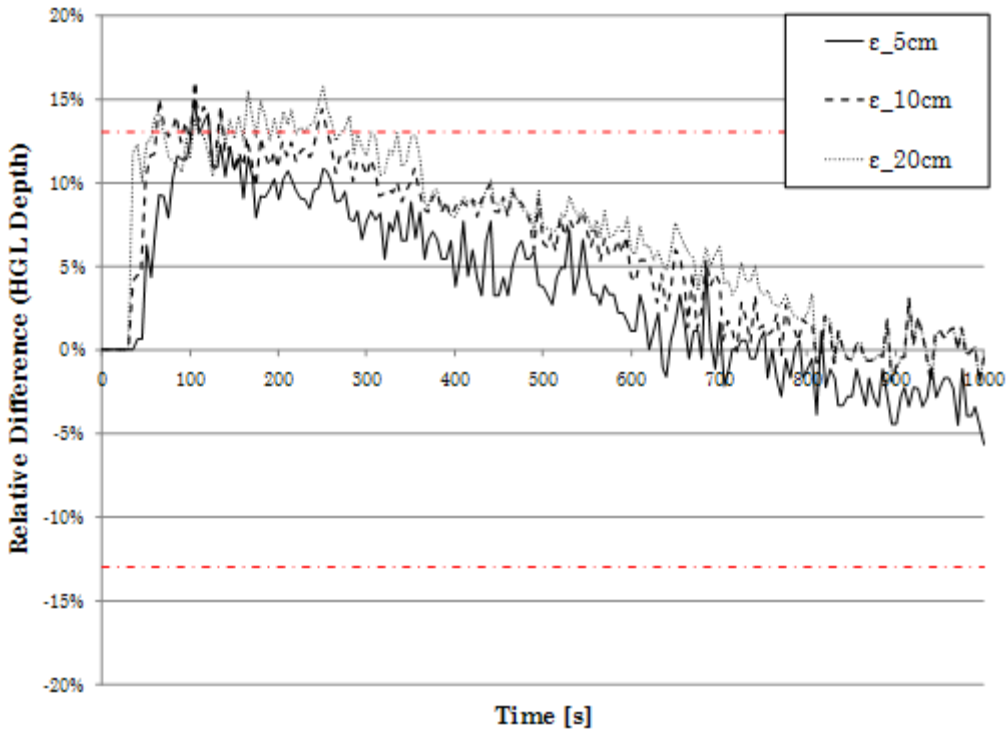

Figure 5-16: Relative difference, ε, versus time for HGL depth

5.1.7 Final Mesh Resolution

The 0.1m grid cell size was chosen as the final mesh resolution for simulation of the full burn facility. There are two basic reasons for choosing 0.1m for the final mesh resolution: the fidelity of FDS predictions and total elapsed simulation run time.

The most evident change in the fidelity of FDS predictions was displayed in the HGL temperature curves when grid cell size was reduced from 0.2m to 0.1m. The change between 0.1m and 0.05m HGL temperature predictions are negligible, as shown in Figure 5-14.

The change in fidelity of the predicted HGL depths between the 0.5m and 0.1m grid cell sizes are also non-appreciable, as shown in Figure 5-16. The 0.05m and 0.1m cell sizes result in approximately the same peak relative difference at approximately 105 seconds, which lies outside the 13% error bounds. After 105 seconds, both relative difference curves move back within the 13% error bounds at the same approximate time.

The 0.10m mesh resulted in a wall-clock elapsed time of approximately 3 1/3 hours. This total run time made it practical to perform numerous set-up simulations to test input file assumptions. The 0.5m grid cell size resulted in an elapsed wall-clock simulation time of 32 hours. These elapsed wall-clock times were considered in light of the much larger computational demands of the residential-scale model. Simulation times were expected to scale with increases in the computational domain and a subsequent increase in the number of computational cells per mesh.

In summary, the 0.1m grid cell size was chosen because reducing the grid cell size from 0.2m to 0.1m resulted in an appreciable increase in the accuracy of FDS predictions without significantly changing the elapsed wall-clock run time of the simulation. Reducing the grid cell size from 0.1m to 0.05m resulted in a significantly greater elapsed wall-clock simulation time without an appreciable change in the fidelity of FDS predictions.

5.2 Burn Facility Simulations

5.2.1 Domain & Mesh Resolution

The computational domain used for the burn facility simulations measured 13.0m x 15.0m x 5.7m. The simulation was run for 1100 seconds. The boundaries of the domain were extended 1m past the partition walls used to divide the burn facility in half. This allowed the inclusion of measured areas of leakage between halves and provided space in which to resolve flow. It was assumed that this flow can be neglected after leaking from the "test half" burn facility. Extension of the domain past the partition walls is shown on the left in the isometric view of the domain presented in Figure 5-17. The domain was also extended a minimum of 1m beyond the exterior walls of the structure in all directions to resolve leaks from the interior of the building to the ambient atmosphere.

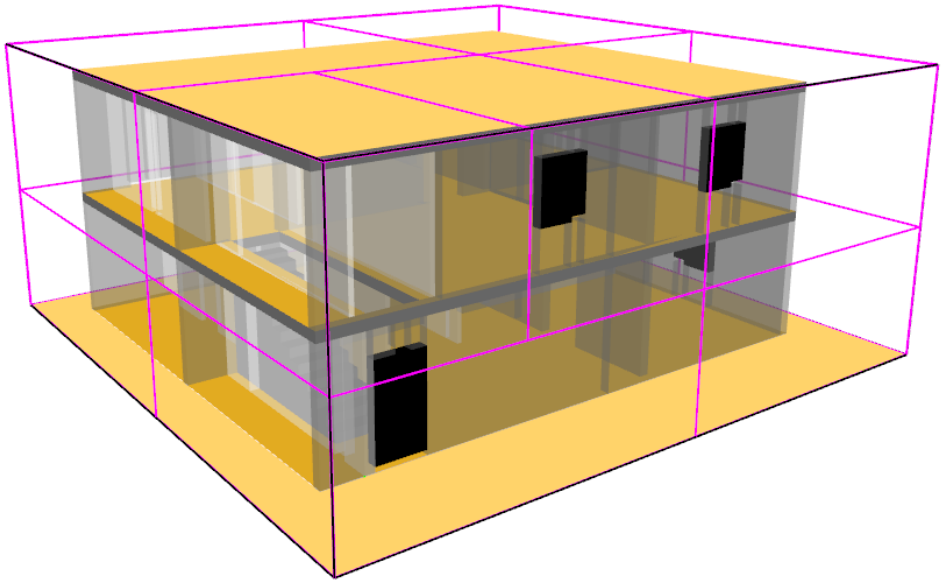

Figure 5-17: Domain used in simulation of field experiments

The mesh size used was 0.1m, based upon the results of the grid cell sensitivity study in Section 5.1. In total, the computational domain was divided into nine meshes. All but two meshes were equally sized. These two meshes, prescribed in the area of the stairwell, ensured that the perturbation pressure was being passed correctly between vertical mesh boundaries. Passing perturbation pressure vertically in this region was an obstacle during simulation set-up. The boundaries of the meshes are shown as the outer wire frame edges in Figure 5-17. Figure 5-18 shows the same isometric view as Figure 5-17 with the second floor cut away and the computational mesh overlaid.

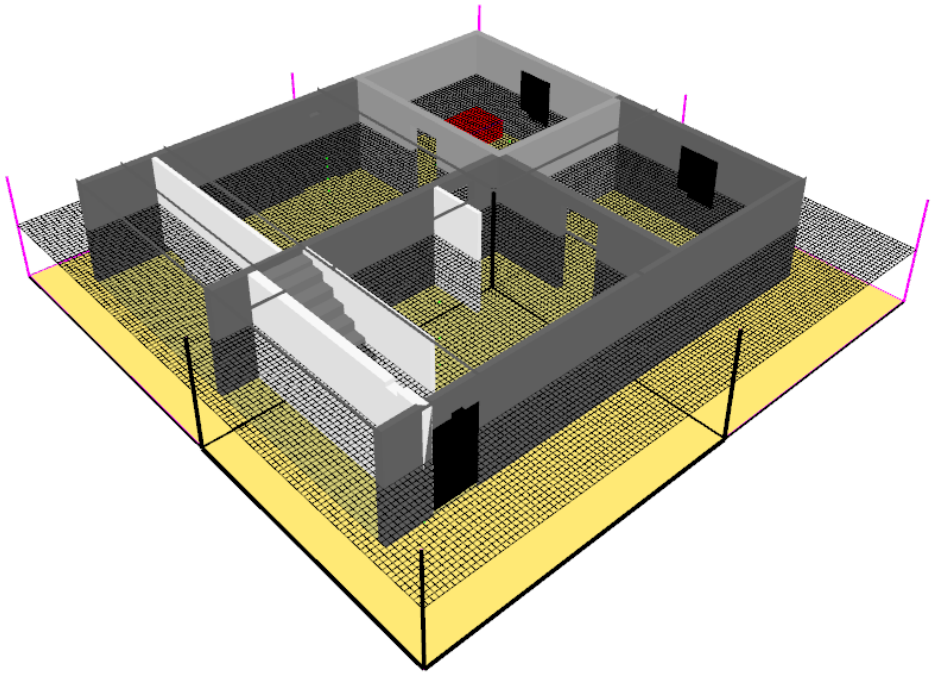

Figure 5-18: Isometric view of domain of burn facility with mesh overlay

5.2.2 Geometry

The geometry of the burn facility was input using the detailed dimensions from Figure 4-6. All of the geometry was prescribed using rectangular obstructions that conformed with the 0.1m mesh used throughout the domain. The 0.1m mesh allowed the geometry of the structure to be specified with excellent spatial agreement, resulting in minimal variations in dimensions. The non-combustible obstructions contained in the burn facility were not included in the simulation. Details of ventilation and leakage are described in Section 5.2.4.

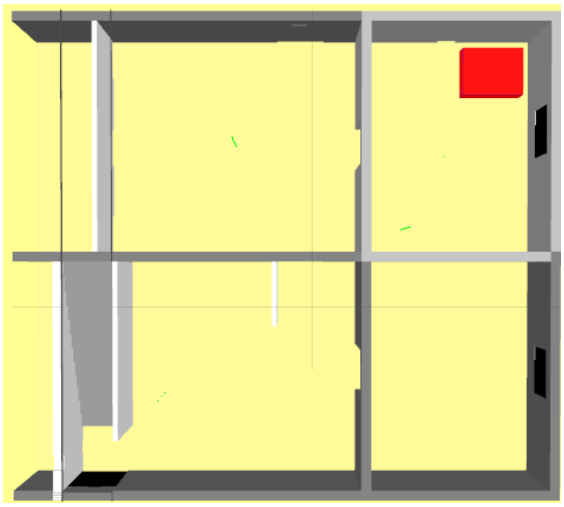

Figure 5-19: Top-down view of the first floor of the burn facility

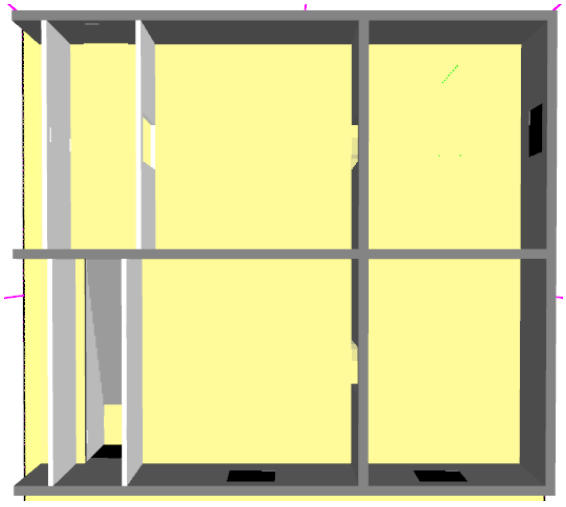

Figure 5-20: Top-down view of the second floor of the burn facility

5.2.3 Materials

The materials used in the simulations were assigned with the best-informed thermo-physical and chemical properties from common fire protection engineering literature. Where possible, material properties were gathered from manufacturer's specification literature. Where materials overlapped, such as in the burn compartment, the multiple-layer feature of FDS was used. Table 8 lists the material inputs for the simulations.

Material	Specific heat [kJ/kg·K]	Conductivity [W/m·K]	Density [kg/m3]	Thickness [m]	Location
Cement Board [60]	0.84	0.12	1153.0	0.013	Burn compartment walls, all ceilings
Gypsum [61]	1.09	0.18	677.6	0.013	All partition walls, behind cement board in burn compartment
Concrete [63]	1.13	2.0	2300.0	0.1	All floor surfaces
Steel [64]	0.46	45.8	7850.0	0.003	Stairs

Table 8: Material properties used in simulations of field experiments

The fuel was approximated as Douglas Fir, with a chemical formula of $CH_{1.7}O_{0.74}N_{0.002}$, a heat of combustion of 16400 J/kg·K, a CO yield of 0.01 kg/kg and a soot yield of 0.015 kg/kg [62].

5.2.4 Vents & Initial/Boundary Conditions

All boundaries of the computational domain were set to "open." This simulated a no-wind condition outside the structure. Open boundary conditions allowed hot, smoky gasses escaping the "test half" of the structure to flow to the boundaries of the domain where they were no longer calculated, or "out of the simulation."

The front door and windows were created by first adding holes the exterior walls of the simulated burn facility. These holes were then filled back in with obstructions assigned with logic control devices. The control devices allowed the obstructions to be removed at set points in time, simulating operability. The windows and doors are shown in black in Figure 5-21.

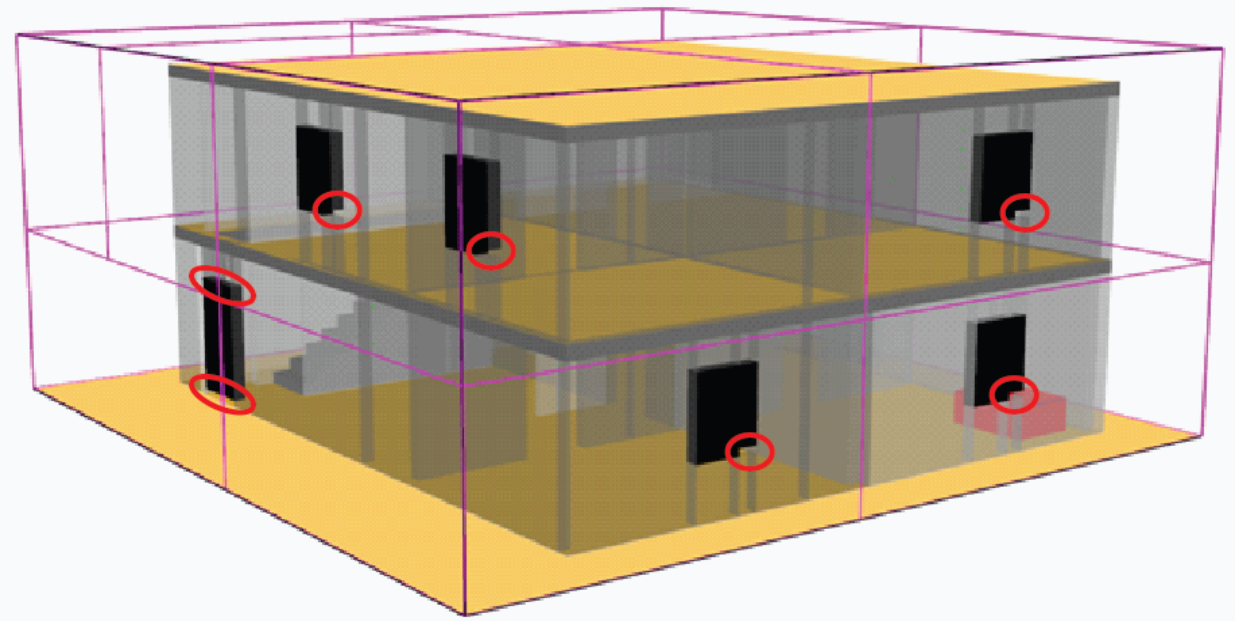

Figure 5-21: Isometric view of field structure showing window & door obstructions and leakage points (circled in red).

Numerous leakage points existed throughout the structure. Leaks were assigned with holes in the areas where visible leak paths existed in the burn facility. In the case of leaks with dimensions smaller than the resolution of the computational mesh, a lumped analysis was used. For example, the area of the seams around the perimeter of the windows were summed and approximated by creating a single hole through the bottom of the window obstruction. The dimensions of the hole were defined such that the area of the hole matched the summed leakage area as accurately as possible. Holes representing window leakage and door leakage are circled in red Figure 5-21.

Walls were assigned materials according to the locations indicated in Table 8 and given backing conditions that simulated being open to a void. The floors were assigned to be concrete. On the first floor, the floor was assumed to have an insulated backing condition. The second floor was assigned to have a void backing condition. All ceiling surfaces were assigned a void backing condition.

The fire was simulated by an obstruction representing the pallet stack shown in red, in Figure 5-21. The laboratory-measured HRR was used as the input for the field experiments. At the time of fire suppression, the HRR is manipulated as part of the assumption to simulate suppression. This is described in greater detail in the section that follows.

5.2.5 Assumptions for Simulating Door Opening and Fire Suppression

To simulate the front door opening a simple assumption is made. A physical obstruction of the same size and location as the front door, is instantaneously removed from the model. The obstruction is removed at the moment measured by the timing staff in the field experiments.

The suppression sub-model built into FDS was determined inappropriate for this simulation because it is based on research of sprinkler suppression of the Factory Mutual (FM) Class II commodity and FM plastic commodity in a rack-storage array. To simulate fire suppression, a simple assumption was used and is based on more appropriate wood crib suppression research and supported by video documentation of fire suppression in this study. The assumption in the simulation is that the user-defined HRR input is exponentially ramped down to zero over 4 seconds, beginning at the time that fire suppression was initiated. The research of Madrzykowski and Vettori provided an algorithm for estimating the HRR as a function of time [65]. Evans updated the algorithm to include variable sprinkler spray densities [66]:

$$\dot{Q}(t - t_{act}) = \dot{Q}(t_{act}) exp\left[{-(t - t_{act})}/{3.0(\dot{w}'')^{-1.85}}\right]$$

Where $\dot{Q}$ is the HRR, t_{act} is the time that suppression begins, and $\dot{w}''$ is the water spray density. Figure 5-22 plots this algorithm with two of the spray densities provided in the research and also plots the estimated spray density of the hose stream used in the field experiments ($\dot{w}''$ =2.59). The spray density of the hose was estimated using the known flow rate of the hose (100gpm) and the surface area of the pallets impinged upon by the hose stream (~26ft^2). The flow rate of the hose resulted in a spray density that was approximately 21 times greater than sprinkler density used in the suppression research. Consequently the fire was near-instantaneously suppressed.

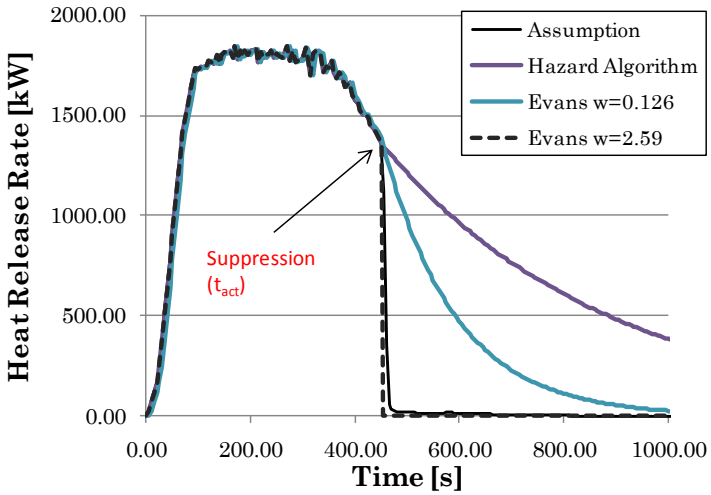

Figure 5-22: Suppression algorithm plotted for hose stream and two different sprinkler spray densities

The second means for determining the appropriateness of this assumption is by video analysis. Figure 5-23 through Figure 5-26 show how the fire was suppressed with respect to time. Fire suppression begins at 24:08 (with respect to the start of the recording) and ends and at 24:12. The estimated maximum water delivery is 6.5 gallons. Given this relatively small amount of water, the additional effects of water are neglected. The duration of fire suppression was consistent for each test.

Figure 5-23: 24:08 min, immediately prior to suppression

Figure 5-24: 24:09, after one second of water application

Figure 5-25: 24:10, after two seconds of water application

Figure 5-26: 24:12, fire completely extinguished after 4 seconds of water application

6 Comparison of Field Experiments and Simulations

Section 6 provides comparison of the field experiments with the simulations in three sub-sections. Section 6.1 focuses on the spread of heat and smoke throughout the multi-level, multi-compartment training structure. Section 6.2 focuses on changes in the thermal environment near the front door after the front door is opened. Section 6.3 focuses on changes in the thermal environment in the burn compartment after fire suppression. The results of simulation should be considered in light of the uncertainty of the laboratory-measured HRR as an input parameter.

6.1 Heat and Smoke Spread

Three characteristics are observed using TC measurements to establish how the heat and smoke spread (i.e., how the thermal environment developed) throughout the structure prior to the front door opening: the rate of temperature rise, the times that hot gasses begin to arrive in each measurement location, and the peak temperatures. These characteristics benchmark the experimental rate of temperature rise, the rate that heat and smoke spread through the structure and approximate the energy lost by the hot gasses as they spread. The characteristics were devised as a means to compare the simulated spread of heat and smoke from the burn compartment to the bedroom, separated by one floor and multiple compartments.

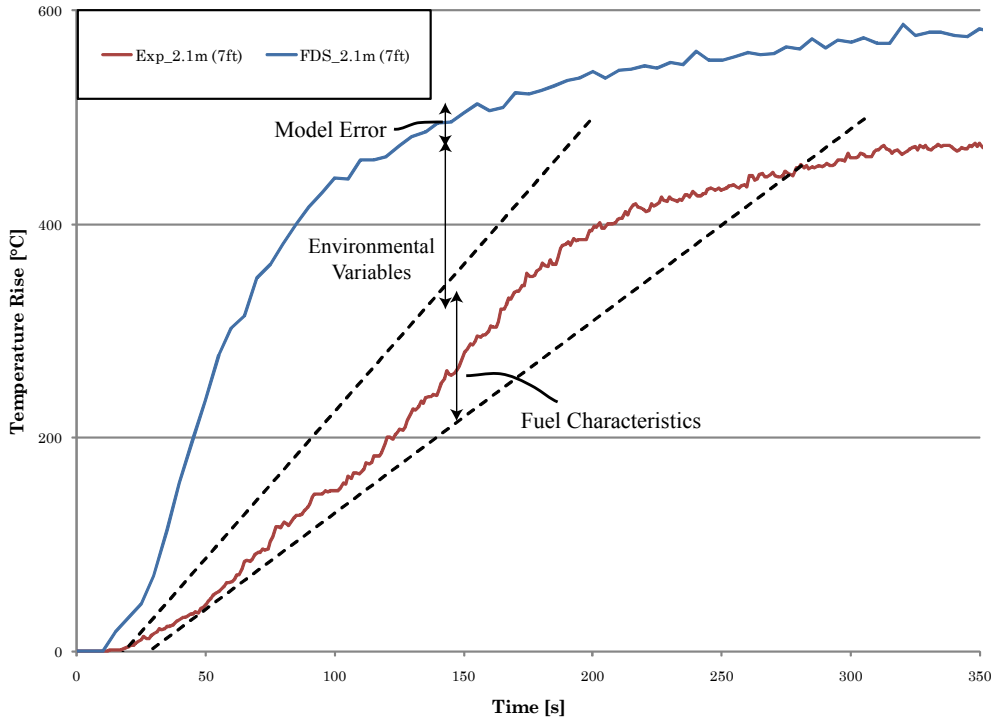

Figure 6-1: Comparison of measured simulated temperature at 7ft in the burn room

Temperature data from the experiment that most closely matches the average experimental rate of temperature rise and simulation data are plotted in Figure 6-1. This

experimental data was selected for comparison, because it was established that the rest of the experimental rates of rise vary by ±21%. Figure 6-1 shows the effectively the same separation between compared temperatures that is shown in Figure 4-31; The field experiment temperatures peak lower and later, due to the environmental variables discussed in Section 4.5. Given that the laboratory-measured HRR was used as an input parameter for simulation of the field experiments, this repeat of separation is expected. Included in the figure are arrows which qualitatively mark the contribution of the model, the testing environment and the fuel causing the separation. The portion due to intrinsic model error is relatively small compared to the total effects of the environmental variables and natural variation in the temperature measurements due to the characteristics of the fuel that cause changes in burning behavior. The model error is shown overlapping the simulated temperature. Although the model may have a bias in error for this particular quantity, the existence of such a bias was not investigated. The overlap is drawn to show that the model error contributes to the separation between the two plots, and does vary positively and negatively slightly from simulation to simulation due to the numerical solver. It is however known that this contribution in error is small, from previous FDS validation studies. Overlap is shown for the arrows marking error contribution of the environmental variables and the fuel characteristics because it is known that the characteristics of the fuel caused variation in burning leading to differences in measured temperature, but that the environmental variables also caused variation in the measured temperatures. The majority of the separation, marked by the environmental.

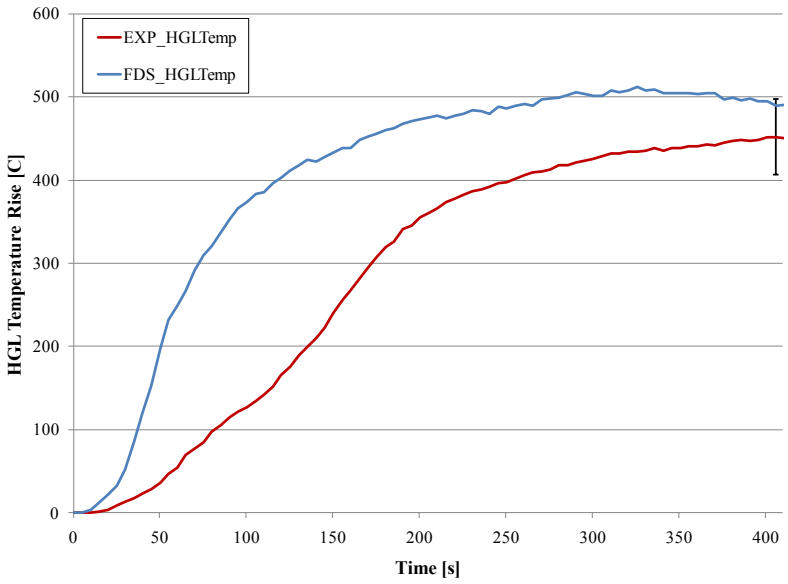

Figure 6-2: Comparison of measured and simulated HGL temperature in the burn compartment

Figure 6-2 compares the simulated and measured HGL temperature and shows that the HGL peak temperatures have an approximate 10% relative difference. The simulated HGL depth is shown in
Figure 6-3, with the experimentally measured HGL depth overlaid. The comparison in Figure 6-3 shows that FDS simulates the HGL depth to be approximately 0.2m, or approximately 10% of the room height, deeper than in the experiments.

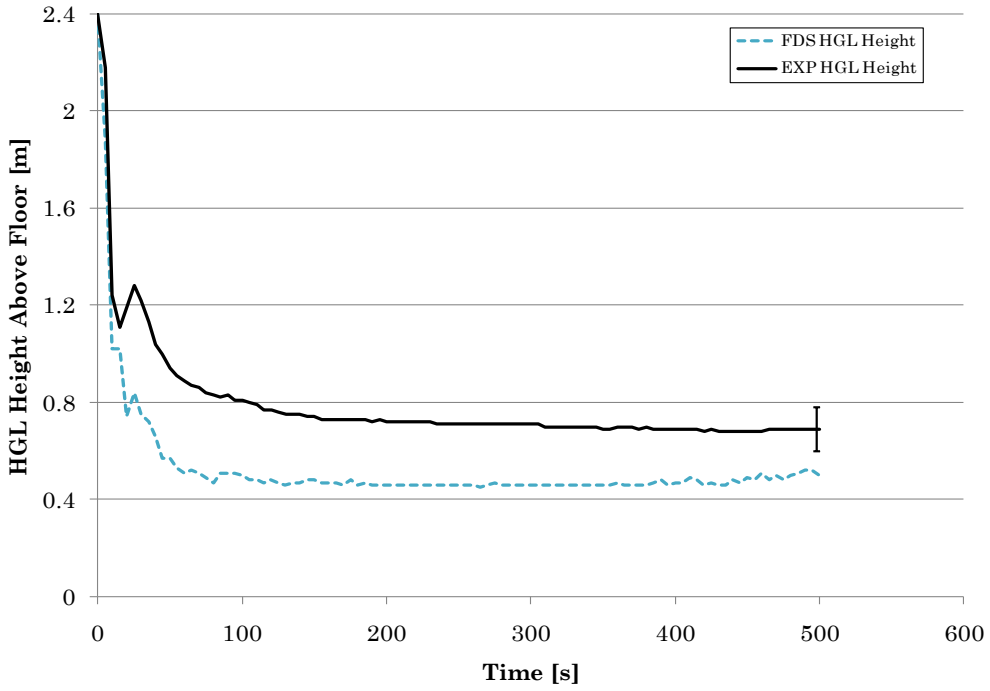

Figure 6-3: Comparison of the HGL depth calculated from measured and TC temperatures in the burn compartment

Statistical analyses of the seventeen experiments were performed to find the repeatability of the times of hot gas arrival and peak temperatures at the highest TC in each measurement location. These measurements are demonstrated in Figure 6-4 and Figure 6-5 for the front door and bedroom TC arrays. Statistical analyses of the seventeen experiments were performed to find the repeatability of the times of hot gas arrival and peak temperatures at the highest TC in each measurement location. These measurements are demonstrated in Figure 6-4 and Figure 6-5 for the front door and bedroom TC arrays.

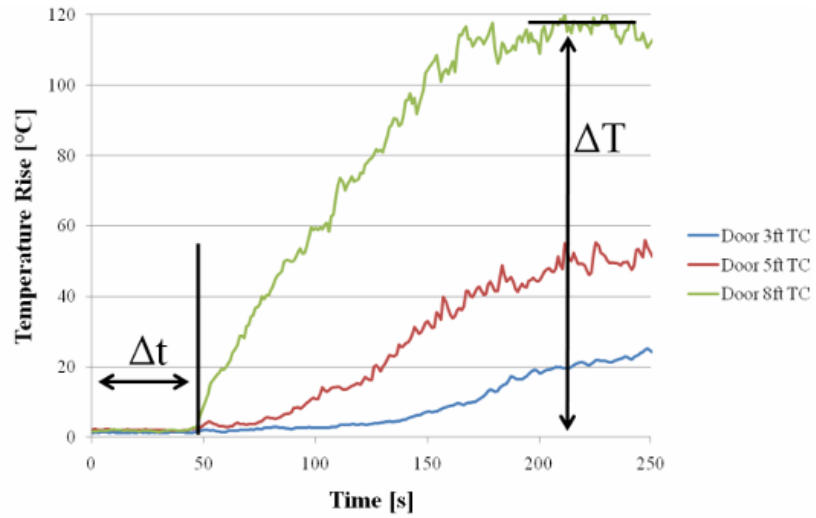

Figure 6-4: Time of hot gas arrival and peak temperature measurements for the front door TC array

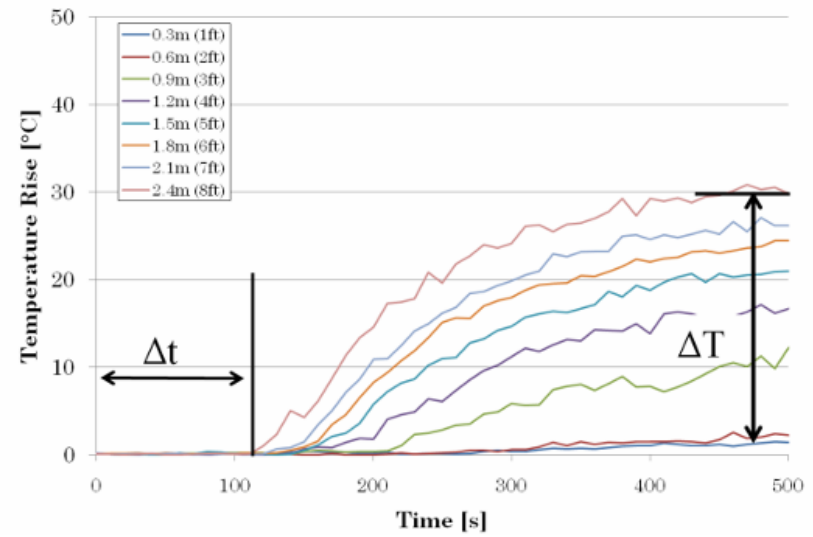

Figure 6-5: Time of hot gas arrival and peak temperature measurements for the bedroom TC array

The results of the statistical analysis, including simulation results are summarized in Table 9. All statistics in this document are reported within a 95% confidence interval. The simulated transport times of hot gasses are statistically similar to the transport times of hot gasses in the experiments. The peak temperatures in the burn compartment and near the front door are approximately 20% higher in the simulation than in the experiments. In the bedroom, the peak temperatures are approximately the same.

TC Array Location	Measured hot gas arrival time [s]	Simulated hot gas arrival time [s]	Measured peak temperature [ºC]	Simulated peak temperature [ºC]
Burn Compartment	17.2 ± 5.6	15	474 ± 48	587.6
Near Front Door	54.1 ± 12.2	50	139 ± 8.9	187.7
Bedroom	131.9 ± 44.2	110	37.1 ± 3.2	43.4

Table 9: Statistical analyses of hot gas arrival time and peak temperature at the highest location in each TC array

For the period of fire growth until peak burning, the simulated temperatures rose faster and peaked at higher temperatures than the experimentally measured temperatures. Peak temperatures were approximately 20% greater in the burn compartment and near the front door and nearly the same in the bedroom. The simulated fire also produced a deeper and hotter gas layer than measured in the experiments. The transport times of hot gasses throughout the structure were marginally faster in the simulation than the average transport times measured in the experiments. Previous FDS validation studies show closer agreement between measured and predicted temperatures for simple single burn compartment laboratory experiment simulations. The majority of the differences in fire growth rate and peak temperatures in this comparison are due to the "reality" of environmental conditions outside the laboratory. The field testing environment introduces numerous uncontrollable environmental variables existent at real structure fires (e.g., moisture, wind, lower ambient temperature, etc.) that are otherwise non-existent in the

lab. Inclusion of these environmental variables into FDS is an area of ongoing research. Regardless, the general behavior of the temperature rise and the spread of heat and smoke throughout the structure agrees well with the experiments.

6.2 Temperature Changes After the Front Door is Opened

Temperatures measured near the front door and in the burn compartment were studied to establish how the thermal environment changed after the front door was opened in the experiments. Figure 6-6 and Figure 6-7 show plots of temperatures from the TC arrays in the burn compartment and the array near the front door for one set of test data. The figures are provided to show how the thermal environment changed in response to the front door opening and help to explain how the change in the thermal environment was measured. The times that the front door opened and the fire was suppressed are marked with vertical lines in both figures.

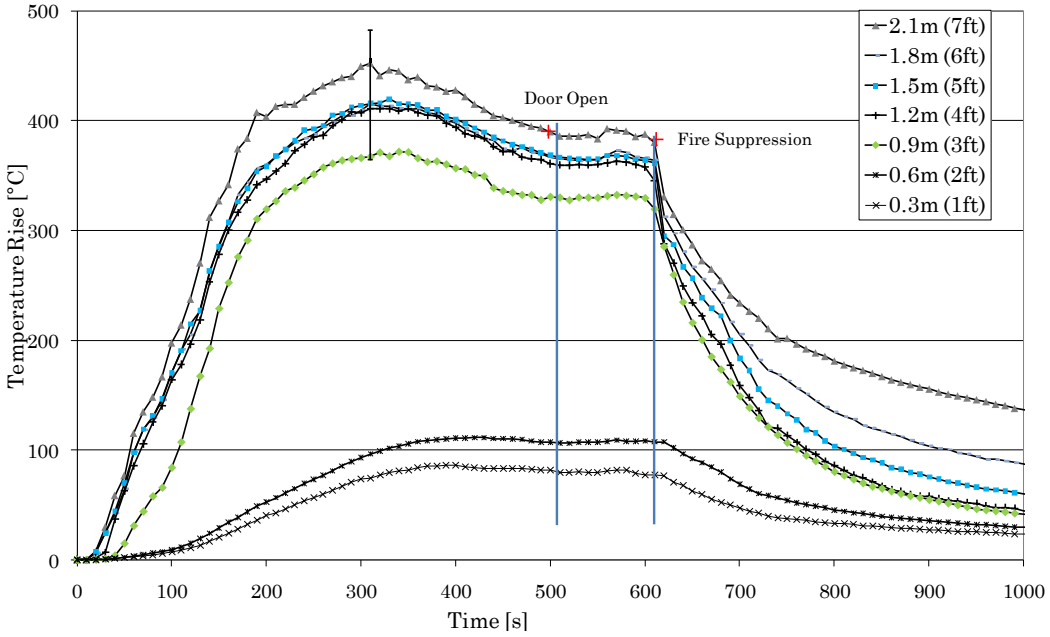

Figure 6-6: Temperatures measured by TC array in the burn compartment

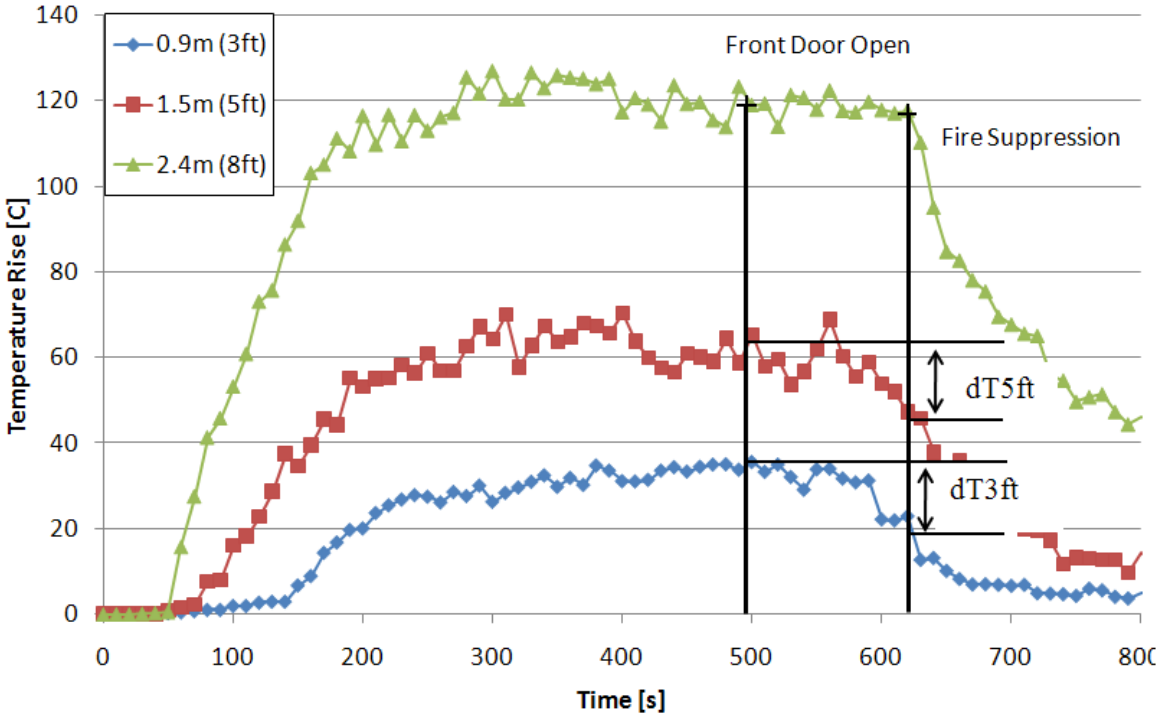

Figure 6-7: Temperatures measured by the TC array near the front door

Figure 6-6 shows that after the front door is opened, the thermal environment remains unchanged until fire suppression. Figure 6-7 shows that opening the front door caused temperatures to decrease at the 1.2 m and 0.9 m heights, while the temperature at 2.4 m stayed relatively constant. A statistical analysis was performed to determine how much temperatures near the front door decreased in all 17 tests fire suppression. Figure 6-7 shows how temperature change was measured; temperature change was taken as the difference in temperature between the time the front was opened and the time of fire suppression. Temperature changes were normalized by the temperature measured at the time the door opened in consideration of measurement uncertainty (+6/-20%). Six tests registered temperature changes greater than measurement uncertainty at 0.9 m and 1.2 m. In all six of these tests, greater than 60 seconds elapsed between the front door opening and fire suppression. In all 11 other tests, less than 60 seconds elapsed between events. In other words, a minimum of 60 seconds of elapsed time between the door opening and fire suppression was needed for the thermal environment to undergo a temperature change greater than measurement uncertainty. At the 1.2 m height temperature changed by 48.7 ± 21.1% and at the 0.9 m height, a 30.8 ± 13.9% change in temperature was recorded. In all tests, temperature changes at 2.4 m were negligible. These statistics support the temperature behavior shown in Figure 6-7. The statistics quantify how much the thermal environment changed near the front door, after it was opened, in order that it can be determined if the simulation reproduces the same amount of change in the thermal environment.

The times chosen to simulate the door opening and fire suppression are based off of the field experiment with the longest amount of time elapsed between these two events. This

gave the model the longest time to reproduce the same measure of temperature changes recorded in the experiments. The temperature changes in the simulation that resulted from opening the front door were 9.7% at the 2.4 m height, 7.4% at the 1.2 m height and 37.6% at the 0.9 m height. The simulation results show agreement within a 95% confidence interval for temperature change at the 0.9m height. The simulated temperature changes at the 1.2 m height are below the lower confidence bound of temperature change. Temperature change at 2.4 m is simulated as appropriately as can be determined by the preceding statistical analysis because changes in both the experiments are smaller than measurement uncertainty.

The cause of discrepancy between measured and simulated temperature changes at 1.2 m was thoroughly investigated using Smokeview visualizations. In the experiments, temperatures at 0.9m and 1.2m change as if they are located below the thermal interface of the HGL; they cool after the door is opened, while the temperature at 2.4 m stays relatively constant. In the simulation, the temperature at 0.9m changes as if it is below the thermal interface of the HGL and the temperature at 1.2m and 2.4m behave as if they are in the HGL. Figure 6-8 through Figure 6-11 show a sequence of temperature slice files for the period of time starting when the door opens and ending just prior to suppression. The location of the thermal interface is marked with a dashed black line and the TCs are outlined in black, to aid in visualization. The sequence shows that the thermal interface of the HGL is initially located at around 0.8 m, and rises above 0.9 m within 60 seconds. Before fire suppression the interface rises to approximately 1.1m. This sequence shows cooling at 0.9 m, and that the HGL is below 1.2 m and above 0.9 m in the simulation. In Figure 6-3, the HGL depth is over-predicted by approximately 0.2 m in the burn room. Assuming that this amount of HGL depth over-prediction is constant, the HGL depth near the front door in the experiments should start at approximately 1.0 m (0.8 m + 0.2 m) and rise to approximately 1.3 m (1.1 m + 0.2 m) resulting in the cooling seen at 1.2 m in the experiments but not in the simulation.

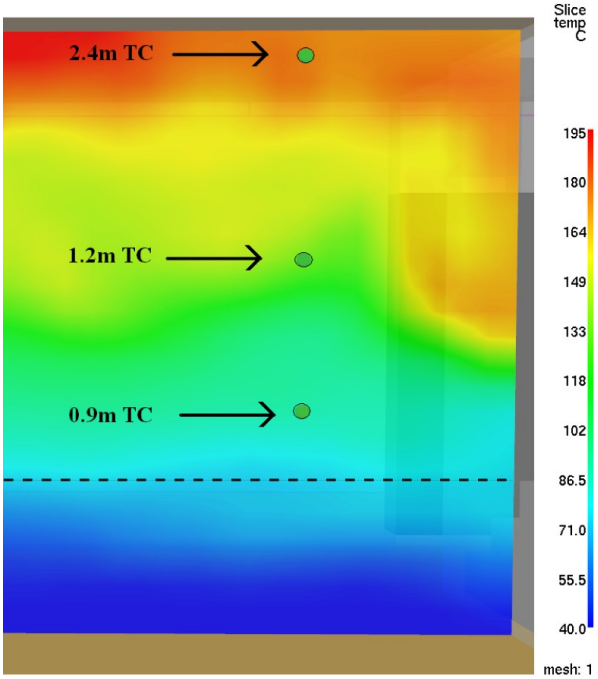

Figure 6-8: Vertical thermal profile of the room proximate to the front door at t = 498 sec (time the door opens)

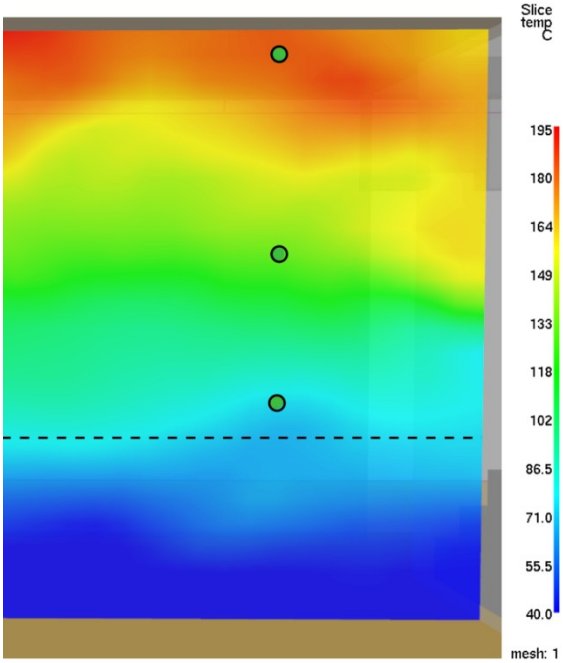

Figure 6-9: Vertical thermal profile 9.7 seconds after the door opens, showing the thermal interface immediately near the 0.9 m TC.

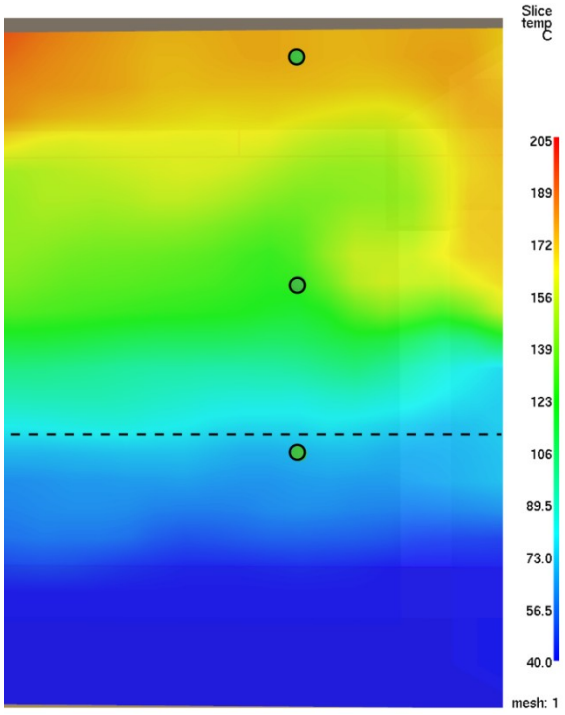

Figure 6-10: Vertical thermal profile 59 seconds after the door opens, showing the thermal interface as it rises above 0.9 m

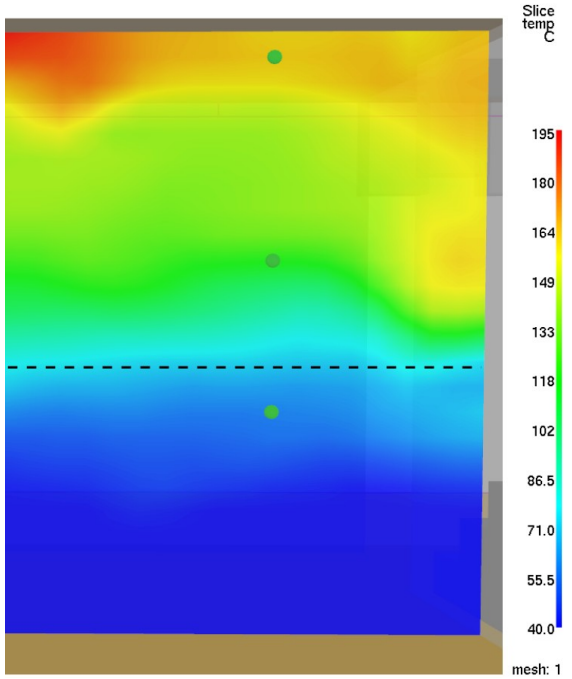

Figure 6-11: Vertical thermal profile 109.7 seconds after the door opens, showing the thermal interface between the 0.9 m and 1.2 m TCs

6.3 Temperature Changes Caused by Fire Suppression

Changes in the thermal environment caused by fire suppression are determined by examining the HGL temperature and depth in the burn compartment. Specifically, the rate of HGL temperature decay, the amount of time it takes for the HGL depth to respond to fire suppression and the rate at which the depth changes are examined. The HGL temperature is examined for two reasons. First, the HGL temperature describes the bulk temperature change of all of the TCs in the HGL. If the decay of the measured and simulated HGL temperatures match, then the general temperature behavior of all the TCs in the HGLs match which eliminates the need to compare temperature changes at each TC location. Second, the HGL temperature will be a primary visualization of the computer-based fire fighter trainer, so it is necessary to know how well the simulated HGL temperature change matches the experimental HGL temperature change. The HGL depth is examined because it describes the location of the HGL interface and therefore is a component in visualizing the HGL.

To analyze the temperature decay of the HGL for the seventeen tests, the time of fire suppression was set as time zero and each set of data were normalized by the temperature at this time. The result is shown in Figure 6-12 for 300 seconds after the initiation of fire suppression.

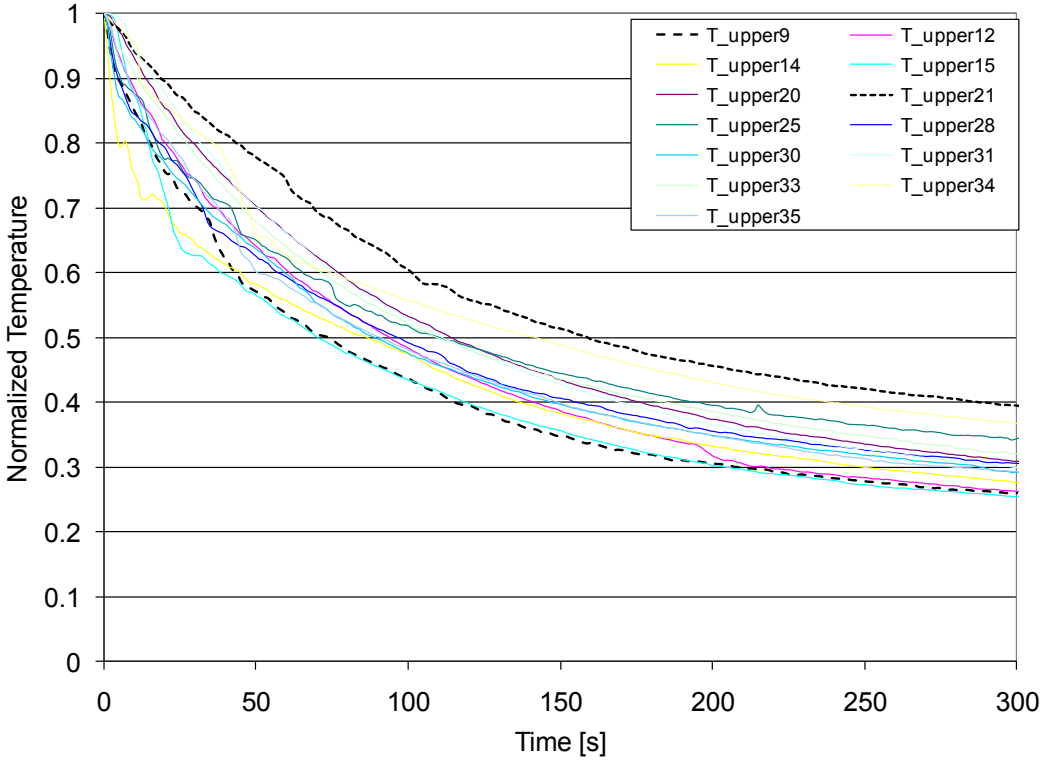

Figure 6-12: Normalized HGL temperature curves of seventeen tests, with t= 0 the time of suppression

It is apparent in Figure 6-12 that the HGL temperatures for all the tests decay in the same manner, but at varying rates. It is also seen that two tests (test 9 and test 21) bound the rates of temperature decay. These two tests are chosen for further analysis and

comparison with the rate of HGL temperature decay in the simulation. If the simulation properly reproduces HGL temperature decay, the rate of decay should fall between these two tests. To determine their decay rates, a single phase exponential decay trend line was fit to each test. Figure 6-13 shows the results.

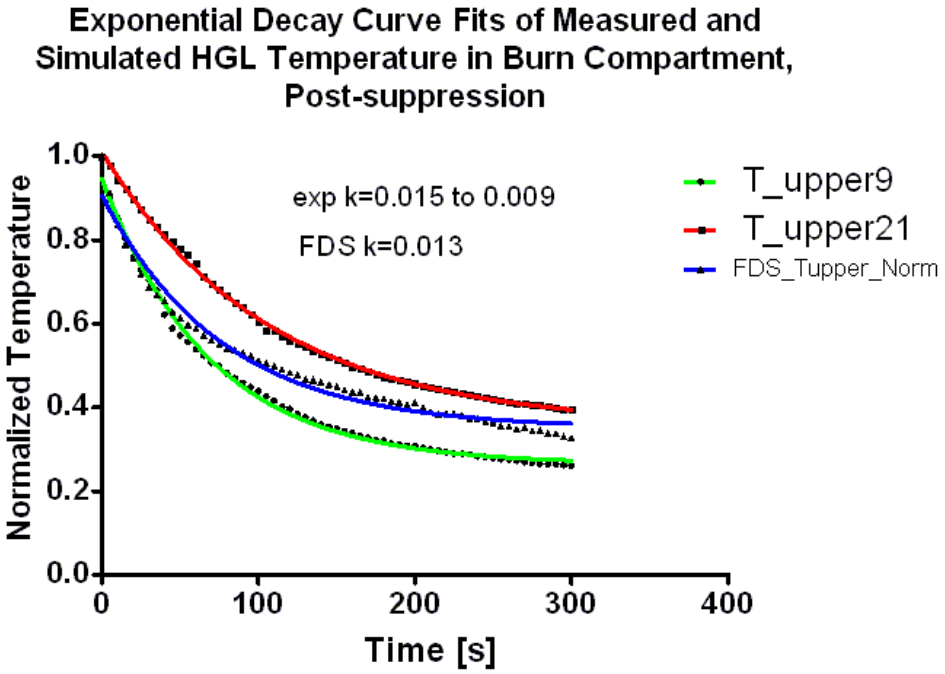

Figure 6-13: Single-phase exponential decay curve fits of measured HGL temperatures after fire suppression

The decay constants k = 0.015 and k = 0.009 were determined from the exponential curve fits, which correspond to the faster decaying HGL temperature in test 9 and slower decaying HGL temperature in test 21. Also included in Figure 6-13 is the plot of the simulated HGL temperature decay and the matching decay constant. The exponential decay curves fit well to the data and the decay constant for the simulation falls close to the middle of the range of temperature decay in the experiments.

A similar analysis was carried out for the HGL depth, and is shown in Figure 6-14. The time of fire suppression was set as time zero and HGL depth is plotted for all 17 tests and the simulation. The comparison shows that the simulated HGL depth rapidly rises approximately 0.4 m within the first 50 seconds. After 50 seconds the HGL rise slows, transitioning into a linear rate of rise. For experiments it takes approximately 50 seconds for the HGL depth to begin to rise. After 50 seconds, the rate of rise is linear. After approximately 225 seconds, the experimental HGL depth has risen 0.4 m and "caught up" to the simulated HGL depth. The comparison is kept to 250 seconds from fire suppression. After 250 seconds, faster performing fire crews started ventilating the burn compartment window and comparison with the simulation is no longer appropriate.

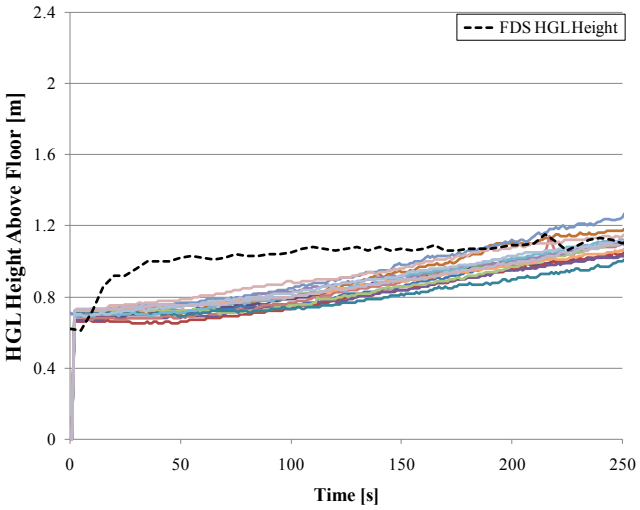

Figure 6-14: Comparison of measured simulated HGL depth after suppression

7 Conclusions

A sensitivity study was carried out that simulated the laboratory experiments with different mesh resolutions to determine the cell size necessary to accurately simulate the fire dynamics inside the burn compartment. Results were considered in light of the computational requirements for simulation of the considerably larger, residential-scale burn facility. A mesh resolution of 0.1 m (per cell dimension) was determined to provide a practical wall-clock simulation time and to predict floor to ceiling temperatures and HGL temperature and depth to within established measurement uncertainties.

Given the assumptions used for the input parameters, particularly the HRR, heat and smoke spread to measurement locations throughout the test structure at times matching experimentally measured times within a 95% confidence interval. Predictions of peak temperatures near the ceiling were within approximately 20% of corresponding experimental measurements in the burn compartment, near the front door and in the bedroom. In the burn compartment, where the HGL reduction method could be used to produce reliable calculations, the hot gas layer temperature was predicted to within 10% of the experimental HGL temperature and the HGL depth was predicted to within 10% of the room height.

This study also investigated changes in the simulated thermal environment due to ordinary fire department operations. Two fire fighter actions were focused on: opening the front door (thus changing the ventilation of conditions of the structure) and fire suppression. After the front door was opened, the temperature change near the door, at 0.9m and 2.4 m, is correctly simulated to within a 95% confidence interval. A slight over-prediction of the HGL depth caused the mismatch of temperature between the temperatures simulated and measured at 1.2m. However, Smokeview visualizations were used to show that the HGL interface rose after the door opened, which demonstrated the expected cooling behavior at a slightly lower location. With the flow rate of the typical hose stream, fires the size of the fire in this study can be assumed to be instantaneously suppressed. With this assumption, the simulation provides excellent agreement in the rate of HGL temperature decay after fire suppression; the HGL temperature decayed at a rate between the fastest and slowest rate decay measured in the experiments. After fire suppression, initially the simulation HGL depth rose faster than the experiments, but throughout the duration of 250 second period examined the HGL depth raised the same amount for both the simulation and the experiments.

Within the limitations of the data and given the relatively large input parameter uncertainty, FDS appropriately simulated the spread of heat and smoke throughout the two-story burn facility prior to any fire fighter actions, changes in the thermal environment after the front door is opened, and the changes in the thermal environment caused by fire fighters performing fire suppression.

8 Future Work

This research demonstrated the ability of the FDS to simulate the spread of heat and smoke and the changes in the thermal environment due to fire fighter actions. However, it remains to be determined whether FDS simulations can produce discernibly different visualizations of the thermal environment and fire behavior that result from different times that fire fighter actions are performed. For instance, whether it is observable how the temperature throughout the structure is affected when the front door is opened early to perform a rapid search and rescue and left open until fire attack versus if the door is left closed for longer until a suppression team is prepared to attack the fire.

To take the next step, future research should consider the limitations of the field experiments in this study in the design of further experiments. The major limitations to the field experiments were the control of environmental variables, a known heat release rate and the availability and positioning of instrumentation. Having gained knowledge and experience from the field experiments in this study the following is a list of suggestions, categorized by environmental variable, which could provide improved control over the environment in the field experiments:

- Ambient temperature – if possible, conduct the field experiments during a season with temperatures closer to room temperature
- Fuel mass and moisture content – ideally, use a flow-controlled gas burner as a fire source to limit temperature changes in the thermal environment related to issues specific to wood pallets (pallets absorbed suppression water, diminishing burning prior to fire fighter action). Given a certain flow, a good estimate of HRR would be possible.
- Moisture of wall linings – if possible, allow longer times for a burn compartment to dry out after fire suppression, replace wall linings or use a different burn compartment
- Thermo-physical properties of construction materials – collect samples of construction materials and perform bench scale tests to characterize the thermo-physical properties to inform model inputs.

- Wind direction/magnitude – although the magnitude and direction of the wind cannot be controlled, portable weather stations should be deployed to gather weather data. In this particular study, wind conditions were investigated using publicly available data from nearby weather stations and vetted with videos taken during the experiments. An improvement would be to record this information on-site. This information could potentially be used to allow the user to impose a wind condition in FDS simulations.
- Building envelope leakage – The total leakage of the test structure in this study was difficult to quantify with the dimensional measurements of visible leakage paths. For the experiments, leakage testing equipment was unavailable. It is suggested that this equipment be used to at a minimum be used to quantify the total leakage of a test structure, if not quantifying the leakage of rooms inside the structure.

Improving the control of environmental testing conditions, while making the experiments less representative of the variability of "real world" fires, would simplify the determination of the impacts of different fire fighter actions or different fireground tactics. Later experiments could reincorporate a greater level of variability in environmental conditions to consider the bigger picture of possible fire scenarios.

Further instrumentation should be included in future experiments to make it possible to perform more detailed analyses of the impact of fire fighter actions on the thermal environment. The instrumentation plan for the field experiments in this study was designed to satisfy the requirements of the parent study, the Multiphase Study on Fire Fighter Safety and the Deployment of Resources. For instance, locating a standard 8-TC array to the center of the compartment near the front door would have allowed examination of the impact of the front door opening on hot gas layer calculations. However, for these experiments in this study, the TC array would have become tangled and destroyed by the movement of fire fighters inside the structure. Instrumentation should also be included in ventilation openings to measure the flow after a ventilation action is performed.

During the design of the simulations better assumptions may be possible if more information were available regarding the environmental conditions during experimentation. For instance, it may be possible to use wind measurements to impose a wind condition in the simulation. This would be of particular value when observing changes in the thermal environment that result from non-mechanical ventilation.

9 References

[1] K. McGrattan, S. Hostikka, and J. Floyd, "Fire Dynamics Simulator (Version 5) User's Guide," NIST SP 1019-5, 2009.

[2] K. McGrattan, S. Hostikka, J. Floyd, B. Klein, and K. Prasad, Fire Dynamics Simulator (Version 5) Technical Reference Guide, 2009.

[3] G.P. Forney, "User's Guide for Smokeview Version 5: A Tool for Visualizing Fire Dynamics Simulation Data," NIST, Gaithersburg, MD, SP 1017-1 2007.

[4] National Fallen Firefighters Foundation, "Report of the National Fire Service Research Agenda Symposium," , Emmitsburg, MD, 2005.

[5] United States Department of Energy. (2008) 2005 Residential Energy Consumption Survey--Detailed Tables. Spreadsheet.

[6] Delmar, Cengage Learning, *Firefighter's Handbook: Firefighting and Emergency Response*. Florence, KY: Cengage Learning, Inc., 2008.

[7] J. Loyd and J. Richardson, *Fire and Emergency Services*.: Bradybooks, 2009.

[8] The International Fire Service Training Association, *Essentials of Fire Fighting, 5th Ed.* Stillwater, OK: Fire Protection Publications, 2008.

[9] National Fire Protection Association, NFPA 1403: Standard on Live Fire Training Evolutions, 2007.

[10] W. L. Grosshandler, N. P. Bryner, D. Madrzykowski, and K. Kuntz, "Report of the Technical Investigation of The Station Nightclub Fire. Volume 1.," NIST, Gaithersburg, MD, NCSTAR 2, 2005.

[11] Daniel Madrzykowski and Robert L. Vettori, "Simulation of the Dynamics of the Fire at 3146 Cherry Road NE Washington D.C., May 30, 1999," NIST, Gaithersburg, MD, NISTIR 6510, 2000.

[12] D. Madrzykowski, G.P. Forney, and D. Walton, "Simulation of the Dynamics of a Fire in a Two-Story Duplex -," Gaithersburg, MD, NISTIR 6854, 2002.

[13] R. L. Vettori, D. Madrzykowski, and W. D. Walton, "Simulation of the Dynamics of a Fire in a One-Story Restaurant, Texas, February 14, 2000.," NIST, Gaithersburg, MD, NISTIR 6923, 2002.

[14] American Society for Testing and Materials, ASTM E 1355: Standard Guide for Evaluating the Predictive Capability of Deterministic Fire Models, 2005.

[15] N. Dembsey, M. Janssens, and M. Hurley. (2009) Fire Pyrolysis Parameter Guidance. [Online]. http://sites.google.com/a/fire-pyrolysis-parameter-guidance.org/fire-pyrolysis-parameter-guidance/

[16] Michael J. Jr. Karter, "Fire Loss in the United States 2008," Quincy, MA, 2009.

[17] Michael J. Jr. Karter, "Fire Loss in the United States 2007," Quincy, Ma, 2008.

[18] Michael J. Jr. Karter, "Fire Loss in the United States During 2006," Quincy, MA, 2007.

[19] M Ahrens, "Trends and Patterns of U.S. Fire Losses in 2008," Quincy, MA, 2009.

[20] National Fire Protection Association, NFPA 1710: Standard for the Organization and Deployment of Fire Suppression Operations, Emergency Medical Operations, and Special Operations to the Public by Career Fire Departments, 2010 Edition., 2009.

[21] Michael J. Jr. Karter, "Patterns of Firefighter Fireground Injuries," Quincy, MA, 2009.

[22] United States Fire Administration, "Firefighter Fatalities in the United States in 2008," Emmitsburg, MD, 2009.

[23] Divergent Simulations, LLC. (2009) True Hero Simulations. [Online]. http://www.trueherosims.com/index.php?option=com_content&task=view&id=23&Itemid=39

[24] Flame-Sim LLC. (2008) FLAME-SIM — Fire Department Training Simulation Software. [Online]. http://www.flame-sim.com/upload/presentationmaterials/11/presentationmaterials-1243353093.pdf

[25] VSTEP. (2009) Vstep RescueSim - Virtual Emergency Response Training. [Online]. http://www.rescuesim.com/

[26] Action Training Systems, Inc. (2009) Fire Simulator: StageIT the Ultimate Fire Simulator. [Online]. http://www.action-training.com/product.aspx?training=StageIT_Emergency_Response_Simulator&pid=541

[27] D. Tate, S. Sibert, and T. King, "Using Virtual Environments to Train Firefighters," *IEEE Computer Graphics and Applications*, vol. 17, no. 6, pp. 23-29, 1997.

[28] T. St. Julien and C. Shaw, "Firefighter Command Training Virtual Envrionment," pp. 30-33, 2003.

[29] The College of Computing at Georgia Tech. (2005) Georgia Tech College of Computing. [Online]. http://www.cc.gatech.edu/news/helping-firefighters-with-virtual-reality-technology

[30] University of Greenwich. (2009) Fire Safety Engineering Group (FSEG). [Online]. http://fseg.gre.ac.uk/smartfire/index.html

[31] Cranfield University, "SOFIE (Simulation of Fires in Enclosures) - User's Manual," Cranfield, Bedfordshire, U.K., 2006.

[32] R. Yin and W.K. Chow, "Building Fire Simulation with a Field Model Based on Large Eddy Simulation," vol. 45, 2002.

[33] Y. Xin, J.P. Gore, K.B. McGrattan, R.G. Rehm, and H.R. Baum, "Large Eddy Simulation of Buoyant Turbulent Pool Fires.," in *Twenty-Ninth Symposium (International) on Combustion*, Pittsburgh, Pennsylvania, 2002, pp. 259-266.

[34] S. Cochard, "Validation of Fire Dynamics Simulator (Version 2.0) Freeware," *Tunnel Management International Journal*, vol. 6, no. 4, December 2003.

[35] K.M. Liang, T. Ma, J.G. Quintiere, and D. Rouson, "Application of CFD Modeling to Room Fire Growth on Walls.," National Institute of Standards and Technology, Gaithersburg, MD, NIST GCR 03-849 2003.

[36] K. Hill, J. Dreisbach, K. McGrattan, R. Peacock, and A. Hamins, Verification and Validation of Selected Fire Models for Nuclear Power Plant Applications, 2007.

[37] J. Floyd, "Comparison of CFAST and FDS for Fire Simulation with the HDR T52 and T52 Tests," Gaithersburg, MD, 6866, 2002.

[38] S.P. Nowlen, "A summary of the fire testing program at the German HDR test facility," Rockville, MD, CR-6173, 1995.

[39] E. Zalok and G.V. Hadjisophocleous, "Assessment of the Use of Fire Dyanmics Simulator in Performance-Based Design," *Fire Technology*, no. Online, November 2009.

[40] Yun Jiang, "Smoke Detection Performance and FDS Modelling for Full-Scale Fire Tests," Xtralis (UK) Ltd., Bentleigh East, VIC 3165, Australia, 2010.

[41] J.L. Lee, and H.C. Kung. H.Z. Yu, "Suppression of Rack-Storage Fires by Water," in *International Association For Fire Safety Science*, Ottowa, Ontario, Canada, 1994, p. 901–912.

[42] Daniel Madrzykowski. (October, 2009) BFRL Project: Hose Stream Characterization and Effectiveness Modeling. [Online]. http://www.nist.gov/bfrl/fire_protection/fireservice/hose_stream_charact_effect_modeling.cfm

[43] L. Y. Cooper, M. F. Harkleroad, J. G. Quintiere, and W. J. Rinkinen, "Experimental Study of Upper Hot Layer Stratification in Full-Scale Multiroom Fire Scenarios.," in *20th Joint ASME/AIChE National Heat Transfer Conference*, Milwaukee, WI, 1982, pp. 1-12.

[44] United States Nuclear Regulatory Commission, "Verification and Validation of Selected Fire Models for Nuclear Power Plant Applications: Volume 2 Experimental Uncertainty," United States Nuclear Regulatory Commission, Rockville, MD, NUREG-1824, 2007.

[45] J. D., Moore-Merrell, L. , Barowy, A. , Santos, R. , Peacock, R. D., Notarianni, K. , Wissoker, D. Averill, "Report on Residential Fireground Field Experiments," National Institute of Standards and Technology, Gaithersburg, MD, TN-1661 April 27, 2010.

[46] B. Taylor and C. Kuyatt, "Guidelines for Evaluating and Expressing the Uncertainty of NIST Measurement Results," Gaithersburg, MD, TN-1297, 1994.

[47] R. A. Bryant and G.W. Mulholland, "A Guide to Characterizing heat release rate measurement uncertainty for full-scale fire tests," *Fire and Materials*, vol. 32, pp. 121-139, January 2008.

[48] L.G. Blevins, "Behavior of Bare and Aspirated Thermocouples in Compartment Fires," in *National Heat Ransfer Conference*, Albuquerque, NM, August 15-17, 1999.

[49] W.M. Pitts et al., "Temperature Uncertainties for Bare-Bead and Aspirated Thermocouple Measurements in Fire Envinronments," in *Thermal Measurements: The Foundation of Fire Standards.*, Dallas, TX, December 3, 2001.

[50] A. Lock and et al., "Experimental Study of the Effects of Fuel Type, Fuel Distribution, and Vent Size on Full-Scale Underventilated Compartment Fires in an ISO 9705 Room," NIST, Gaithersburg, MD, TN 1603, 2008.

[51] Delmhorst Instrument Co., J-2000 Owner's Manual, 2006.

[52] J. Gust, R. Graham, and M. Lombardi, "Stopwatch and Timer Calibrations," Gaithersburg, MD, SP 960-12, 2004.

[53] W. Thornton, "The Relation of Oxygen to the Heat of Combustion of Organic Compounds," vol. 33, 1917.

[54] C. Hugget, "Estimation of the Rate of Heat Release by Means of Oxygen Consumption," vol. 12, pp. 61-65, 1980.

[55] W. Parker, "Calculations of the Heat Release Rate by Oxygen-Consumption for Various Applications.," vol. 4, pp. 380-395, 1984.

[56] M. L. Janssens, "Measuring Rate of Heat Release by Oxygen-Consumption," vol. 27, pp. 234-249, 1991.

[57] F. Tamanini, "Defining the Effects of Ambient Conditions in Large-Scale Fire Tests," *Experimental Thermal and Fluid Science*, 2009.

[58] Andrew H. Buchanan, *Structural Design for Fire Safety*. Chichcester, West Sussex, England: John Wiley & Sons, 2001.

[59] D. Gawin, J Kosny, and K. Wilkes, "Thermal Conductivity of Moist Cellular Concrete - Experimental and Numerical Study," Oak Ridge National Laboratory, Oak Ridge, Tennessee, 2004.

[60] United States Gypsum Company, Submittal Sheet 10310 - Durock Cement Board, 2007.

[61] United States Gypsum Company, Submittal Sheet 09250 - Sheetrock Gypsum Panels, 2007.

[62] A. Tewarson, "Generation of Heat and Chemical Compounds in Fires," in *The SFPE Handbook of Fire Protection Engineering*, P J DiNenno et al., Eds. Quincy, MA, U.S.A.: National Fire Protection Association, 2002, ch. 3-4, pp. 3-112.

[63] V. Kodur and T. Harmanthy, "Properties of Building Materials," in *The SFPE Handbook of Fire Protection Engineering*, P. DiNenno et al., Eds. Quincy, MA, U.S.A.: National Fire Protection Association, 2002, ch. 1-10, pp. 1-171.

[64] D. Drysdale, *An Introduction to Fire Dynamics*, 2nd ed. West Sussex, England: John Wiley & Sons, 1998.

[65] D Madrzykowski and R. L. Vettori, "Sprinkler Fire Suppression Algorithm for the GSA Engineering Fire Assessment System," NIST, Gaithersburg, MD, NISTIR 4833, May 1992.

[66] D.D. Evans, "Sprinkler Fire Suppression Algorithm for HAZARD," NIST, Gaithersburg, MD, NISTIR 5254, August 1993.

[67] S. Kerber and P. Fuss. (2008) BFRL Program - Advanced Fire Service Technologies. [Online]. http://www.bfrl.nist.gov/goals_programs/PDF/AFST/2009pd8661016_000.pdf

[68] J. Averill et al., "Report on Residential Fire Ground Field Experiments ," Gaithersburg, MD, Publication Pending, 2010.

[69] B. McCaffrey, J. Quintiere, and M. Harkleroad, "Estimating Room Fire Temperatures and the Likelihood of Flashover using Fire Test Data Correlations," *Fire Technology*, vol. 17, no. 2, pp. 98-119, 1981.

[70] Glenn P. Forney, "Smokeview (Version 5) - A Tool for Visualizing Fire Dynamics Simulation Data," Gaithersburg, MD, NIST SP 1017-1, 2008.

[71] Glenn P. Forney, "Visualization, A Tool For Understanding Fire Dynamics," Gaithersburg, MD, NISTIR 7431, 2007.

[72] G. P. Forney, D. Madrzykowski, K. B. McGrattan, and L. Sheppard, "Understanding Fire and Smoke Flow Through Modeling and Visualization," *IEEE Computer Graphics and Applications*, vol. 23, no. 4, pp. 6-13, July/August 2003.

[73] K. B. McGrattan, S. Hostikka, J. E. Floyd, H. R. Baum, and R. G. Rehm, "Fire Dynamics Simulator (Version 5): Technical Reference Guide.," Gaithersburg, MD, SP 1018-5, 2007.

[74] S. Kerber, "Characterizing positive pressure ventilation using computational fluid dynamics," Gaithersburg, MD, 7065, 2003.

[75] André Bakker. (2009, Dec.) CFD Class. [Online]. http://www.bakker.org/dartmouth06/engs150/01-intro.pdf

[76] Omega Engineering, Inc., *The Temperature Handbook, 5th Edition*. Stamford, CT: Omega Engineering, Inc., 2007.

[77] D. Madrzykowski and S. I. Kerber, "Fire Fighting Tactics Under Wind Driven Conditions: Laboratory Experiments.," Gaithersburg, MD, TN 1618, 2009.

[78] National Fire Protection Association, *Fire Protection Handbook, 20th Edition*. Quincy, MA: National Fire Protection Association, 2008.

[79] Daniel Madrzykowski. (2009, October) BFRL Project: Hose Stream Characterization and Effectiveness Modeling. [Online]. http://www.nist.gov/bfrl/fire_protection/fireservice/hose_stream_charact_effect_modeling.cfm

Appendix A: Grid Cell Sensitivity Temperature Comparison Plots

The following set of graphs contains comparisons of predicted and measured temperatures at all thermocouple locations for grid cell sensitivity study described in Section 5.1. The 0.03m thermocouple height is not included, it was not possible to simulate this thermocouple with the any of the grid resolutions. The "snap to grid" feature of FDS caused this thermocouple to measured the temperature of the surface material, rather than the gas temperature.

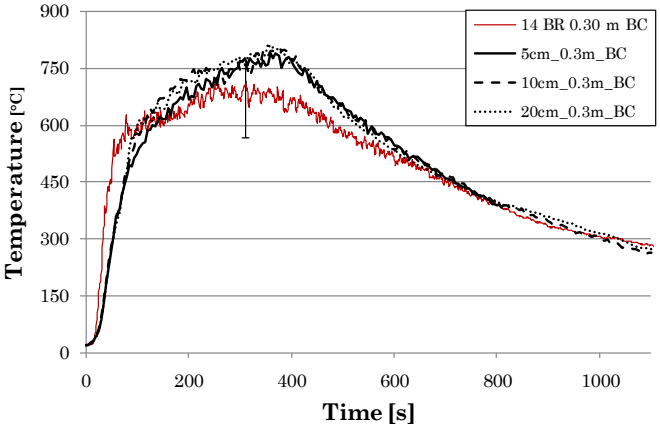

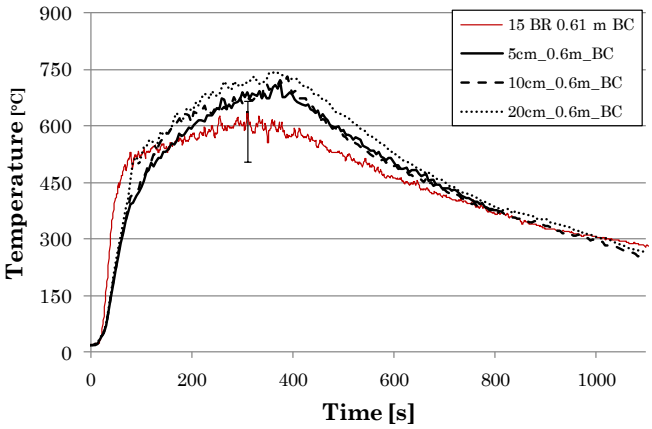

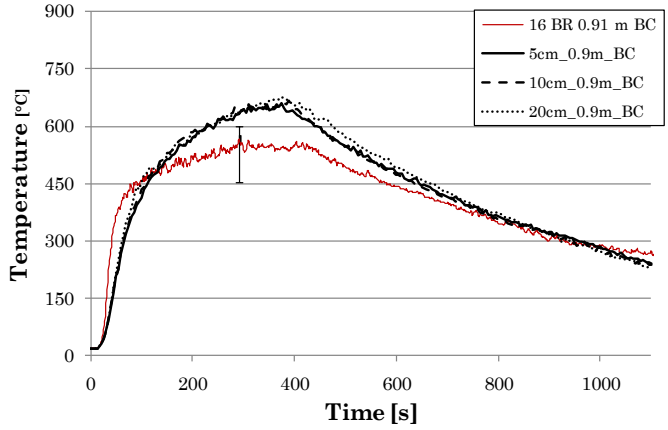

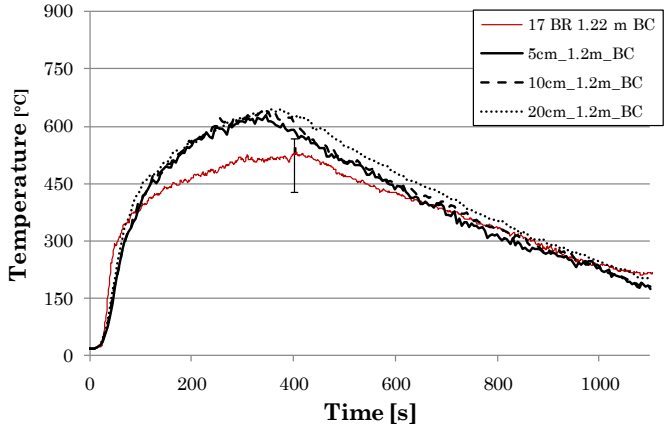

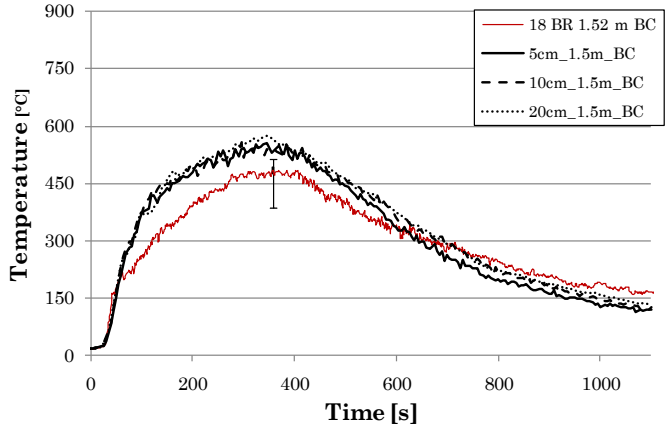

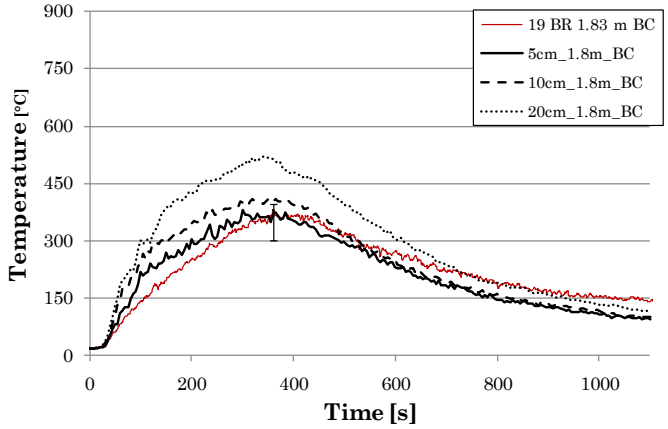

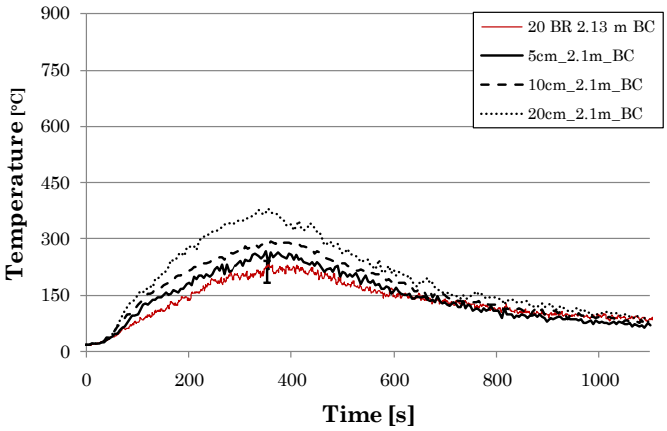
900
750
600
450
300
150
0
0
200
400
600
800
1000
Temperature [°C]
Time [s]
20 BR 2.13 m BC
5cm_2.1m_BC
10cm_2.1m_BC
20cm_2.1m_BC

Appendix B: Pallet Data

Test No.	Burn Side	Date	Excelsior Mass [kg]	Pallet No.	Pallet Mass [kg]
3 (2Far Rep. #1)	South	1/28/2009	2.2	1	18.6
				2	18.8
				3	15.4
				4	18.6
9 (2Far Rep. #2)	South	1/30/2009	2.9	1	15.7
				2	19.2
				3	17
				4	24.9
21 (2Far Rep. #3)	South	2/3/2009	3.4	1	18.2
				2	20.7
				3	17.5
				4	18.4
22 (5Close Rep. #1)	South	2/3/2009	3.5	1	21
				2	20
				3	14.6
				4	19.9
27 (5Close Rep. #2)	North	2/4/2009	3.1	1	17.4
				2	19.2
				3	17.7
				4	15.6
				4	15.8
34 (5Close Rep. #3)	North	2/6/2009	3.5	1	19.7
				2	15.5
				3	16.2
				4	18.6

Pallet #	Mass [kg]	MC1 [%]	MC2 [%]	MC3 [%]
1	16.9	9	9.1	7
2	17.2	10.9	11	11.1
3	19.2	12.4	10.3	9.2
4	15.6	12.7	13.3	13.1
5	17.7	14	13.4	14
6	18.6	9.7	10.9	10.1
7	16.2	7.9	8	7
8	16.1	9.1	7.1	7.8
9	18.7	8.1	10.3	6.9
10	20.8	10.6	11.5	11.7
Ave MC [%]	10.24			
Std Dev	2.21			